

Preparation, and ex vivo and in vivo Characterization of Favipiravir-Loaded Aspasomes and Niosomes for Nose-to-Brain Administration

Maryana Salamah ^{1,2}, Balázs Volk ³, István Lekli ⁴, István Bak ⁴, Alexandra Gyöngyösi ⁴, Gábor Kozma ⁵, Zoltán Kónya ⁵, Ágnes Szalencó-Tőkés ⁶, Ágnes Kiricsi ⁶, László Rovó ⁶, Diána Balogh-Weiser ^{7,8}, István Zupkó ², Ildikó Csóka ¹, Gábor Katona ^{1,*}, György Tibor Balogh ^{9,10,*}

¹Institute of Pharmaceutical Technology and Regulatory Affairs, Faculty of Pharmacy, University of Szeged, Szeged, Hungary; ²Institute of Pharmacodynamics and Biopharmacy, Faculty of Pharmacy, University of Szeged, Szeged, Hungary; ³Directorate of Drug Substance Development, Egis Pharmaceuticals Plc., Budapest, Hungary; ⁴Department of Pharmacology, Faculty of Pharmacy, University of Debrecen, Debrecen, Hungary; ⁵Faculty of Science and Informatics, Department of Applied & Environmental Chemistry, University of Szeged, Szeged, Hungary; ⁶Department of Oto-Rhino-Laryngology and Head-Neck Surgery, University of Szeged, Szeged, Hungary; ⁷Department of Organic Chemistry and Technology, Faculty of Chemical Technology and Biotechnology, Budapest University of Technology and Economics, Budapest, Hungary; ⁸Department of Physical Chemistry and Materials Science, Faculty of Chemical Technology and Biotechnology, Budapest University of Technology and Economics, Budapest, Hungary; ⁹Department of Pharmaceutical Chemistry, Semmelweis University, Budapest, Hungary; ¹⁰Center for Pharmacology and Drug Research & Development, Department of Pharmaceutical Chemistry, Semmelweis University, Budapest, Hungary

*These authors contributed equally to this work

Correspondence: Gábor Katona, Institute of Pharmaceutical Technology and Regulatory Affairs, Faculty of Pharmacy, University of Szeged, Eötvös Str. 6, Szeged, H-6720, Hungary, Email katona.gabor@szte.hu; György Tibor Balogh, Department of Pharmaceutical Chemistry, Semmelweis University, Hőgyes Endre Str. 9, Budapest, H-1092, Hungary, Email balogh.gyorgy.tibor@semmelweis.hu

Purpose: The present study aimed to develop and compare the intranasal applicability of favipiravir-loaded aspasomes (FAV-ASPs) using film hydration method, and favipiravir-loaded niosomes (FAV-NIOs) using ethanol injection method.

Methods: The FAV-ASP and FAV-NIO formulations were characterized according to nanoparticulate characteristics (DLS, drug loading, drug encapsulation efficacy, droplet size distribution), drug release and permeability behavior.

Results: The optimized FAV-ASP formulation (FAV-ASP8) consisted of FAV, ascorbyl palmitate, Span® 60 and cholesterol (30:25:25:50 w/w) with nano-scale size range (292.06 ± 2.10 nm), narrow polydispersity index (PDI) value (0.36 ± 0.03), adequate zeta potential (-74.73 ± 3.28 mV) and acceptable encapsulation efficiency ($55.33 \pm 0.41\%$). The optimized FAV-NIO formulation (FAV-NIO9) contained FAV, Span® 60 and cholesterol (30:30:40 w/w) with nano-scale size range (167.13 ± 1.60 nm), narrow PDI value (0.07 ± 0.01), adequate zeta potential (-27.1 ± 1.24 mV) and acceptable encapsulation efficiency ($51.30 \pm 0.69\%$). FAV-ASP8 and FAV-NIO9 were suitable for spraying into the nasal cavity (droplet size distribution <200 μ m). In vitro drug release and permeability studies demonstrated enhanced solubility and increased blood–brain barrier (BBB) permeability of FAV formulations, respectively. The ex vivo human nasal permeability study revealed that FAV diffusion from FAV-ASP8 was higher than from FAV-NIO9 or initial FAV. Furthermore, the in vivo animal study showed that FAV-ASP8 had a higher BBB penetration compared to FAV-NIO9 and pure FAV. The in vitro–in vivo correlation study showed good correlation between the in vitro and the in vivo pharmacokinetic data.

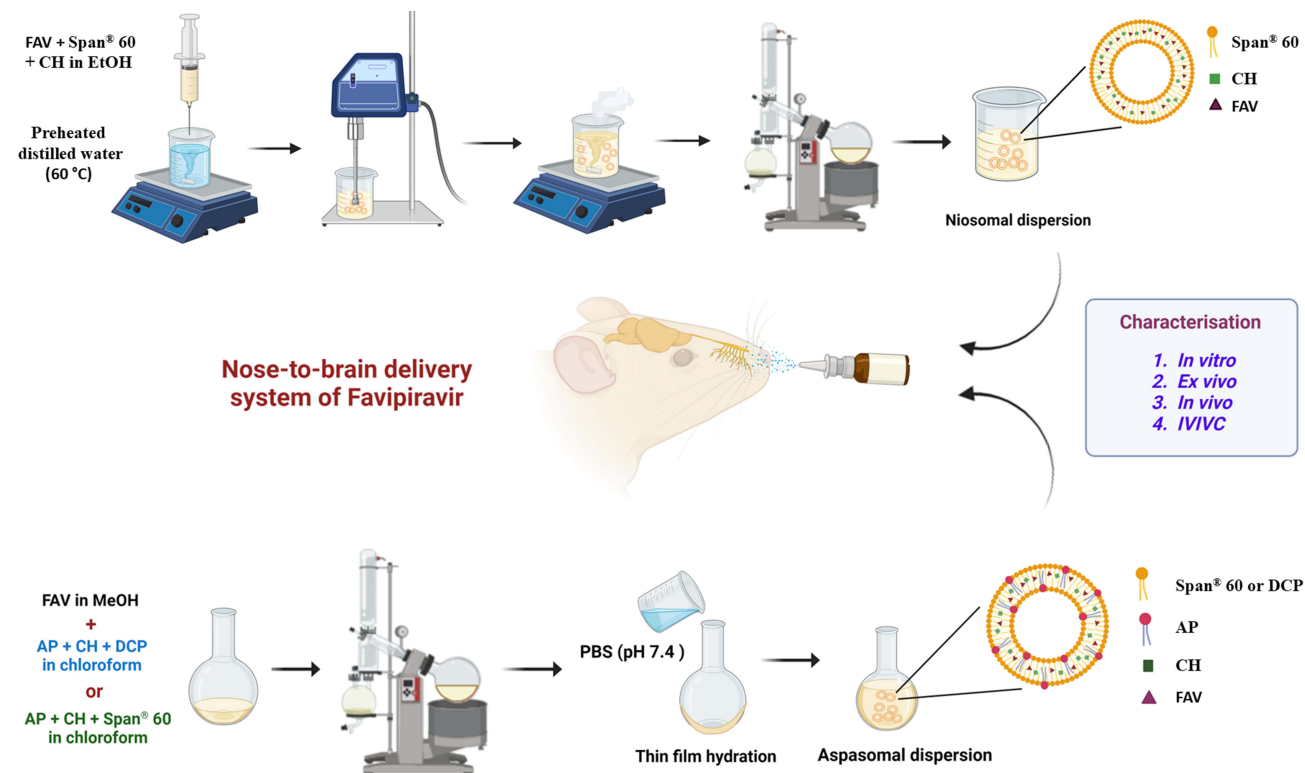
Conclusion: FAV-ASP8 for nose-to-brain delivery system could be a promising formulation to improve FAV bioavailability compared to FAV-NIO9.

Keywords: aspasomes, niosomes, favipiravir, nose-to-brain delivery, ex vivo nasal permeability, in vivo nasal permeability

Introduction

Neurotropic viruses including RNA viruses, such as poliovirus, Zika virus, influenza A and B, severe acute respiratory syndrome coronavirus 2 (SARS-CoV-2), mumps virus, and measles virus, are able to access the brain and infect the central nervous system

Graphical Abstract



(CNS), resulting in meningitis, myelitis, encephalitis, or meningoencephalitis.¹⁻³ Neurotropic viruses can access CNS by crossing the blood–brain barrier (BBB) or blood-cerebrospinal fluid barrier (BCSFB), nerve terminals in the nasal olfactory epithelium, or the pseudounipolar sensory neurons of the peripheral nervous system (PNS).³⁻⁵ This viral infection of the CNS leads to alteration or degeneration of neuronal cell function, which causes several neurodegenerative diseases, such as Alzheimer’s disease, Parkinson’s disease, and amyotrophic lateral sclerosis.⁵⁻⁷ Therefore, it has become urgent to search for potential drugs for the treatment of viral CNS infections. Considering these facts, intranasal delivery can be a proper choice to deliver the drug directly to the brain via the systemic pathway, olfactory and trigeminal nerve pathways.⁸⁻¹⁰ Several possible candidates exist for the intranasal delivery of virucidal drugs and agents, such as favipiravir (FAV).^{11,12}

FAV (FAV, 6-fluoro-3-hydroxypyrazine-2-carboxamide, [Figure 1](#)), as an antiviral prodrug, was approved in Japan in 2014 for the treatment of new-onset or recurrent pandemic influenza as well as for experimental drug for Ebola virus

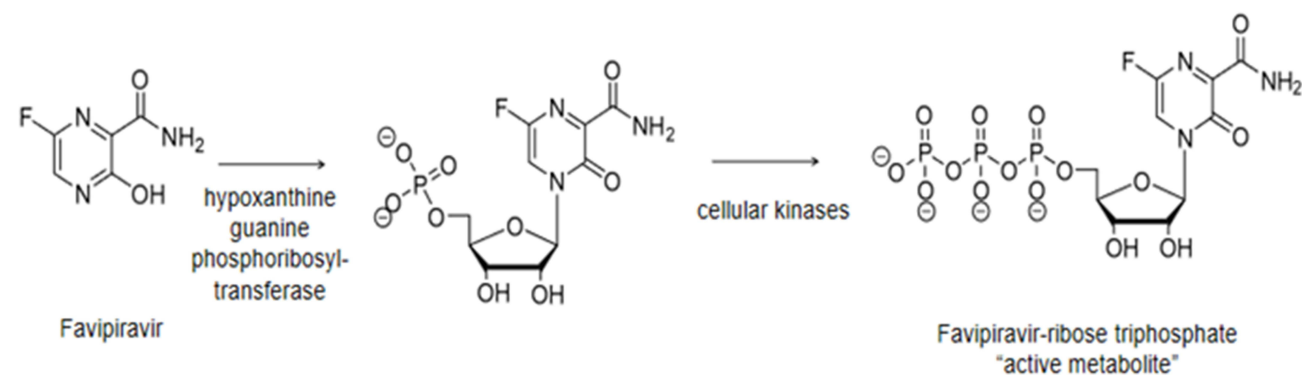


Figure 1 Chemical structure of FAV and its metabolic activation.¹⁴

infections. FAV is first converted by hypoxanthine-guanine phosphoribosyl transferase (HGPRT) to ribose 5'-monophosphate (T-705-RMP) and then metabolized to the triphosphate form (T-705RTP) by cellular kinases.^{13,14} The compound selectively inhibits viral RNA polymerase in vivo by its triphosphorylated metabolite, translating to broad-spectrum inhibition of RNA viruses.^{15,16}

FAV is available in an oral solid dosage form (Avigan® 200 mg),¹⁷ with a recommended dosage of 1600 mg twice daily on day 1, followed by 600 mg twice daily on days 2 to 5 for the treatment of influenza infection,¹⁸ which leads to patient incompliance, and results in toxicity and limited oral bioavailability (due to its low water solubility, FAV is a Biopharmaceutics Classification System (BCS) class II drug).¹⁹ FAV has a short half-life, leading to rapid renal clearance in its hydroxylated form (inactive metabolite T-705M1) after being metabolized by aldehyde oxidase/xanthine oxidase enzymes (present in the liver, lungs, small and large intestine, kidney, prostate, and adrenal glands).²⁰ Thus, a novel formulation and alternative route of administration are critical to improve bioavailability and therapeutic efficacy while minimizing the adverse effects of FAV (that include mild to moderate diarrhoea, increase of blood uric acid and transaminase level, and decrease in the neutrophil counts).^{21,22}

Intranasal delivery of FAV means further advantages, including improved systemic bioavailability due to increased drug solubility, absorption and nasal permeability through a highly vascularized and less acidic environment, avoiding hepatic first-pass metabolism in comparison to the gastrointestinal tract.^{23,24} FAV shows low brain penetrance because it has a low log P value (0.72), the critical factor for CNS penetration, and low lipophilicity, which decreases brain uptake.²⁵ Therefore, intranasal delivery can be utilized to deliver FAV directly to the brain, where it could be activated by the HGPRT enzyme within the infected cells by neurotropic viruses, as HGPRT is also found in the CNS. Moreover, the administration of lower doses may be therapeutically effective with fewer systemic side effects.

Lipid nanoparticles, including liposomes and niosomes, are considered a suitable antiviral drug carrier to enhance the BBB penetrating, protect the drug against enzymatic degradation, and improve its bioavailability, hence, prevent viral spread.^{26–28} Niosomes (NIOs), a newer generation of liposomes, rise from the self-assembly of non-ionic surfactants of the alkyl or dialkyl polyglycerol ether class and cholesterol (CH) with subsequent hydration in aqueous media.^{29,30} Recently, amphiphilic materials, such as ascorbyl palmitate (AP), have been used to prepare bilayer vesicles called aspasomes (ascorbyl palmitate-based nanocarriers; ASPs), a newer generation of NIOs, to enhance the stability and biological activity of NIOs.³¹ ASPs contain AP in combination with CH and an anionic or nonionic surfactant in various molar ratios. AP is an ester form of ascorbic acid, which is amphiphilic by nature and more stable in liquid form than ascorbic acid.^{31–35}

These colloidal vesicles have several advantages, like the development of an effective drug delivery system to achieve a maximum effective concentration and the formation of vesicles that are able to entrap both hydrophilic and hydrophobic drug molecules with higher stability compared to liposomes. Moreover, modification of the nanoparticulate composition or surface can adjust the affinity for the target site and/or the drug release rate.

According to our knowledge, several FAV-nanocarriers for intranasal administration have been developed such as favipiravir-pyridinecarboxamide cocrystal nasal powder formulation,³⁶ crystalline favipiravir Sodium Salt liquid formulation,³⁷ favipiravir loaded PLGA nanoparticles,³⁸ and favipiravir loaded mucoadhesive chitosan–alginate nanoparticles.³⁹ Moreover, ASPs have been used for transdermal delivery, such as Acyclovir loaded aspasomal gel,⁴⁰ Quercetin loaded aspasomal gel,⁴¹ Idebenone/Naproxen co-loaded aspasomes,⁴² and based on the literature, there are no available reported ASP formulations for intranasal administration. Therefore, FAV-loaded aspasome formulations (FAV-ASPs) and FAV-loaded niosome formulations (FAV-NIOs) seem to be a novel approach.

In this study, our aim was to develop and compare novel FAV-ASPs and FAV-NIOs intended for intranasal administration in order to improve the poor solubility of FAV, as a potential treatment for viral infections of CNS. A further aim was the characterization of nasal applicability of optimized FAV-ASP and FAV-NIO formulations.

Materials and Methods

Chemicals and Solvents

FAV was provided by Egis Pharmaceuticals Plc. (Budapest, Hungary) with a purity of 99.6% w/w (according to supplier certificate of analysis). Methanol 99.99% v/v (HPLC grade), *ortho*-phosphoric acid 85% v/v (HPLC grade) and

anhydrous disodium hydrogen phosphate were purchased from Molar Chemicals Kft. (Budapest, Hungary). Acetonitrile 99.8% v/v (HPLC grade) was purchased from PromoChem (Wesel, Germany). Ascorbyl acid-6-palmitate (AP), sorbitan monostearate (Span® 60), chloroform, ethanol 96% v/v, dimethyl sulfoxide (DMSO) and dodecane were purchased from Merck KGaA (Darmstadt, Germany). Porcine brain polar lipid extract, dicetyl phosphate (DCP) and cholesterol (CH) were purchased from Sigma Aldrich Co. Ltd. (Budapest, Hungary). For redispersion of formulations, pH 7.4 Dulbecco's phosphate-buffered saline (DPBS) acquired from Capricorn Scientific GmbH (Ebsdorfergrund, Germany) was applied. As nasal dissolution medium, Simulated Nasal Electrolyte Solution (SNES) was freshly prepared, containing 8.77 g sodium chloride (NaCl), 2.98 g potassium chloride (KCl), and 0.59 g anhydrous calcium chloride (CaCl₂) in 1000 mL of deionized water at pH 5.6. These chemicals were acquired from Sigma-Aldrich Co. Ltd. (Budapest, Hungary). In all experiments, purified water was filtered using the Millipore Milli-Q® (Merck Ltd., Budapest, Hungary) Gradient Water Purification System.

Quantitative Analysis by RP-HPLC-DAD

FAV concentration in the experiments was analyzed using an Agilent 1260 hPLC (Agilent Technologies, San Diego, CA, USA) and Zorbax® SB-CN C18 column (5 µm, 250 mm × 4.6 mm, 100 Å). As mobile phase acetonitrile–disodium hydrogen phosphate anhydrous buffer (pH 3.1, 20 mM) in a ratio of 10:90 (v/v) was used, and FAV was eluted at an isocratic flow rate of 1.0 mL/min up to 10 min at 30°C. The injection volume was 10 µL. Chromatograms were detected at 323 nm using a UV-VIS diode-array detector.

Preparation of FAV-ASP Formulations

A modified film hydration method was used for the preparation of FAV-ASPs^{31,34} (Table 1). For anionic surfactant-based FAV-ASPs, various ratios of lipid mixture (AP:CH:DCP) (w/w) were dissolved in 10 mL of chloroform, whereas for nonionic surfactant-based FAV-ASPs, different ratio of AP/Span® 60 with a constant amount of CH (50 mg) were dissolved in 10 mL of chloroform. A fixed amount of FAV (30 mg) was dissolved in 5 mL of methanol. Then, the FAV solution was mixed with each lipid solution in a round bottom flask, and the organic solvent was evaporated at 60 °C and 633 mbar pressure using a Büchi R-210 rotary vacuum evaporator (Flawil, Switzerland), and the rotation was set at 100 rpm for 1 h, until the appearance of a thin film on the wall of the flask. Thereafter, the thin lipid film was hydrated with 15 mL of pH 7.4 phosphate-buffered saline (PBS) for 1 h.

Table 1 Composition of FAV-Loaded Aspasome Formulations (FAV-ASP)

Formulation	FAV (mg)	Anionic Surfactant-Based FAV-ASP			Nonionic Surfactant-Based FAV-ASP		
		AP (mg)	CH (mg)	DCP (mg)	AP (mg)	Span® 60 (mg)	CH (mg)
FAV-ASP1	30	40	40	10	–	–	–
FAV-ASP2	30	30	40	10	–	–	–
FAV-ASP3	30	20	40	10	–	–	–
FAV-ASP4	30	10	40	10	–	–	–
FAV-ASP5	30	40	10	10	–	–	–
FAV-ASP6	30	40	20	10	–	–	–
FAV-ASP7	30	40	30	10	–	–	–
FAV-ASP8	30	–	–	–	25	25	50
FAV-ASP9	30	–	–	–	25	50	50
FAV-ASP10	30	–	–	–	50	25	50
FAV-ASP11	30	–	–	–	50	50	50

Preparation of FAV-NIO Formulations

FAV-NIOs were formulated by a modified ethanol injection method.⁴³ Various amounts of Span® 60 and CH (as shown in Table 2) were dissolved in 2 mL ethanol using ultrasonication (for 10 min at 30°C). A fixed amount of FAV (30 mg) was dissolved in the ethanolic solution, followed by sonication until the formation of a clear solution. Then, it was injected rapidly in 15 mL of distilled water (previously heated to 60°C) under constant stirring, followed by probe sonication (0.5 cycles for 2 min at ultrasonic power input 80%). Then, it was stirred for 1 h at room temperature, followed by a complete evaporation of ethanol at 60°C and 633 mbar pressure using a rotary vacuum evaporator, and the rotation was set at 100 rpm for 1 h. To reach the final volume (15 mL) of niosomal dispersion, distilled water was added.

Lyophilization

For freeze-drying a Scanvac, CoolSafe 100–9 Pro type apparatus (LaboGeneApS, Lyngø, Denmark) was applied. Formulations were divided in 1.5 mL portions, and 5% w/v of mannitol was added as a cryoprotectant. Freeze-drying was performed at –40°C for 12 h at reduced pressure (0.013 mbar) controlled by Scanlaf CTS16a02 software. After that, a secondary drying at 25°C was applied for 3 hours. Freeze-dried samples were stored in the refrigerator at 4°C until further analysis. The samples were redispersed in adequate medium before each test.

Vesicle Size Analysis, Polydispersity Index and Zeta Potential Determination

The mean hydrodynamic diameter of vesicles (Z-average), polydispersity index (PDI) and zeta potential (ZP) for FAV-ASP and FAV-NIO formulations were investigated using a Malvern NanoZS equipment (Malvern Instrument). Samples were redispersed in distilled water and suitably diluted (1:10) before assessments. All measurements were carried out in triplicate, and results are presented as means ± SD.

Determination of Drug Content, Drug Encapsulation Efficiency (EE%) and Drug Loading (DL%)

For drug content determination 1–1 mL of formulations were diluted with 4 mL of methanol using ultrasonication bath for 10 min. Then, the suspensions were filtered using 0.45 µm syringe filters and analyzed with HPLC to determine FAV concentration. Encapsulation efficiency (EE%), ie the percentage amount of FAV that has been loaded in the vesicles, was determined by using the dialysis technique in order to select the proper formulations with the highest EE% for further studies.⁴⁴ The formulations were redispersed in distilled water, and then 3 mL of each sample was transferred into a dialysis bag (12 kDa MWCO, Sigma-Aldrich, St. Louis, USA) immersed in 100 mL of purified water and constantly

Table 2 Composition of FAV-Loaded Niosome Formulations (FAV-NIO)

Formulation	FAV (mg)	Span 60® (mg)	CH (mg)
FAV-NIO1	30	40	10
FAV-NIO2	30	30	10
FAV-NIO3	30	20	10
FAV-NIO4	30	40	20
FAV-NIO5	30	40	30
FAV-NIO6	30	40	40
FAV-NIO7	30	10	40
FAV-NIO8	30	20	40
FAV-NIO9	30	30	40

stirred for 30 min. The concentration of free FAV that diffused from the dialysis bag to the purified water was determined by using HPLC, and EE% and DL% were calculated as follows:⁴⁵

$$EE\% = \frac{C_{\text{before dialysis}} - C_{\text{after dialysis}}}{C_{\text{before dialysis}}} \times 100\% \quad (1)$$

$$DL\% = \frac{\text{Mass of drug encapsulated}}{\text{Mass of nanoparticles components}} \times 100\% \quad (2)$$

Residual Solvent Determination

To determine the residual organic solvents (ethanol, methanol and chloroform) in the freeze-dried formulations, gas chromatography-mass spectroscopy (GC-MS) measurements were performed using a Shimadzu GCMS-QP2010 SE (Shimadzu Europa GmbH, Duisburg, Germany) with a ZBWax-Plus column (length: 30 m, diameter: 0.25 mm) and helium carrier gas.

In vitro Permeability Measurements

A blood–brain barrier-specific parallel artificial membrane permeability assay (BBB-PAMPA) was used to investigate FAV permeability (cm/s) of initial API solution and in the selected formulations (according to the EE% results) in order to find the optimal one.⁴⁶ 10 mm FAV solution was prepared in dimethyl sulfoxide (DMSO), which was further diluted with DPBS solution (pH 7.4) to obtain reference solution with 100 μM concentration. The donor plate (Multiscreen™-IP, with pore size 0.45 μm ; Millipore, Merck Ltd., Budapest, Hungary) was preliminary coated with 5 μL of lipid solution (24 mg porcine brain polar lipid extract dissolved in 840 μL hexane and 360 μL dodecane). Then, the donor plate was inserted to the acceptor plate (Multiscreen Acceptor Plate, Millipore, Merck Ltd., Budapest, Hungary), which contained 300 μL of DPBS solution (pH 7.4). 150–150 μL of reference FAV solution, as well as of the redispersed freeze-dried formulations with DPBS (with 2 mg/mL FAV nominal concentration) were transferred on the lipid membrane of the donor plate. The plates were incubated at 37°C for 4 h (Heidolph Titramax 1000, Heidolph Instruments, Schwabach, Germany). After that the PAMPA plates were separated and the FAV concentrations both in the donor and acceptor chambers were determined using HPLC. The effective permeability and membrane retention of drugs were calculated using the following equation (3):

$$P_e = -\frac{2.303 \cdot V_A}{A(t - \tau_{ss})} \cdot \log\left(1 - \frac{C_A(t)}{S}\right) \quad (3)$$

where P_e means the effective permeability coefficient (cm/s), V_A is the volume of the acceptor well (0.3 cm^3), A indicates the surface area of one well (0.24 cm^2), t is the incubation time (s), τ_{ss} is the time to reach the steady state (s), $C_A(t)$ is the concentration of the compound in the acceptor phase at time point t (mol/cm^3), and S is the solubility of FAV in the donor phase. The flux of the samples was calculated as follows (4):

$$\text{Flux} = P_e \cdot S \quad (4)$$

Six parallel measurements were performed, and data are presented as means \pm SD.

Rapid Equilibrium Dialysis Measurement (RED)

RED method (Thermo Scientific™, Waltham, MA, USA) was applied for the determination of the time-dependent drug release profiles of FAV and the selected optimal formulations (according to PAMPA results) after nasal absorption. For the measurement, the reference was prepared by suspending 2 mg of FAV in 1 mL DPBS solution (pH 7.4) using an Eppendorf MixMate (Thermo Scientific™, Waltham, MA, USA) vortex mixer for 30 s. RED inserts (8K MWCO) were fitted into the reusable Teflon base plate, and then 150–150 μL of reference FAV solution, as well as of the lyophilized formulations redispersed in DPBS (with 2 mg/mL FAV nominal concentration) were pipetted into the donor chambers. Then, 300 μL of DPBS was pipetted to the acceptor chambers, and the device was covered with a sealing tape to avoid evaporation and incubated at 37°C for 4 h. Aliquots from the acceptor chambers were withdrawn at predetermined time

points and replaced with fresh DPBS.⁴⁶ FAV concentrations were determined using HPLC. Six parallel measurements were conducted, and data were presented as means \pm SD.

In vitro Drug Release Under Nasal Conditions

In vitro drug release study under nasal conditions is an important test during the development of intranasal formulations to determine the absorption through the nasal cavity. Using the modified paddle method (Hanson SR8 Plus, Teledyne Hanson Research, Chatsworth, CA, USA) drug release profile for reference FAV suspension, and the optimal freeze-dried formulations redispersed in SNES (with 2 mg/mL FAV nominal concentration⁴⁷) were determined at 32°C at 50 rpm paddle rotation speed in 100 mL SNES medium for 60 min. 1 mL of reference suspension and formulations were loaded in pre-treated dialysis bags (Spectra/Por® Dialysis Membrane with 12–14 kDa MWCO, Spectrum Laboratories Inc., Rancho Dominguez, CA, USA) sealed at both ends. Quantification of aliquots was performed by HPLC.

Evaluation of in vitro Drug Release Data

Drug release profiles were compared with model-independent approaches based on calculating the area under the curve (AUC), dissolution efficiency (DE), and mean dissolution time (MDT). In addition, the model-dependent kinetic analysis (zero order, first order, Higuchi, and Korsmeyer-Peppas kinetic profiles) was fit to evaluated. Microsoft Excel DDSolver® add-in software was used for the mathematical evaluation of the release kinetics, and the fitting of each model by comparing the correlation coefficient (R^2), rate constant (K), Akaike Information Criterion (AIC), and Model Selection Criterion (MSC).^{48–51}

Storage Stability

The optimal formulations were stored at 4°C and the storage stability study was conducted for 4 weeks and analyzed in terms of Z-average, PDI, ZP to evaluate the physical stability and in terms of drug content to evaluate the chemical stability every week (as described previously).

Droplet Size Distribution Measurement

Laser diffraction method was used to evaluate the droplet size distribution of the optimal formulations.⁵² The evaluation was performed using a Malvern Spraytec® system (Malvern Instruments Ltd., Malvern, UK), equipped with a 300 mm lens capable of analysing droplet sizes in a range of 0.1–900 μ m (Dv50: 0.5–600 μ m). The tip of the nasal spray device was aligned and positioned at 45° from the horizontal plane. Measurements were conducted at room temperature. The formulations were redispersed in distilled water and placed in a nasal spray container. Each nasal spray was manually actuated three times and discharged into waste, allowing the device to function optimally. The data were analyzed using the Spraytec® software v4.00 (Malvern Panalytical Ltd., Malvern, UK), with volume diameter and described as 10% (Dv10), 50% (Dv50), and 90% (Dv90) of the cumulative volume distribution. The results were presented as means \pm SD.

Ex vivo Nasal Permeability Study on Human Nasal Mucosa

The ex vivo transmucosal permeability of the optimized formulation (based on BBB-PAMPA, nasal dissolution, and RED results) and reference FAV suspension (with 2 mg/mL nominal FAV concentration) was studied in a modified Side-Bi-Side® type horizontal diffusion apparatus under artificial nasal conditions.⁵³ Human nasal mucosa were collected during routine nasal and sinus surgeries (septoplasty, Functional Endoscopic Sinus Surgery (FESS)) under general or local anesthesia. The surgical field was infiltrated with locally administered 1% lidocaine-adrenalin injection, and the mucosa was excised with a raspatorium or Cottle elevator. Excised nasal mucosa was stored in physiological saline until further investigation. All investigations were conducted freshly within 30 min after the removal of the tissue. The experiments have been performed in line with the principles of the Declaration of Helsinki under approval of University of Szeged's institutional ethics committee (ETT-TUKEB: IV/3880-1/2021/EKU). The participants were briefed on the study procedures, and written informed consent was obtained from all subjects prior to conducting the procedure. Nasal mucosa was cut with a surgical scalpel into uniform segments with a diameter of 6 mm and inserted between donor and acceptor phases to provide an appropriate surface for permeability study.⁵⁴ To the donor Phase 8 mL of SNES was added, whereas

to the acceptor Phase 9 mL of DPBS solution (pH 7.4) was pipetted. The temperature of both chambers was thermostated at $32 \pm 0.5^\circ\text{C}$ using a heating circulator (ThermoHaake C 10-P5, Sigma–Aldrich Co. Ltd., Budapest, Hungary). For the measurement, both FAV reference suspension and selected freeze-dried formulation were redispersed in 1 mL SNES (with 2 mg/mL FAV nominal concentration) and added to the donor compartment. Both compartments were continuously stirred at 300 rpm using magnetic stirrers. Aliquots were withdrawn (100 μL) from the acceptor phase at 5, 10, 15, 30, and 60 min and replaced with fresh DPBS. FAV concentration was determined using HPLC. The steady-state flux (J_{ss}), permeability coefficient (K_p), and enhancement ratio (ER) were calculated as follows:⁵⁵

$$J_{ss} = \frac{m_t}{A \times t} \quad (5)$$

$$K_p = \frac{J_{ss}}{C_d} \quad (6)$$

$$ER = \frac{J_{ss \text{ formulation}}}{J_{ss \text{ Reference}}} \quad (7)$$

where J_{ss} is the steady-state flux ($\mu\text{g}/\text{cm}^2/\text{h}$), m_t is the quantity of FAV permeated through the nasal mucosa, A is the permeability surface of nasal mucosa (0.785 cm^2), t is the duration of the investigation (h), K_p is the permeability coefficient (cm/h) and C_d is the drug concentration in the donor phase ($\mu\text{g}/\text{cm}^3$).

The theoretical steady-state plasma concentration (C_{ss}) of the drug can be used for estimation of the concentration of drug that could be reached in the blood after nasal administration, was calculated as follows:⁵⁶

$$C_{ss} = J_{ss} \frac{A}{Cl_p} \quad (8)$$

where J_{ss} is the steady-state flux, A is the surface area of nasal mucosa used for the permeation study (cm^2), and Cl_p is the plasmatic clearance (human Cl_p value for FAV is 5.11 L/h).⁵⁷

In vivo Study

Animals and Samples Collection

The animals were kept at room temperature (approximately 23°C) and light was adjusted to alternate darkness and light for 12 hours. The rats were fed with normal rodent chow and tap water ad libitum. All animals received humane care, in compliance with the “Principles of Laboratory Animal Care” according to the National Society for Medical Research and the Guide for the Care and Use of Laboratory Animals, formulated by the National Academy of Sciences, and published by the National Institute of Health (NIH Publication No. 86–23, revised 1985). Healthy male Sprague-Dawley rats ($339 \pm 39 \text{ g}$, mean \pm SD) were anaesthetized with an *i.p.* injection of ketamine (50 mg/kg) and xylazine (10 mg/kg). The femoral vein was cannulated for plasma collection.⁵⁸ A total of 50 μL FAV (2 $\mu\text{g}/\mu\text{L}$) or the corresponding formulation of FAV was administered nasally. Animals were divided into three groups (FAV, FAV-ASP8, and FAV-NIO9), and 0.5 mL of blood samples were taken at 0, 5, 10, 15, 30 and 60 min post-FAV administration, then cerebrospinal fluid samples were collected at the end of the experiments. After 45 min, the clot was removed by centrifuging at $1000 \times g$ for 10 min. The resulting supernatant (non-hemolytic serum) was extracted with 2 volumes of acetonitrile. Accordingly, acetonitrile is suitable for precipitating and removing high-abundance proteins from the serum and eliminate the intra-molecular protein interactions. The precipitate was removed by centrifuging at $1000 \times g$ for 10 min. The animal study protocol was approved by the Institutional Review Board (or Ethics Committee) of Institutional Animal Care and Use Committee of the University of Debrecen, Debrecen, Hungary. (Approval number: 2/2021/DEMÁB)

Sample Preparation

Real or spiked (standard) plasma or cerebrospinal fluid samples were precipitated with acetonitrile (1:2) and centrifuged at $1000 \times g$ for 10 min. The supernatants were collected, and the samples were dried under a gentle stream of N_2 at 60°C using a Turbovap LV concentrator. The samples were re-dissolved in 50 μL pyridine, and then 50 μL *N*,

O-bis(trimethylsilyl)tri- fluoroacetamide (BSTFA) with 1% of trimethylchlorosilane (TMCS) was added into the tubes. The solutions were transferred into 1.5 mL vials sealed, and derivatization was carried out at 80°C for 30 min at 500 rpm using an Eppendorf Thermomixer C device.⁵⁹ Finally, 1 µL of the reaction mixture was injected into GC-MS equipment.

Gas Chromatograph-Mass Spectrometric (GC-MS) Analysis

Derivatized FAV was measured by GC-MS using a Shimadzu GCMS-QP2010 (Shimadzu, Kyoto, Japan) equipment. The GC was equipped with an SLB-5 MS capillary column (Supelco, Bellefonte, PA, USA) (30 m × 0.25 mm i.d.; 0.25 µm film thickness). Operating conditions were as follows: carrier gas: He, flow rate 32 cm/s; column temperature program: 1 min at 60°C, 60–250°C at 40°C/min and finally 7 min at 250°C. The temperature of the injection port and the interface were 250°C and 270°C, respectively. 1 µL of the samples was injected into the GC-MS using an AOC-20i autosampler; the split ratio was 1:10. The MS was equipped with an electron ionization (EI) ion source, and the operating conditions were as follows: ionization energy 70 eV, ion source temperature 200°C, solvent cut time 4 min. The measurements were carried out in selected ion monitoring (SIM) mode. The registered ions were 301 m/z, 286 m/z and 270 m/z, which were selected based on the EI spectrum measured in SCAN mode.

Evaluation of Pharmacokinetic (PK) Parameters

The PK parameters of pure FAV, FAV-ASP8, and FAV-NIO9 were determined in the plasma and the CSF following a single intranasal dose to evaluate the brain targeting. PK Solver 2.0 software was used to determine pharmacokinetic parameters by non-compartmental analysis.⁶⁰ The maximum concentrations (C_{max}) and times taken to reach these concentrations (T_{max}) were determined from the mean concentration-time profiles. The elimination rate constant (k_e) was determined by plotting log-linear concentration versus time. The elimination half-life ($t_{1/2}$) was calculated using equation (9):⁶¹

$$t_{1/2} = 0.693/k_e \quad (9)$$

The area under the plasma concentration versus time curve (AUC_{0-t}) was calculated using the linear trapezoidal method from time 0 to time t (the last time point to withdraw blood samples), then the AUC from 0 to infinity, $AUC_{0-\infty}$ (µg hour/mL) was calculated using the following equation:^{61,62}

$$AUC_{0-\infty} = AUC_{0-t} + C_t/k_e \quad (10)$$

where C_t (µg/mL) is the last measured concentration at time t .

The clearance (C_L), the apparent volume of distribution (V_d), the mean residence time (MRT), and the relative bioavailability ($F\%$) were calculated using the following equations:^{46,63–66}

$$C_L = dose/AUC_{0-\infty} \quad (11)$$

$$V_d = \frac{C_L}{k_e} \quad (12)$$

$$MRT = \frac{\int C \cdot t dt}{\int C dt} = \frac{AUMC}{AUC} \quad (13)$$

$$F(\%) = \frac{(AUC_{0-t})_{formulation}}{(AUC_{0-t})_{reference}} \times 100 \quad (14)$$

where AUMC is the first moment of the concentration-time integral.

Evaluation of in vitro-in vivo Correlations (IVIVC)

A point-to-point IVIVC for pure FAV, FAV-ASP8, and FAV-NIO9 was mathematically examined based on the in vitro data (release and permeation) and the in vivo pharmacokinetics data (based on FDA guidance^{67–69}). The relationship between in vitro values of AUC_{0-t} (µg×min/mL) and in vivo values of AUC_{0-t} (µg×min/mL) were evaluated using linear regression. R^2 values have been calculated for each graph.

Statistical Analysis

All experimental results are expressed as the mean \pm SD. For statistical analysis, GraphPad Prism version 10.12 software (GraphPad Software, San Diego, CA) was used. A one-way analysis of variance (ANOVA) and Tukey's post-hoc test were performed to compare the groups. The significance level was set at p -value < 0.05 , where (ns) means non-significant, * p -value < 0.05 , ** p -value < 0.01 , and *** p -value < 0.001 , **** p -value < 0.0001 .

Results and Discussion

Quantitative Analysis by RP-HPLC-DAD

The optimized method showed a good retention time (4.95 ± 0.01 min), symmetrical peak shape (0.87 ± 0.02) and the required number of theoretical plates (12722.12 ± 89.21) as per United States Pharmacopoeia (USP) and International Council for Harmonization of Technical Requirements for Pharmaceuticals for Human Use (ICH) Q2 (R1) guidelines.^{70,71} The correlation coefficient (R^2) was 0.9996, which suggests an excellent correlation and good linearity for the method. System suitability is related to the reproducibility and capability of the method for routine analysis. The optimized method showed good system suitability (Table 3).

Preparation of FAV-ASP and FAV-NIO Formulations

Anionic surfactant-based FAV-ASP consisted of AP, CH and DCP. AP has a hydrophilic–lipophilic balance (HLB) value of about 8.4, which is suitable for vesicle formation.⁷² However, these AP vesicles are not stable. In contrast, AP may form stable ASPs when combined with CH and the negatively charged lipid DCP.^{42,73,74} CH is necessary to improve physical stability as it provides rigidity to the bilayer membrane. DCP is used as a negative charge inducer to create vesicles with stronger interaction with the mucosal surface, achieving improved delivery. It also forms electrostatic repulsion between the vesicles, inhibiting aggregations. In addition, the double hydrocarbon chains in DCP results in tighter packing of the bilayer membrane, increasing the encapsulation efficiency in ASP formulations.^{75,76}

Nonionic surfactant-based FAV-ASPs were formed by combining AP, CH and nonionic surfactants (Span® 60). All Span types have the same head group but a different alkyl chain, and increasing the alkyl chain length leads to a higher encapsulation efficiency. In this study, Span® 60 (HLB = 4.7) was used as a vesicle stabilizer due to its long chain length (C18) and high transition temperature (53 – 55°C).³⁴ The temperature of the rotary evaporator was 60°C , above the gel-to-liquid phase transition temperature of Span® 60.

The NIO vesicles were formed by the combination of CH and Span® 60. The impact of CH and Span® 60 on the formation of the vesicles was described previously. According to the literature, Span® 60 can form vesicles-NIOs only in the presence of a suitable amount of cholesterol.^{77,78}

The optimal formulations were selected based on the critical parameters of the drug carrier for the nose-to-brain delivery system, as summarized in Table 4. Firstly, we selected the formulations within the acceptable range of Z-average, PDI and ZP. Then, we selected those with the highest EE% and DL%. After that, depending on PAMPA results, we selected those with the highest permeability and flux values to evaluate the release rate, permeation through the human nasal mucosa and in vivo permeability. Finally, we selected the promising formulation based on the in vivo pharmacokinetics results.

Table 3 Results of System Suitability (n = 6)

Parameter	FAV (323 nm)	USP Requirements	Result
Theoretical plates/meter	12722.12 ± 89.21	> 2000	Accepted
Tailing factor	0.87 ± 0.02	< 2	Accepted
RSD% (for t_R)	0.38	< 2	Accepted
RSD% (for AUC)	0.70	< 2	Accepted

Table 4 The Critical Parameters for the Selection of the Optimal Formulations and the Justification

Parameters	Target	Justification
Z-average	< 300 nm	It effects the pharmacokinetics (solubility, absorption, distribution), toxicity, stability, thus, the bioavailability and therapeutic effect. ^{79,80}
PDI	< 0.5	It reflects the homogeneous degree of the particles. The smallest PDI values, the more stable with lower aggregation and larger surface area, resulting in higher release rate. ^{81,82}
ZP	> \pm 30 mV	ZP is a predictive indicator of the kinetic stability of the vesicles, ^{83,84} and the ability to bypass the BBB and prevent the aggregation in blood circulation. ⁸⁵
EE% & DL%	EE% > 50% DL% > 5%	To ensure the efficiency of the drug carrier in improving the therapeutic effect and minimizing adverse effects. ⁸⁶
Release rate	> initial FAV	To ensure the improving in the solubility, thus, the improving in the absorption and pharmacokinetics of FAV.
Permeability rate (in vitro & in vivo)	> initial FAV	To improve the absorption through the nasal mucosa into the systemic circulation hence to CNS, resulting in increased the bioavailability and therapeutic effect.

Vesicle Size (Z-Average), Polydispersity Index (PDI) and Zeta Potential (ZP) Analysis

Table 5 shows the results of Z-average, PDI and ZP for the selected formulations (Z-average, PDI and ZP results of all formulations are presented in [Supplementary Table 1](#)). The results for FAV-ASPs showed that when the amount of AP was decreased, the vesicle size of the ASPs significantly increased (p-value < 0.0001). Furthermore, the vesicle size significantly increased with increasing CH amount (p-value < 0.0001). This result was similar to the findings of a previous study by Babar et al (2025), where they developed Acyclovir loaded aspasomal gel for transdermal delivery system. Their results revealed that the amount of AP and CH had a positive impact on Z-average.⁴⁰ CH intercalates in the bilayer with its polar head, and due to its hydrophobic properties, it occupies the interior portion of lipid bilayers and can fill the gaps. The nonionic surfactant-based FAV-ASP and FAV-NIO formulations showed that with the increase in Span®

Table 5 Z-Average, PDI and ZP of Selected Formulations. Results are Expressed as Means \pm SD (n = 3)

Formulation		Z-Average (nm)	PDI	ZP (mV)
Anionic surfactant-based FAV-ASPs	FAV-ASP1	283.20 \pm 1.51	0.31 \pm 0.01	-67.567 \pm 0.850
Nonionic surfactant-based FAV-ASPs	FAV-ASP8	292.06 \pm 2.10	0.36 \pm 0.03	-74.73 \pm 3.28
	FAV-ASP9	292.76 \pm 3.80	0.31 \pm 0.05	-73.16 \pm 4.65
	FAV-ASP10	284.60 \pm 6.71	0.29 \pm 0.06	-65.66 \pm 2.70
FAV-NIOs	FAV-NIO1	195.13 \pm 2.55	0.13 \pm 0.03	-51.70 \pm 2.49
	FAV-NIO2	194.55 \pm 2.18	0.18 \pm 0.04	-32.46 \pm 1.36
	FAV-NIO3	160.23 \pm 2.65	0.07 \pm 0.01	-28.43 \pm 2.42
	FAV-NIO4	272.75 \pm 0.71	0.38 \pm 0.02	-30.00 \pm 0.87
	FAV-NIO5	292.80 \pm 1.95	0.12 \pm 0.05	-31.63 \pm 1.42
	FAV-NIO6	274.30 \pm 1.37	0.13 \pm 0.05	-30.70 \pm 1.76
	FAV-NIO7	262.60 \pm 4.51	0.26 \pm 0.02	-11.34 \pm 2.41
	FAV-NIO8	180.70 \pm 1.61	0.12 \pm 0.04	-17.60 \pm 0.73
	FAV-NIO9	157.60 \pm 1.62	0.07 \pm 0.01	-27.20 \pm 0.26

60 amount, the Z-average significantly increased (p -value < 0.0001). This result was also in accord with a previous study by Mathure et al (2018). They developed Buspirone loaded niosomes for nose-to-brain delivery system. Their results revealed that Z-average increased by increasing Span® 60 amount from 20 to 40 mg.⁸⁷ Soni et al (2024) explained the effect of Span® 60 on Z-average by the high interfacial activity and a critical packing parameter between 0.5 and 1, where the lower value means tight packed vesicles, thus a smaller Z-average, while the further increase in Span® 60 amount led to an increase in Z-average due to increase CH amount to fill the gaps and counteract the effect of Span® 60 leading to higher rigidity of the Methotrexate loaded niosomes.⁸⁸

Anionic surfactant-based FAV-ASPs exhibited bigger vesicles, which could be attributed to the influence of DCP that had a negative charge, leading to an increase in the interbilayer distance and the surface area of the vesicles. Similar results obtained by Varshosaz et al (2003) for Insulin loaded niosomes.⁸⁹

Moreover, FAV-ASP formulations had a broad size distribution ($PDI > 0.3$). However, PDI values < 0.5 were reported to be acceptable.⁸¹ Whereas FAV-NIO formulations showed a significantly smaller particle size compared with FAV-ASP formulations (p -value < 0.0001), and a narrow size distribution ($PDI < 0.3$). The results of the prepared formulations showed an acceptably homogenous size distribution; this distribution may depend on the synthesis of mixed multi-lamellar and large unilamellar vesicles during the hydration stage, as reported in previous studies.^{42,72}

ZP is a predictive indicator of the intensity of repulsive and attractive forces between vesicles, which allows the evaluation of the vesicle stability. The formulations had negative values of ZP, which maintain electric repulsion. These negative values depended on the chemical properties of AP and CH, also because of the application of negatively charged lipids (anionic surfactant-based FAV-ASP formulations). These results agreed with data previously reported by Gopinath et al.³¹ According to these results, the produced FAV-ASPs and FAV-NIOs were physically stable, preventing vesicle aggregation, and they have a longer residence time inside the brain without being effluxed.⁹⁰

Z-average, PDI and ZP are critical parameters which could impact the release, transport through direct or indirect pathways, biodistribution and stability.^{91,92} As reported in the literature, nanoparticles with a Z-average of 150–300 nm were successfully taken up into the brain.⁷⁹ Accordingly, we selected the formulations with a Z-average < 300 nm for further investigations.

Determination of Drug Content, Encapsulation Efficiency (EE%) and Drug Loading (DL%)

The evaluation of the selected formulations (with a Z-average < 300 nm) indicating that FAV was successfully encapsulated into the vesicles with drug content ranged from 1.60 ± 0.36 mg to 1.85 ± 0.60 mg, and EE% values ranging between $41.01 \pm 1.07\%$ and $55.33 \pm 0.41\%$. Drug content of the selected formulations did not alter significantly with the compositions of the formulations (p -value > 0.05). The EE% of FAV-NIOs was varied, and it did not alter significantly with changing of CH amount (p -value > 0.05), and the same result was obtained by Gopinath et al,³¹ while increasing the ratio of Span® 60 to CH increased EE% (p -value < 0.01). This outcome might be explained by an increase in the rigidity of the NIO membrane as CH amount increased to fill the gaps and counteract the effect of Span® 60, leading to higher rigidity; thus, the membrane fluidity decreased.⁹³ El-Sayed et al (2017) studied the effect of CH amount on EE% of Flurbiprofen loaded niosomes, and the results revealed a significant increment in EE% upon increasing CH amount.⁹⁴ The results of FAV-ASPs demonstrated that nonionic surfactant-based FAV-ASPs had a significantly higher EE% compared to anionic surfactant-based FAV-ASPs (p -value < 0.0001), which could be related to the impact of using AP and Span® 60. Moreover, EE% increased significantly by increasing the amount of Span® 60 (p -value < 0.0001), or by increasing the amount of AP (p -value < 0.01), or by increasing both AP and Span® 60 amounts (p -value < 0.0001).

Most nanoparticle systems have relatively low drug loading (< 10 w%). It is critical to increase drug loading in order to improve the therapeutic effect and minimize adverse effects.⁹⁵ The nano-carrier system can be considered efficient if EE% $> 50\%$ and DL% $> 5\%$.⁸⁶ The results showed that using ASP and NIO formulations enhanced DL % of FAV (as shown in Figure 2). FAV-ASP8, FAV-ASP10 and FAV-NIO9 showed acceptable EE % ($> 50\%$), high DL % ($> 5\%$) and drug content. Accordingly, we selected these formulations for further investigation. The results of drug content, EE % and DL % of the selected formulations are presented in [Supplementary Table 2](#).

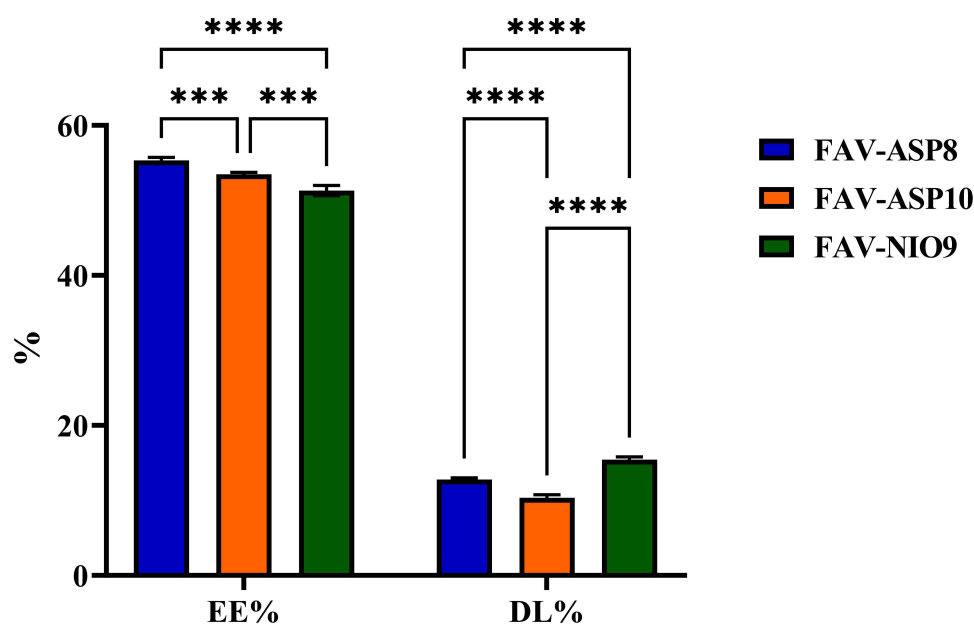


Figure 2 EE% and DL% results of FAV-ASP8, FAV-ASP10 and FAV-NIO9. Results are expressed as means \pm SD ($n = 3$), ***p-value < 0.001, ****p-value < 0.0001.

Residual Solvent Determination

Residual solvents are classified into four classes based on the toxicity level and the degree to which they can be considered as an environmental hazard. Both chloroform and methanol belong to Class II solvents; thus, their residual concentration should be less than 60 ppm and 3000 ppm, respectively, while ethanol belongs to Class III solvents (the accepted residual limit is 5000 ppm) in the daily dose of final product as a requirement of the International Council of Harmonisation (ICH) Q3C (R5) guideline for residual solvents. The results of GC measurement showed that the residual organic solvent contents were under LOD (less than 1 ppm for chloroform, methanol and ethanol), which supports that they were totally evaporated from the ASP and NIO vesicles during the film hydration method, ethanol injection method and freeze-drying.

In vitro Permeability Measurements

PAMPA is a cost-effective, relative, and reproducible technique for rapidly predicting passive transcellular transport,^{96,97} which is one of the absorption routes of lipophilic molecules through the nasal mucosa and BBB,^{98,99} so it is unable to give a complete description of the permeability via the BBB. However, PAMPA would be useful for choosing the most promising formulation, hence reducing in vitro and in vivo testing.¹⁰⁰

The BBB-PAMPA results showed that the formulations (FAV-ASP8, FAV-ASP10 and FAV-NIO9) had significantly higher permeability than pure FAV (Figure 3A). The addition of the surfactant agent to the formulations enhanced the solubility of FAV and increased its membrane permeability through BBB.⁸⁷ The effect of Span® 60 could also be observed in the flux values in the PAMPA study (Figure 3B). Based on these results, we selected FAV-ASP8 and FAV-NIO9 as optimal formulations due to the high permeability and flux values through the porcine brain polar lipid extract, high EE% and DL%. The results of the optimal formulations were summarized in Table 6.

Rapid Equilibrium Dialysis Measurement (RED)

RED assay was used to investigate the in vitro drug release of FAV from ASPs and NIOs vesicles at blood circulation conditions (DPBS, pH = 7.4). The incubation time of 4 h was sufficient for test formulations to reach equilibrium. The result showed that the dissolution rate of the optimal formulations was increased by approximately 3.5-fold compared to pure FAV (p-value < 0.0001), which could be related to the nanosized particles and the effect of AP and Span® 60. As shown in Figure 4, the amount released of FAV increased rapidly during the first hour, and the equilibrium state of the

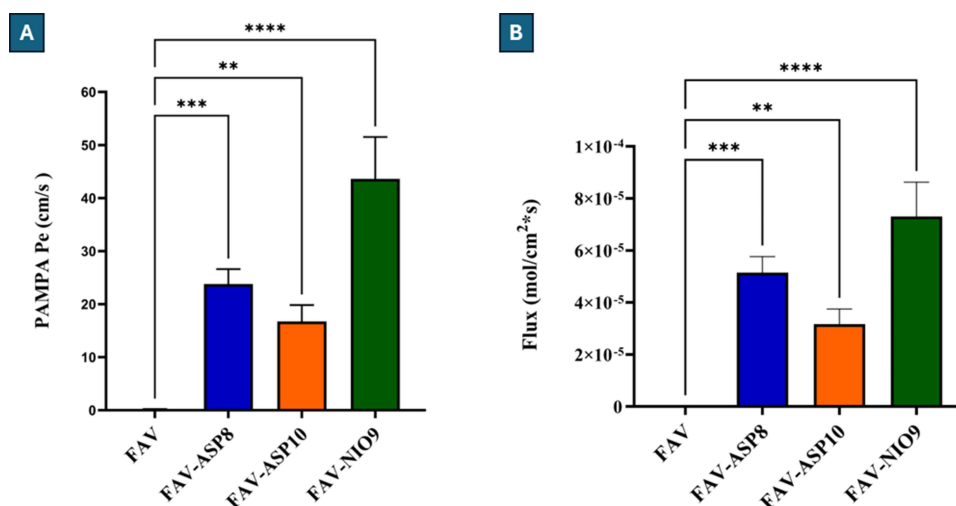


Figure 3 BBB-PAMPA results for FAV-ASP8, FAV-ASP10 and FAV-NIO9 in comparison with pure FAV. **(A):** permeability results, **(B):** flux results. Results are expressed as means \pm SD ($n = 6$), **p-value < 0.01, and ***p-value < 0.001, ****p-value < 0.0001.

formulations started after 2 h. This result could be related to the release of desorption FAV from the surface of the vesicles, followed by diffusion of FAV through the bilayers. Similar result obtained by Taymouri et al (2016).¹⁰¹

In vitro Drug Release Under Nasal Conditions

Figure 5 presents the cumulative in vitro release of FAV from the optimal formulations in SNES. The study indicated that all formulations had a significantly higher release rate than FAV suspension. FAV-ASP8 released $77.31 \pm 1.96\%$ of the loaded drug after 60 min (p-value < 0.001), whereas FAV-NIO9 released $57.01 \pm 1.22\%$ (p-value < 0.05), in comparison with pure FAV ($46.31 \pm 1.83\%$). AP is a more stable amphiphilic derivative of ascorbic acid. It reduces the surface tension, especially when integrated into a phospholipid monolayer.¹⁰² Therefore, the integration of AP with CH and Span® 60 could effect on the fluidity of the vesicle membrane resulting in higher release rate compared to NIOs. Moreover, AP is pH neutral, so the hydrolysis of AP at pH 5.6 is slow, which could impact FAV release by diffusion without affecting the vesicle membrane integrity. In addition, increasing Span® 60:CH ratio may improve the integrity of NIOs membrane and reduce the FAV leakage, resulting in less drug release from the vesicles compared to ASPs. The result indicated that the dialysis bag did not restrict the diffusion of FAV. Furthermore, the use of ASPs and NIOs as

Table 6 The Summarized Results of the Optimal Formulations

Optimal Formulations	FAV-ASP8				FAV-NIO9		
	FAV	AP	Span® 60	CH	FAV	Span® 60	CH
Amount (mg)	30	25	25	50	30	30	40
Z-average (nm)	292.06 ± 2.10				167.13 ± 1.60		
PDI	0.36 ± 0.03				0.07 ± 0.01		
ZP (mV)	-74.73 ± 3.28				-27.1 ± 1.24		
EE (%)	55.33 ± 0.41				51.30 ± 0.69		
DL (%)	12.79 ± 0.22				15.42 ± 0.38		
Pe (cm/s)	23.78 ± 2.84				43.64 ± 7.86		
Flux (mol/cm²*s)	51.47 ± 6.17				73.03 ± 7.61		

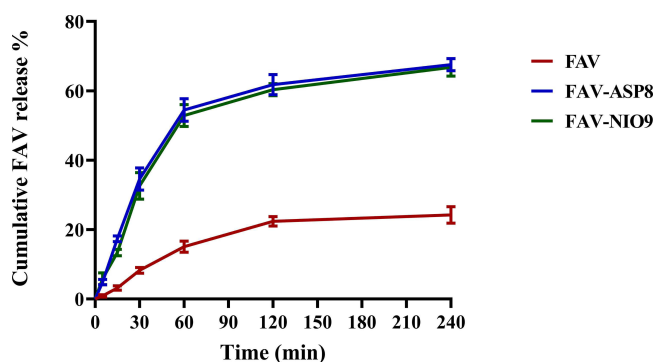


Figure 4 Rapid equilibrium dialysis (RED) of the optimal formulations in comparison with pure FAV. Results are expressed as means \pm SD ($n = 6$).

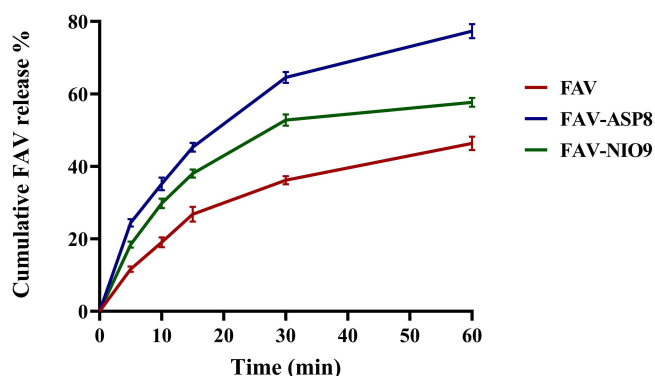


Figure 5 Cumulative in vitro release profile of the optimal formulations compared to pure FAV. Results are expressed as means \pm SD ($n = 3$).

carriers enhanced the encapsulation of FAV and increased the release rate due to the small particle size of the carrier, which increased the surface area and its hydrophilic properties.

In vitro Drug Release Data Evaluation

The release kinetics of the optimal formulations were statically compared with pure FAV using DDSolver®. The results showed that FAV-ASP8 had the highest AUC and DE values (Table 7). The AUC and DE values of all the optimal formulations were significantly higher than the AUC value of pure FAV. Moreover, the MDT values of FAV-ASP8 were significantly lower than those of pure FAV, which means a faster release rate in comparison to pure FAV and FAV-NIO9, which could increase the absorption through the nasal cavity.^{103,104}

The model with the highest R^2 , the smallest AIC, and the highest MSC values is the best kinetics model.^{50,51,105} The release profiles of the optimal formulations were fitted Korsmeyer-Peppas kinetic model. The release exponent “ n ” values of FAV-ASP8 and FAV-NIO9 were 0.44 ± 0.01 and 0.38 ± 0.01 , respectively, which refers to a quasi-Fickian diffusion ($n < 0.45$)^{50,106} (Supplementary Table 3).

Table 7 Comparison of Release Profiles Using Model-Independent Approaches. Results are Expressed as Means \pm SD ($n = 3$)

Sample	AUC ($\mu\text{g min/mL}$)	DE (%)	MDT (min)
FAV	1922.26 ± 62.97	0.32 ± 0.01	18.48 ± 0.50
FAV-ASP8	3354.79 ± 49.43^b	0.55 ± 0.01^b	16.60 ± 0.45^a
FAV-NIO9	2639.32 ± 14.75^b	0.43 ± 0.002^b	60.16 ± 80.26^b

Notes: ^ap-value < 0.001. ^bp-value < 0.0001.

Storage Stability

The stability test is important for the evaluation of the ability of the vesicles to resist environmental conditions, such as temperature, and for the protection of the drug from degradation, thus determining the recommended storage conditions and the retest period for the drug. The stability results for the optimal formulations showed that there was a decrease in Z-average value after 4 weeks (p-value < 0.0001) in case of FAV-ASP8, which can be explained by the change of mean intensity distribution of the size (Z-average is calculated by the intensity of the particle),¹⁰⁷ and the effect of AP as antioxidant which prevents the oxidative degradation of lipid bilayer. However, FAV-NIO9 showed a significant increase in Z-average value (p-value < 0.0001), presumably because of the aggregation of NIOs over time due to attractive forces (Van der Waals forces) or electrostatic interactions (repulsive forces). Moreover, the evaluation of PDI for FAV-ASP8 and FAV-NIO9 showed a non-significant increase, and both formulations maintained acceptably homogenous size distribution. The evaluation of ZP over time showed that FAV-ASP8 had a non-significant change in ZP, while FAV-NIO9 exhibited a decrease in ZP (non-significant), indicating a higher possibility to aggregate over time.¹⁰⁸ Furthermore, the six hydroxyl groups of mannitol can form hydrogen bonds with FAV (using the hydroxyl and carboxamide groups), which could impact the crystallization of mannitol and form a partially amorphous state. The amorphous state is less chemical stability and more hygroscopic.^{109,110} Therefore, hydrolysis or oxidative degradation could occur over time. FAV-NIO9 showed a higher reduction of FAV concentration compared to FAV-ASP8. Thus, we can conclude that FAV-ASP8 had a higher stability than FAV-NIO9 ([Supplementary Figures 1–4](#)).

Droplet Size Distribution Measurement

Targeting the CNS requires particle deposition in the posterior region of the nasal cavity (to reach the olfactory and trigeminal nerves).¹¹¹ The deposition depends on many factors, including the interaction of the spray device with the nose (the angle of insertion and the plume angle),¹¹² nasal cavity (the mucociliary clearance mechanism and the human variabilities),¹¹³ and the formulation characteristics (droplet size, viscosity, elasticity).¹¹⁴

US FDA and EMA recommended the droplet size distribution measurement as an indicator of in vitro bioavailability for the liquid nasal formulation.^{113,114} The nasal spray is recommended to be placed 3 cm below the receiving lens,¹¹³ with an application angle of 45°. A study by Jüptner et al (2025) demonstrated a more posterior deposition profile for 45° compared to 60° due to increased deposition in the turbinate region, and the overall nasal deposition was excellent at ~98%, with minimal loss from the nose.¹¹¹

The recommended droplet size ranges between 20 to around 200 µm.¹¹² Droplets with Dv50 < 10 µm can be inhaled through the nasopharynx and reach the lungs,¹¹⁵ or deposited in the anterior region of the nasal cavity which enhances formulation clearance from the nasal cavity.¹¹³

The results demonstrated that FAV-ASP8 and FAV-NIO9 were suitable for nasal administration (Dv50 values were 174.80 ± 12.08 and 89.05 ± 7.33 µm, respectively), which indicates a more posterior deposition, thus, increasing the absorption through the nasal cavity.

FAV-ASP8 showed a significantly higher Dv50 values compared to FAV-NIO9 (p-value < 0.01), which could be attributed to the effect of AP and Span® 60. Span® 60, as a non-ionic surfactant, reduced the interfacial tension and facilitated the formation of smaller droplets (FAV-NIO9),¹¹⁴ while the incorporation of AP could counteract the effect of Span® 60 leading to larger droplets (FAV-ASP8). Moreover, FAV-ASP8 and FAV-NIO9 showed small Span values (no significant differences), indicating a narrow width of droplet size distribution¹¹⁶ ([Table 8](#)).

Table 8 Droplet Size Distribution of the Optimal Formulations. Results are Presented as Means ± SD (n = 3)

Formulation	Dv10 (µm)	Dv50 (µm)	Dv90 (µm)	Span (µm)
FAV-ASP8	61.07 ± 6.23	174.80 ± 12.08	500.50 ± 65.80	2.02 ± 0.86
FAV-NIO9	42.10 ± 2.99	89.05 ± 7.33	257.20 ± 76.47	2.37 ± 0.67

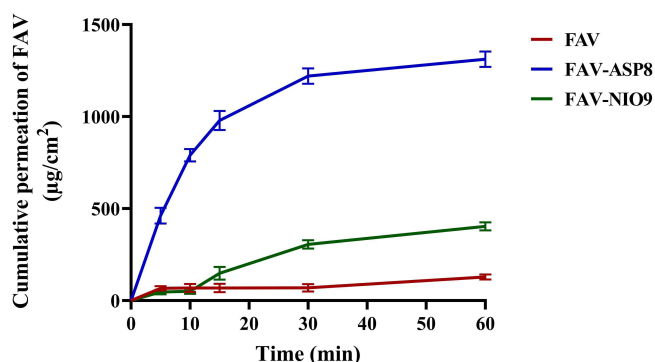


Figure 6 Ex vivo permeability study of FAV-ASP8 and FAV-NIO9 in comparison with pure FAV. Results are expressed as means \pm SD ($n = 3$).

Ex vivo Nasal Diffusion Study on Human Nasal Mucosa

The transmucosal permeability measurement of the optimal formulations in comparison with pure FAV was performed using human nasal mucosa. The study showed that both FAV-ASP8 and FAV-NIO9 had a higher amount of FAV diffused through the human nasal mucosa to the acceptor chamber within 60 min ($1311.74 \pm 41.70 \mu\text{g}/\text{cm}^2$ and $402.94 \pm 22.32 \mu\text{g}/\text{cm}^2$, respectively) compared to pure FAV ($128.17 \pm 13.64 \mu\text{g}/\text{cm}^2$, $p\text{-value} < 0.0001$), which means an enhancement in the absorption and permeation through the nasal mucosa (Figure 6). These results could be attributed to the nanosized particles (particle sizes < 500 nm can pass through the aqueous, non-viscous holes of the mucin network, resulting in higher mucosal penetration and absorption into the mucosal cells), negative ZP value (avoid slow penetration by limiting adherence to the negatively charged membrane), in addition to the effect of vesicles components.¹¹⁷ Furthermore, FAV suspension has high fluidity and negligible mucosal adherence.³⁸ As a result of the shorter contact time with the nasal mucosa, FAV suspension has a lower permeability.

Moreover, FAV-ASP8 showed a significantly higher permeability compared to FAV-NIO9 ($p\text{-value} < 0.0001$), which could be attributed to the surfactant-like property of AP (like sorbitan derivatives), Its lipophilic properties which enhance the tissue penetration, and its deformability which allowed ASPs to bypass through the tight junctions of the nasal cavity. D'Avanzo et al (2022) evaluated the permeation profile of Idebenone/Naproxen co-loaded aspasomes by human stratum corneum and viable epidermis (SCE) membrane, and the results demonstrated enhancement in the permeability due to the impact of AP.⁴²

Table 9 summarizes the biopharmaceutical parameters, including permeation and prediction parameters. FAV-ASP8 had higher steady-state flux (J_{ss}), permeability coefficient (K_p) and theoretical plasma concentration at the steady-state in humans compared to FAV-NIO9 and pure FAV.

In vivo Study

Pharmacokinetic Parameters

FAV has a low solubility in water ($8.7 \text{ mg}/\text{mL}$) and a low CNS permeability, which could be attributed to the low passive permeability due to its three H-bonding donors.²⁵ The capacity of FAV-ASP8 and FAV-NIO9 to deliver FAV to the CNS via the intranasal route was evaluated using Sprague–Dawley rats.

Table 9 The Biopharmaceutical Parameters of the Formulations are Compared to the Initial FAV. Results are Expressed as Means \pm SD ($n = 3$)

Sample	Flux ($\mu\text{g}/\text{cm}^2/\text{h}$)	K_p (cm/h)	ER	C_{ss} ($\mu\text{g}/\text{mL}$)
FAV	2.13 ± 0.06	$0.002 \pm 7.12 \times 10^{-5}$	–	0.32 ± 0.01
FAV-ASP8	21.86 ± 0.02^a	$0.011 \pm 1.45 \times 10^{-5a}$	10.23 ± 0.28^a	3.35 ± 0.01^a
FAV-NIO9	6.71 ± 0.03^a	$0.004 \pm 1.95 \times 10^{-5a}$	3.14 ± 0.07^a	1.03 ± 2.31^a

Note: ^a $p\text{-value} < 0.0001$.

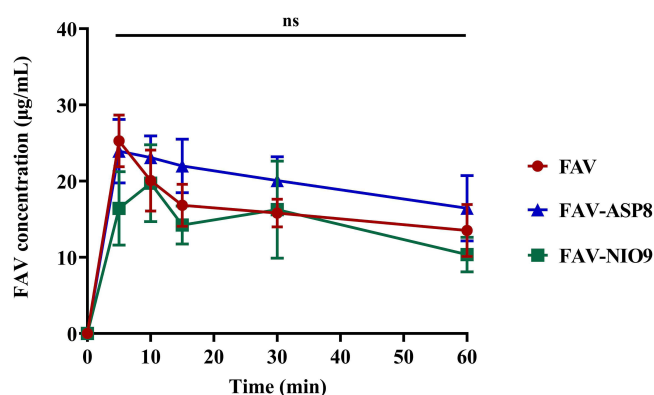


Figure 7 Plasma concentration–time profile after nasal administration of FAV-ASP8, FAV-NIO9 and pure FAV in rats. Results are expressed as means \pm SD ($n = 4$), (ns) means non-significant.

The average plasma drug concentration–time curves after a single nasal dose of pure FAV, FAV-ASP8 and FAV-NIO9 are demonstrated in Figure 7. FAV was detected and reached a plasma concentration peak (C_{\max}) of 26.24 ± 7.382 , 27.03 ± 6.88 , and 20.32 ± 11.08 $\mu\text{g/mL}$ at 7.5 ± 2.88 , 7.5 ± 2.88 , and 10 ± 4.08 min (T_{\max}) after the administration of pure FAV, FAV-ASP8 and FAV-NIO9, respectively. These results indicate that the nasal mucosa effectively and rapidly transports FAV into the systemic circulation. In addition, FAV-ASP8 showed the highest $t_{1/2}$ value (226.42 ± 337.06 min) compared to pure FAV and FAV-NIO9. This could be related to the use of AP to prepare the drug carrier, which may reduce the elimination rate and thus extend the duration in the systemic circulation (C_L value was 0.79 ± 0.56 mL/min). The relative bioavailability ($F\%$) values of FAV-ASP8 and FAV-NIO9 were $124.53 \pm 35.33\%$ and $85.28 \pm 33.24\%$, respectively (Table 10).

Due to restrictions in CNS tissue access, CSF drug concentrations are used as an alternative for CNS tissue delivery, with the hypothesis that there is a direct, though not absolute, link between CSF and CNS tissue penetration.¹¹⁸ Furthermore, the olfactory nerves in the nasal cavity provide additional link with the CSF in the subarachnoid space through the interstitial fluid surrounding the olfactory nerve bundle.^{119,120} In our study, FAV was detected in the CSF samples (Figure 8). The evaluation of CSF samples showed a significant elevation of FAV concentration into CSF after 1 hour of nasal administration of FAV-ASP8 compared to FAV suspension (* p -value < 0.05) and FAV-NIO9 (** p -value < 0.001), while there was no significant increase in the case of FAV-NIO9 compared to FAV suspension. These results can be attributed to an increase in the extent of drug

Table 10 Pharmacokinetic (PK) Parameters of Pure FAV, FAV-ASP8, and FAV-NIO9 Obtained After Non-Compartmental Analysis Using PK Solver Software. Results are Expressed as Means \pm SD ($n = 4$)

PK Parameters	FAV	FAV-ASP8	FAV-NIO9
C_{\max} ($\mu\text{g/mL}$)	26.24 ± 7.38	27.03 ± 6.88	20.32 ± 11.08
T_{\max} (min)	7.50 ± 2.88	7.50 ± 2.88	10.00 ± 4.08
k_e (min^{-1})	0.007 ± 0.01	0.009 ± 0.005	0.01 ± 0.01
$t_{1/2}$ (min)	127.54 ± 103.60	226.42 ± 337.06	94.33 ± 70.07
AUC_{0-t} ($\mu\text{g} \times \text{min/mL}$)	953.56 ± 282.31	1153.01 ± 364.87	792.76 ± 384.97
$AUC_{0-\infty}$ ($\mu\text{g} \times \text{min/mL}$)	4134.94 ± 4133.03	$9305.40 \pm 14,438.56$	2039.36 ± 764.72
C_L (mL/min)	0.88 ± 0.62	0.79 ± 0.56	1.10 ± 0.43
V_d (mL)	104.57 ± 27.35	80.55 ± 19.01	130.90 ± 68.02
MRT (min)	185.23 ± 153.68	329.96 ± 486.03	139.13 ± 97.91
F (%)	–	124.53 ± 35.33	85.28 ± 33.24

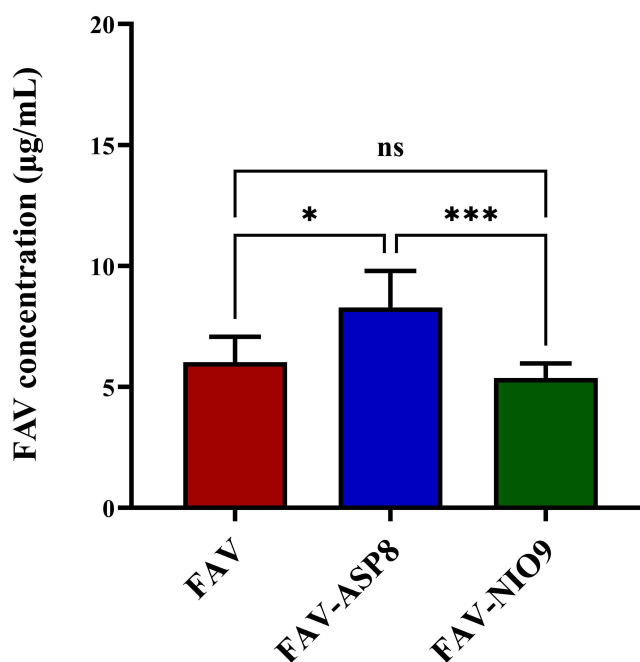


Figure 8 The concentration of FAV in cerebrospinal fluid (CSF) after 1 hour of nasal administration. Results are expressed as means \pm SD ($n = 4$), (ns) means non-significant, * p -value < 0.05 , *** p -value < 0.001 .

absorption through the nasal mucosa (olfactory nerves) due to the physical parameter, the lipophilicity nature of the vesicles and the presence of a permeation enhancer (Span® 60), which improves the membrane penetration. Furthermore, AP can overcome biological barriers, enter the brain¹²¹ and resist hydrolysis,¹²² thereby preventing the degradation of FAV. According to the chemical structure of FAV, amide hydrolysis and oxidation are the potential major degradation pathways.¹²³

Abou-Taleb et al (2018) developed Nefopam loaded niosomes for intranasal administration using CH:Span® 80 (1:1.85 molar ratio). Their study illustrated a 4.77-fold increase in bioavailability compared with oral solution of drug.⁶¹ Moreover, Ammar et al (2017) developed Diltiazem loaded niosomes using CH:Span® 60 (1:1 molar ratio), which showed the highest EE% and release rate. The in vivo study on male Wistar rats showed an increase in MRT, $t_{1/2}$ and AUC with a decrease in K_e .¹²⁴

Due to the lipophilic nature of AP, it can easily bypass phospholipid bilayers of membranes, especially neuronal ones and BBB.^{121,125,126} AP has been used in nasal formulations as a cross-linker, as reported by J. Varshosaz et al (2004). They developed insulin chitosan microspheres by emulsification-cross linking process using ascorbic acid or ascorbyl palmitate as a cross-linker. The formulation consists of 400 mg of chitosan and 70 mg of AP showed a 67% reduction of blood glucose compared to IV route.¹²⁷

Evaluation of in vitro–in vivo Correlations (IVIVC)

IVIVC is a useful tool to predict the in vivo performance of FAV based on its in vitro data. Figure 9 demonstrates the IVIVC graphs for the comparison of AUC_{0-t} values between the in vitro release and the in vivo PK data. The correlation coefficient (R^2) values were 0.971, 0.982, and 0.903 for pure FAV, FAV-ASP8, and FAV-NIO9, respectively. Furthermore, R^2 values obtained from IVIVC graphs for the comparison of AUC_{0-t} values between the in vitro permeation and the in vivo PK data (Figure 10) showed a good point-to-point correlation (0.977, 0.992, and 0.839 for pure FAV, FAV-ASP8, and FAV-NIO9, respectively). This result indicates that the use of in vitro release and permeation data to establish the IVIVC could be useful in predicting the in vivo properties of the formulations.

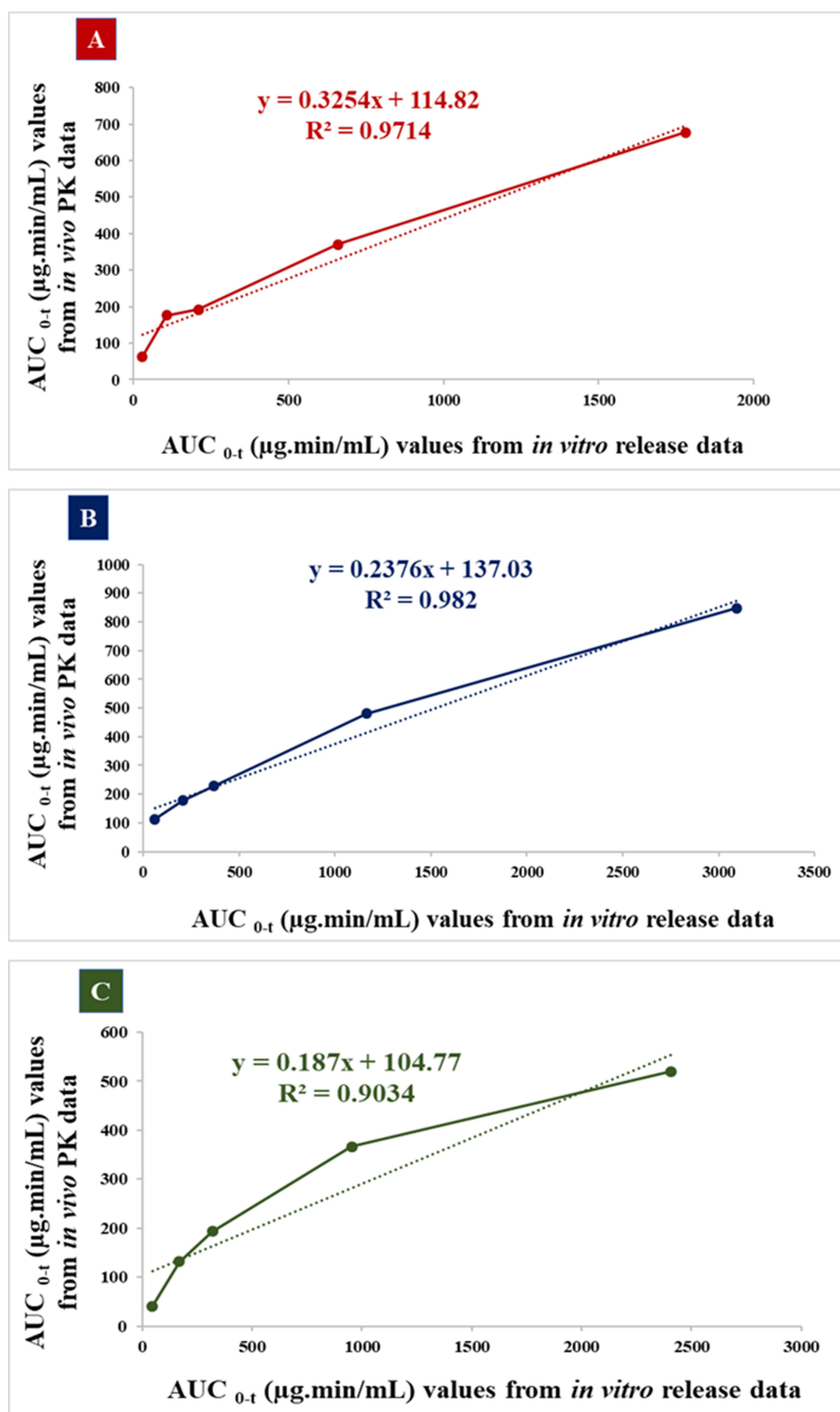


Figure 9 IVIVC graphs for the comparison of AUC_{0-t} values between the in vitro release and the in vivo PK data. Where **(A)**: IVIVC for pure FAV, **(B)**: IVIVC for FAV-ASP8, and **(C)**: IVIVC for FAV-NIO9.

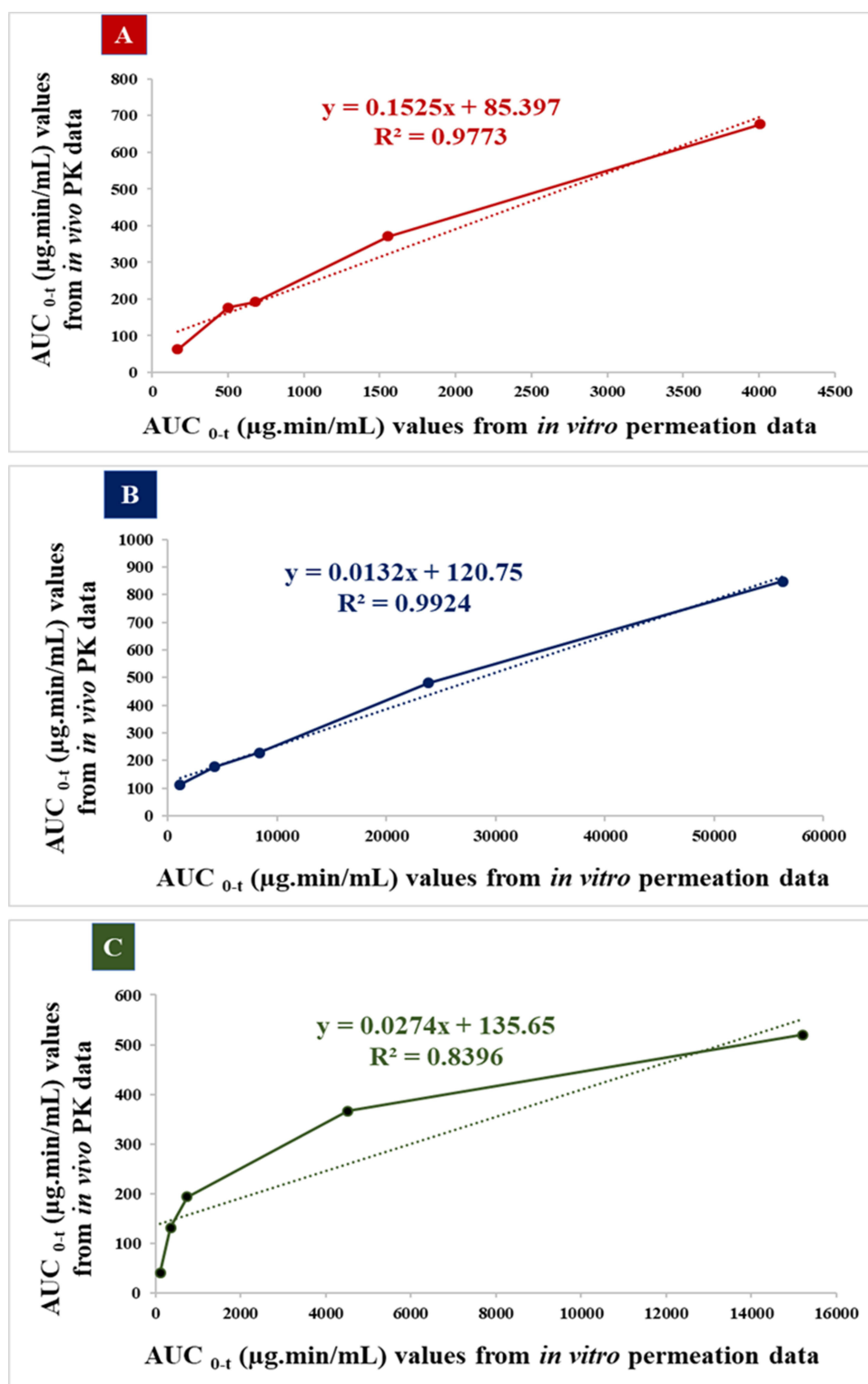


Figure 10 IVIVC graphs for the comparison of AUC_{0-t} values between the *in vitro* permeation and the *in vivo* PK data. (A): IVIVC for pure FAV, (B): IVIVC for FAV-ASP8, and (C): IVIVC for FAV-NIO9.

Conclusion

In the present study, ASP and NIO formulations have been developed as promising intranasal delivery systems for FAV to enhance its bioavailability. The optimized formulation FAV-ASP8 (consisting of FAV:AP:Span® 60:CH in 30:25:25:50 w/w ratio) can encapsulate FAV inside ASP vesicles with an encapsulation efficiency of $55.33 \pm 0.41\%$ drug loading of $12.79 \pm 0.22\%$. The formulation showed a small particle size (292.06 ± 2.10 nm), a narrow PDI value (0.36 ± 0.03) and negative values of ZP (-74.73 ± 3.28 mV), indicating a high physical stability for FAV-ASP8. The other optimized formulation, FAV-NIO9 contained FAV, Span® 60 and CH in 30:30:40 w/w ratio with a Z-average value of 167.13 ± 1.60 nm, a narrow PDI value (0.07 ± 0.01), adequate ZP (-27.1 ± 1.24 mV), acceptable encapsulation efficiency ($51.30 \pm 0.69\%$) and advantageous drug loading ($15.42 \pm 0.38\%$).

FAV-ASP8 and FAV-NIO9 formulations enhanced the solubility of FAV, elevated its membrane permeability through BBB, and increased its release under both nasal (pH = 5.6) and blood circulation conditions (pH = 7.4), with Dv50 values ranged between 20 and 200 μ m. The ex vivo study showed that FAV-ASP8 had a higher amount of FAV diffused through the human nasal mucosa than FAV-NIO9 and pure FAV. The in vivo study indicated that there was no significant difference in plasma concentrations for the optimal formulations in comparison to pure FAV. However, only FAV-ASP8 had higher CSF concentrations than FAV-NIO9 and pure FAV after a single intranasal dose. IVIVC showed a good point-to-point correlation between the in vitro and the in vivo PK data.

These encouraging results suggest that ASPs could be promising intranasal delivery systems for hydrophobic drugs to enhance solubility, avoid first-pass metabolism, and decrease systemic adverse effects.

Data Sharing Statement

The datasets generated during and/or analyzed during the current study are available from the corresponding author on reasonable request.

Author Contributions

All authors made a significant contribution to the work reported, whether that is in the conception, study design, execution, acquisition of data, analysis, and interpretation, or all these areas; took part in drafting, revising, or critically reviewing the article; gave final approval of the version to be published; agreed on the journal to which the article has been submitted; and agree to be accountable for all aspects of the work.

Funding

The publication was funded by The University of Szeged Open Access Fund (FundRef, Grant No. 7468). This work was supported by Project no. TKP2021-EGA-32 implemented with support provided by the Ministry of Culture and Innovation of Hungary from the National Research, Development and Innovation Fund, financed under the TKP2021-EGA funding scheme.

Disclosure

The authors report no conflicts of interest in this work.

References

1. Vazquez C, Jurado KA. Neurotropic RNA Virus Modulation of Immune Responses within the Central Nervous System. *International Journal of Molecular Sciences*. 2022;23(7):4018. doi:10.3390/ijms23074018
2. Salinas S, Funk KE. Editorial: cellular and: molecular Mechanisms of Neurotropic Viral Infection. *Front Cell Neurosci*. 2024;18:1365755. doi:10.3389/fncel.2024.1365755
3. Klein RS, Garber C, Funk KE, et al. Neuroinflammation During RNA Viral Infections. *Annu Rev Immunol*. 2019;37(1):73–95. doi:10.1146/annurev-immunol-042718-041417
4. Yachou Y, El Idrissi A, Belapasov V, Ait Benali S. Neuroinvasion, Neurotropic, and Neuroinflammatory Events of SARS-CoV-2: understanding the Neurological Manifestations in COVID-19 Patients. *Neurol Sci*. 2020;41(10):2657. doi:10.1007/s10072-020-04575-3
5. Sun M, Manson ML, Guo T, De Lange ECM. CNS Viral Infections-What to Consider for Improving Drug Treatment: a Plea for Using Mathematical Modeling Approaches. *CNS Drugs*. 2024;38:349–373. doi:10.1007/s40263-024-01082-3
6. Wongchitrat P, Chanmee T, Govitrapong P. Molecular Mechanisms Associated with Neurodegeneration of Neurotropic Viral Infection. *Mol Neurobiol*. 2024;61(5):2881–2903. doi:10.1007/s12035-023-03761-6
7. Zhao YJ, Xu KF, Shu FX, Zhang F. Neurotropic Virus Infection and Neurodegenerative Diseases: potential Roles of Autophagy Pathway. *CNS Neurosci Ther*. 2024;30:6. doi:10.1111/CNS.14548

8. Rinaldi F, Hanieh P, Chan L, et al. Chitosan Glutamate-Coated Niosomes: a Proposal for Nose-to-Brain Delivery. *Pharmaceutics*. 2018;10(2):38. doi:10.3390/pharmaceutics10020038
9. Djupesland PG, Messina JC, Mahmoud RA. The Nasal Approach to Delivering Treatment for Brain Diseases: an Anatomic, Physiologic, and Delivery Technology Overview. *Ther Deliv*. 2014;5(6):709–733. doi:10.4155/TDE.14.41
10. Martins PP, Smyth HDC, Cui Z. Strategies to Facilitate or Block Nose-to-Brain Drug Delivery. *Int J Pharm*. 2019;570:118635. doi:10.1016/J.IJPHARM.2019.118635
11. Higgins TS, Wu AW, Illing EA, et al. Intranasal Antiviral Drug Delivery and Coronavirus Disease 2019 (COVID-19): a State of the Art Review. *Otolaryngol Head Neck Surg*. 2020;163(4):682–694. doi:10.1177/0194599820933170
12. Delshadi R, Bahrami A, McClements DJ, Moore MD, Williams L. Development of Nanoparticle-Delivery Systems for Antiviral Agents: a Review. *J Control Release*. 2021;331:30–44. doi:10.1016/J.JCONREL.2021.01.017
13. Konstantinova ID, Andronova VL, Fateev IV, Esipov RS. Favipiravir and Its Structural Analogs: antiviral Activity and Synthesis Methods. *Acta Naturae*. 2022;14(2):16–38. doi:10.32607/actanaturae.11652
14. Al-Horani RA, Kar S. Potential Anti-SARS-CoV-2 Therapeutics That Target the Post-Entry Stages of the Viral Life Cycle: a Comprehensive Review. *Viruses*. 2020;12:10. doi:10.3390/V12101092
15. Shiraki K, Daikoku T. Favipiravir, an Anti-Influenza Drug against Life-Threatening RNA Virus Infections. *Pharmacol Ther*. 2020;209:107512. doi:10.1016/j.pharmthera.2020.107512
16. Furuta Y, Komeno T, Nakamura T. Favipiravir (T-705), a Broad Spectrum Inhibitor of Viral RNA Polymerase. *Proceedings Japan Academy Ser B: Physical and Biological Sciences*. 2017;93(7):449–463. doi:10.2183/pjab.93.027
17. Borbone N, Piccialli G, Roviello GN, Oliviero G. Nucleoside Analogs and Nucleoside Precursors as Drugs in the Fight against SARS-CoV-2 and Other Coronaviruses. *Molecules*. 2021;26(4):986. doi:10.3390/molecules26040986
18. Rattanaumpawan P, Jirajariyavej S, Lerdlamyong K, Palavutitotai N, Saiyarin J. Real-World Effectiveness and Optimal Dosage of Favipiravir for Treatment of COVID-19: results from a Multicenter Observational Study in Thailand. *Antibiotics*. 2022;11(6):805. doi:10.3390/ANTIBIOTICS11060805
19. Sajadian SA, Ardestani NS, Esfandiari N, Askarizadeh M, Jouyban A. Solubility of Favipiravir (as an Anti-COVID-19) in Supercritical Carbon Dioxide: an Experimental Analysis and Thermodynamic Modeling. *J Supercrit Fluids*. 2022;183:105539. doi:10.1016/J.SUPFLU.2022.105539
20. Hayden FG, Lenk RP, Epstein C, Kang LL. Oral Favipiravir Exposure and Pharmacodynamic Effects in Adult Outpatients With Acute Influenza. *J Infect Dis*. 2024;230(2):e395–e404. doi:10.1093/INFDIS/JIAD409
21. Du Y, Chen X. Favipiravir: pharmacokinetics and Concerns About Clinical Trials for 2019-nCoV Infection. *Clin Pharmacol Ther*. 2020;108(2):242–247. doi:10.1002/cpt.1844
22. Almutairi AO, El-Readi MZ, Althubiti M, et al. Liver Injury in Favipiravir-Treated COVID-19 Patients: retrospective Single-Center Cohort Study. *Trop Med Infect Dis*. 2023;8(2). doi:10.3390/TROPICALMED8020129
23. Pires A, Fortuna A, Alves G, Falcão A. Intranasal Drug Delivery: how, Why and What For? *J Pharm Pharm Sci*. 2009;12(3):288. doi:10.18433/J3NC79
24. Erdő F, Bors LA, Farkas D, Bajza Á, Gizurarson S. Evaluation of Intranasal Delivery Route of Drug Administration for Brain Targeting. *Brain Res Bull*. 2018;143:155–170. doi:10.1016/j.brainresbull.2018.10.009
25. Rong J, Zhao C, Xia X, et al. Evaluation of [18F]Favipiravir in Rodents and Nonhuman Primates (NHP) with Positron Emission Tomography. *Pharmaceutics*. 2023;16(4):524. doi:10.3390/ph16040524
26. Khan MS, Baskoy SA, Yang C, et al. Lipid-Based Colloidal Nanoparticles for Applications in Targeted Vaccine Delivery. *Nanoscale Adv*. 2023;5(7):1853. doi:10.1039/D2NA00795A
27. Xincheng Y, Jing T, Jiaoqiong G. Lipid-Based Nanoparticles via Nose-to-Brain Delivery: a Mini Review. *Front Cell Dev Biol*. 2023;11:1214450. doi:10.3389/FCELL.2023.1214450/FULL
28. Battaglia L, Panciani PP, Muntoni E, et al. Lipid Nanoparticles for Intranasal Administration: application to Nose-to-Brain Delivery. *Expert Opin Drug Deliv*. 2018;15(4):369–378. doi:10.1080/17425247.2018.1429401
29. Rajera R, Nagpal K, Singh SK, Mishra DN. Niosomes: a Controlled and Novel Drug Delivery System. *Biol Pharm Bull*. 2011;34(7):945–953. doi:10.1248/bpb.34.945
30. Marianecci C, Di Marzio L, Rinaldi F, et al. Niosomes from 80s to Present: the State of the Art. *Adv Colloid Interface Sci*. 2014;205:187–206. doi:10.1016/j.cis.2013.11.018
31. Gopinath D, Ravi D, Rao BR, Apte SS, Renuka D, Rambhau D. Ascorbyl Palmitate Vesicles (Aspasomes): formation, Characterization and Applications. *Int J Pharm*. 2004;271(1–2):95–113. doi:10.1016/j.ijpharm.2003.10.032
32. Moribe K, Limwikrant W, Higashi K, Yamamoto K. Drug Nanoparticle Formulation Using Ascorbic Acid Derivatives. *J Drug Deliv*. 2011;2011:1–9. doi:10.1155/2011/138929
33. Palma S, Manzo R, Lo Nostro P, Allemanni D. Nanostructures from Alkyl Vitamin C Derivatives (ASCn): properties and Potential Platform for Drug Delivery. *Int J Pharm*. 2007;345(1–2):26–34. doi:10.1016/J.IJPHARM.2007.09.014
34. Khalil RM, Abdelbary A, Arini SKE, Basha M, El-Hashemy HA, Farouk F. Development of Tizanidine Loaded Aspasomes as Transdermal Delivery System: ex-vivo and in-vivo Evaluation. *J Liposome Res*. 2021;31(1):19–29. doi:10.1080/08982104.2019.1684940
35. Han S. Structure of Ascorbyl Palmitate Bilayers (Aspasomes) from Molecular Dynamics Simulation. *Bull Korean Chem Soc*. 2018;39(7):887–890. doi:10.1002/BKCS.11475
36. Wong SN, Li S, Low KH, et al. Development of Favipiravir Dry Powders for Intranasal Delivery: an Integrated Cocrystal and Particle Engineering Approach via Spray Freeze Drying. *Int J Pharm*. 2024;653:123896. doi:10.1016/J.IJPHARM.2024.123896
37. Darne P, Vidhate S, Shintre S, et al. Advancements in Antiviral Therapy: favipiravir Sodium in Nasal Formulation. *AAPS Pharm Sci Tech*. 2024;25(8):1–15. doi:10.1208/S12249-024-02986-5/TABLES/4
38. Gattani V, Dawre S. Development of Favipiravir Loaded PLGA Nanoparticles Entrapped in In-Situ Gel for Treatment of Covid-19 via Nasal Route. *J Drug Deliv Sci Technol*. 2023;79:104082. doi:10.1016/j.jddst.2022.104082
39. Alcantara KP, Nalinratana N, Chutiwitoonchai N, et al. Enhanced Nasal Deposition and Anti-Coronavirus Effect of Favipiravir-Loaded Mucoadhesive Chitosan–Alginate Nanoparticles. *Pharmaceutics*. 2022;14(12):2680. doi:10.3390/PHARMACEUTICS14122680/S1
40. Vimalakar Babar A, Prasanna Sutar K, Vijay Usulkar S. S121–S131. Formulation and Evaluation of Acyclovir Loaded Aspasomal Gel for Effective Management of Herpes. *Indian J Pharm Educ Res*. 2025;59(1s). doi:10.5530/ijper.20254263

41. Kar M, Saquib M, Jain DK. Formulation Development and Evaluation of Aspasomes Containing Skin Whitening Agent. *Manipal J Pharma Sci.* 2020; 6(1):47–53.
42. d'Avanzo N, Cristiano MC, Di Marzio L, et al. Multidrug Idebenone/Naproxen Co-Loaded Aspasomes for Significant in vivo Anti-Inflammatory Activity. *ChemMedChem.* 2022;17(9):e202200067. doi:10.1002/CMDC.202200067
43. Sita VG, Jadhav D, Vavia P. Niosomes for Nose-to-Brain Delivery of Bromocriptine: formulation Development, Efficacy Evaluation and Toxicity Profiling. *J Drug Deliv Sci Technol.* 2020;58:101791. doi:10.1016/J.JDDST.2020.101791
44. Tavano L, Muzzalupo R, Trombino S, Cassano R, Pingitore A, Picci N. Effect of Formulations Variables on the in vitro Percutaneous Permeation of Sodium Diclofenac from New Vesicular Systems Obtained from Pluronic Triblock Copolymers. *Colloids Surf B Biointerfaces.* 2010;79(1):227–234. doi:10.1016/j.colsurfb.2010.03.055
45. Peng W, Jiang XY, Zhu Y, et al. Oral Delivery of Capsaicin Using MPEG-PCL Nanoparticles. *Acta Pharmacol Sin.* 2015;36(1):139–148. doi:10.1038/APS.2014.113
46. Katona G, Balogh GT, Dargó G, et al. Development of Meloxicam-Human Serum Albumin Nanoparticles for Nose-to-Brain Delivery via Application of a Quality by Design Approach. *Pharmaceutics.* 2020;12(2):97. doi:10.3390/pharmaceutics12020097
47. Nigam K, Kaur A, Tyagi A, et al. Nose-to-Brain Delivery of Lamotrigine-Loaded PLGA Nanoparticles. *Drug Deliv Transl Res.* 2019;9(5):879–890. doi:10.1007/s13346-019-00622-5
48. Zhang Y, Huo M, Zhou J, et al. DDSolver: an Add-In Program for Modeling and Comparison of Drug Dissolution Profiles. *AAPS J.* 2010;12(3):263. doi:10.1208/S12248-010-9185-1
49. OZ Ameer. In vitro Pharmacokinetic-Equivalence Analysis of Diclofenac Potassium Oral Film-Coated Tablet Relative to Marketed Generics. *JPPRes.* 2023;11:585. doi:10.56499/jppres23.1641_11.4.585
50. Abdul Rasool BK, Mohammed AA, Salem YY. The Optimization of a Dimenhydrinate Transdermal Patch Formulation Based on the Quantitative Analysis of in vitro Release Data by DDSolver through Skin Penetration Studies. *Sci Pharm.* 2021;89(3):33. doi:10.3390/SCIPHARM89030033/S1
51. Pascoal ADSMR, da Silva PM, Coelho Pinheiro MN. Drug Dissolution Profiles from Polymeric Matrices: data versus Numerical Solution of the Diffusion Problem and Kinetic Models. *Int J Heat Mass Transf.* 2015;61:118–127. doi:10.1016/J.ICHEATMASSTRANSFER.2014.12.011
52. Salamah M, Budai-Sz M, Ucs M, et al. Development and Characterization of In Situ Gelling Nasal Cilostazol Spanlastics. *Gels.* 2025;11(2):82. doi:10.3390/GELS11020082
53. Katona G, Sabir F, Sipos B, et al. Development of Lomustine and N-Propyl Gallate Co-Encapsulated Liposomes for Targeting Glioblastoma Multiforme via Intranasal Administration. *Pharmaceutics.* 2022;14(3):631. doi:10.3390/pharmaceutics14030631
54. Sipos B, Bella Z, Gróf I, et al. Soluplus® Promotes Efficient Transport of Meloxicam to the Central Nervous System via Nasal Administration. *Int J Pharm.* 2023;632:122594. doi:10.1016/j.ijpharm.2023.122594
55. Abdullah G, Abdulkarim M, Salman I, et al. In vitro Permeation and in vivo Anti-Inflammatory and Analgesic Properties of Nanoscaled Emulsions Containing Ibuprofen for Topical Delivery. *IJN.* 2011;2011:387. doi:10.2147/IJN.S14667
56. Espinoza LC, Silva-Abreu M, Clares B, et al. Formulation Strategies to Improve Nose-to-Brain Delivery of Donepezil. *Pharmaceutics.* 2019;11(2):64. doi:10.3390/pharmaceutics11020064
57. Irie K, Nakagawa A, Fujita H, et al. Population Pharmacokinetics of Favipiravir in Patients with COVID-19. *CPT Pharmacom Syst Pharma.* 2021;10(10):1161–1170. doi:10.1002/psp4.12685
58. Jespersen B, Knupp L, Northcott CA. Femoral Arterial and Venous Catheterization for Blood Sampling, Drug Administration and Conscious Blood Pressure and Heart Rate Measurements. *JoVE.* 2012;(59):3496. doi:10.3791/3496
59. Jain R, Jain B, Kabir A, Bajaj A, Ch R, Sharma S. Fabric Phase Sorptive Extraction-Gas Chromatography-Mass Spectrometry for the Determination of Favipiravir in Biological and Forensic Samples. *Adv Sample Preparation.* 2023;6:100058. doi:10.1016/j.sampre.2023.100058
60. Zhang Y, Huo M, Zhou J, Xie S. PKSolver: an Add-in Program for Pharmacokinetic and Pharmacodynamic Data Analysis in Microsoft Excel. *Comput Methods Programs Biomed.* 2010;99(3):306–314. doi:10.1016/J.CMPB.2010.01.007
61. Abou-Taleb HA, Khalaf RA, Abdel-Aleem JA. Intranasal Niosomes of Nefopam with Improved Bioavailability: preparation, Optimization, and in-vivo Evaluation. *Drug Des Devel Ther.* 2018;12:3501. doi:10.2147/DDDT.S177746
62. Ahmed TA. Preparation of Finasteride Capsules-Loaded Drug Nanoparticles: formulation, Optimization, in vitro, and Pharmacokinetic Evaluation. *Int J Nanomed.* 2016;11:515–527. doi:10.2147/IJN.S98080
63. Ibrahim MM, Basalious EB, El-Nabarawi MA, Makhlof AIA, Sayyed ME, Ibrahim IT. Nose to Brain Delivery of Mirtazapine via Lipid Nanocapsules: preparation, Statistical Optimization, Radiolabeling, in vivo Biodistribution and Pharmacokinetic Study. *Drug Deliv Transl Res.* 2024;14(9):2539–2557. doi:10.1007/S13346-024-01528-7
64. Rompicherla SKL, Arumugam K, Bojja SL, Kumar N, Rao CM. Pharmacokinetic and Pharmacodynamic Evaluation of Nasal Liposome and Nanoparticle Based Rivastigmine Formulations in Acute and Chronic Models of Alzheimer's Disease. *Naunyn Schmiedeberg Arch Pharmacol.* 2021;394(8):1737–1755. doi:10.1007/S00210-021-02096-0/FIGURES/13
65. Bhandari R, Kaur IP. Pharmacokinetics, Tissue Distribution and Relative Bioavailability of Isoniazid-Solid Lipid Nanoparticles. *Int J Pharm.* 2013;441(1–2):202–212. doi:10.1016/J.IJPHARM.2012.11.042
66. Kohajda Z, Virág L, Hornyik T, et al. In vivo and Cellular Antiarrhythmic and Cardiac Electrophysiological Effects of Desethylamiodarone in Dog Cardiac Preparations. *Br J Pharmacol.* 2022;179(13):3382–3402. doi:10.1111/BPH.15812
67. Akel H, Ismail R, Katona G, Sabir F, Ambrus R, Csóka I. A Comparison Study of Lipid and Polymeric Nanoparticles in the Nasal Delivery of Meloxicam: formulation, Characterization, and in vitro Evaluation. *Int J Pharm.* 2021;604:120724. doi:10.1016/J.IJPHARM.2021.120724
68. D'Souza S, Faraj JA, Giovagnoli S, DeLuca PP. IVIVC from Long Acting Olanzapine Microspheres. *Int J Biomater.* 2014;2014:1–11. doi:10.1155/2014/407065
69. Sipos B, Szabó-Révész P, Csóka I, et al. Quality by Design Based Formulation Study of Meloxicam-Loaded Polymeric Micelles for Intranasal Administration. *Pharmaceutics.* 2020;12(8):1–29. doi:10.3390/PHARMACEUTICS12080697
70. Brill Nijhoff. International Conference On Harmonisation Of Technical Requirements For Registration Of Pharmaceuticals For Human Use. In: Tietje C, Brouder A, editors. *Handbook of Transnational Economic Governance Regimes.* Brill Nijhoff. 2010:1041–1053. doi:10.1163/ej.9789004163300.i-1081.897

71. Shabir GA. Validation of High-Performance Liquid Chromatography Methods for Pharmaceutical Analysis Understanding the Differences and Similarities between Validation Requirements of the US Food and Drug Administration, the US Pharmacopeia and the International Conference on Harmonization. *J Chromatogr A*. 2003;2023:1.
72. Aboul-Einien MH, Kandil SM, Abdou EM, Diab HM, Zaki MSE. Ascorbic Acid Derivative-Loaded Modified Aspasomes: formulation, in vitro, ex vivo and Clinical Evaluation for Melasma Treatment. *J Liposome Res*. 2020;30(1):54–67. doi:10.1080/08982104.2019.1585448
73. Moribe K, Maruyama S, Inoue Y, et al. Ascorbyl Dipalmitate/PEG-Lipid Nanoparticles as a Novel Carrier for Hydrophobic Drugs. *Int J Pharm*. 2010;387(1–2):236–243. doi:10.1016/j.ijpharm.2009.12.007
74. Honary S, Zahir F. Effect of Process Factors on the Properties of Doxycycline Nanovesicles. *Trop J Pharm Res*. 2012;11(2):169–175. doi:10.4314/TJPR.V11I2.1
75. Amer SS, Nasr M, Abdel-Aziz RTA, et al. Cosm-Nutraceutical Nanovesicles for Acne Treatment: physicochemical Characterization and Exploratory Clinical Experimentation. *Int J Pharm*. 2020;577:119092. doi:10.1016/j.ijpharm.2020.119092
76. Zaid Alkilani A, Abu-Zour H, Alshishani A, Abu-Huwajj R, Basheer HA, Abo-Zour H. Formulation and Evaluation of Niosomal Alendronate Sodium Encapsulated in Polymeric Microneedles: in vitro Studies, Stability Study and Cytotoxicity Study. *Nanomaterials*. 2022;12(20):3570. doi:10.3390/NANO12203570
77. Saraswathi TS, Mothilal M. Development of Rivastigmine Loaded Self Assembled Nanostructures of Nonionic Surfactants for Brain Delivery. *Int J Appl Pharm*. 2021;13:205–215. doi:10.22159/ijap.2021v13i5.42664
78. Manosroi A, Wongtrakul P, Manosroi J, et al. Characterization of Vesicles Prepared with Various Non-Ionic Surfactants Mixed with Cholesterol. *Colloids Surf B Biointerfaces*. 2003;30(1–2):129–138. doi:10.1016/S0927-7765(03)00080-8
79. Wohlfart S, Gelperina S, Kreuter J. Transport of Drugs across the Blood–Brain Barrier by Nanoparticles. *J Control Release*. 2012;161(2):264–273. doi:10.1016/j.jconrel.2011.08.017
80. Sahin A, Tonbul H, Çapan Y, Seko I. Brain-Targeted Nanoparticles to Overcome the Blood-Brain Barrier. *jpt*. 2020;1(1):26–40. doi:10.37662/jpt.2020.4
81. Amasya G, Badilli U, Aksu B, Tarimci N. Quality by Design Case Study I: design of 5-Fluorouracil Loaded Lipid Nanoparticles by the W/O/W Double Emulsion — solvent Evaporation Method. *Eur J Pharm Sci*. 2016;84:92–102. doi:10.1016/j.ejps.2016.01.003
82. Dutta L, Mukherjee B, Chakraborty T, et al. Lipid-Based Nanocarrier Efficiently Delivers Highly Water Soluble Drug across the Blood–Brain Barrier into Brain. *Drug Deliv*. 2018;25(1):504–516. doi:10.1080/10717544.2018.1435749
83. Eid HM, Naguib IA, Alsantali RI, Alsalahat I, Hegazy AM. Novel Chitosan-Coated Niosomal Formulation for Improved Management of Bacterial Conjunctivitis: a Highly Permeable and Efficient Ocular Nanocarrier for Azithromycin. *J Pharm Sci*. 2021;110(8):3027–3036. doi:10.1016/J.XPHS.2021.04.020
84. Zolghadri S, Asad AG, Farzi F, et al. Span 60/Cholesterol Niosomal Formulation as a Suitable Vehicle for Gallic Acid Delivery with Potent in vitro Antibacterial, Antimelanoma, and Anti-Tyrosinase Activity. *Pharmaceutics*. 2023;16(12):1680. doi:10.3390/ph16121680
85. Neves AR, Queiroz JF, Reis S. Brain-Targeted Delivery of Resveratrol Using Solid Lipid Nanoparticles Functionalized with Apolipoprotein E. *J Nanobiotechnol*. 2016;14(1):27. doi:10.1186/s12951-016-0177-x
86. Korchia L, Bouilhac C, Aubert A, Robin -J-J, Lapinte V. Light-Switchable Nanoparticles Based on Amphiphilic Diblock, Triblock and Heterograft Polyoxazoline. *RSC Adv*. 2017;7(68):42690–42698. doi:10.1039/C7RA07094B
87. Mathure D, Madan R. Formulation and Evaluation of Niosomal in Situ Nasal Gel of a Serotonin Receptor Agonist, Buspirone Hydrochloride for the Brain Delivery via Intranasal Route. *PNT*. 2018;6(1):69–78. doi:10.2174/2211738506666180130105919
88. Soni S, Baghel K, Soni ML, Kashaw SK, Soni V. Size-Dependent Effects of Niosomes on the Penetration of Methotrexate in Skin Layers. *Future J Pharm Sci*. 2024;10(1):1–18. doi:10.1186/S43094-024-00624-2
89. Varshosaz J, Pardakhty A, Hajhashemi VI, Najafabadi AR. Development and Physical Characterization of Sorbitan Monoester Niosomes for Insulin Oral Delivery. *Drug Delivery*. 2003;10(4):251–262. doi:10.1080/DRD_10_4_251
90. Ammar HO, Ghorab MM, Mahmoud AA, Higazy IM. Lamotrigine Loaded Poly-ε-(d,l-Lactide-Co-Caprolactone) Nanoparticles as Brain Delivery System. *Eur J Pharm Sci*. 2018;115:77–87. doi:10.1016/J.EJPS.2018.01.028
91. Hoseini B, Jaafari MR, Golabpour A, Momtazi-Borojeni AA, Karimi M, Eslami S. Application of Ensemble Machine Learning Approach to Assess the Factors Affecting Size and Polydispersity Index of Liposomal Nanoparticles. *Sci Rep*. 2023;13(1):18012. doi:10.1038/s41598-023-43689-4
92. Danaei M, Dehghankhold M, Ataei S, et al. Impact of Particle Size and Polydispersity Index on the Clinical Applications of Lipidic Nanocarrier Systems. *Pharmaceutics*. 2018;10(2):57. doi:10.3390/pharmaceutics10020057
93. Khallaf RA, Aboud HM, Sayed OM. Surface Modified Niosomes of Olanzapine for Brain Targeting via Nasal Route; Preparation, Optimization, and in vivo Evaluation. *J Liposome Res*. 2020;30(2):163–173. doi:10.1080/08982104.2019.1610435
94. El-Sayed MM, Hussein AK, Sarhan HA, Mansour HF. Flurbiprofen-Loaded Niosomes-in-Gel System Improves the Ocular Bioavailability of Flurbiprofen in the Aqueous Humor. *Drug Dev Ind Pharm*. 2017;43(6):902–910. doi:10.1080/03639045.2016.1272120
95. Yang G, Liu Y, Wang H, et al. Bioinspired Core–Shell Nanoparticles for Hydrophobic Drug Delivery. *Angew Chem Int Ed*. 2019;58(40):14357–14364. doi:10.1002/anie.201908357
96. Passeleu-Le Bourdonnec C, Carrupt P-A, Scherrmann JM, Martel S. Methodologies to Assess Drug Permeation Through the Blood–Brain Barrier for Pharmaceutical Research. *Pharm Res*. 2013;30(11):2729–2756. doi:10.1007/s11095-013-1119-z
97. Józsa L, Nemes D, Pető Á, et al. Recent Options and Techniques to Assess Improved Bioavailability: in vitro and ex vivo Methods. *Pharmaceutics*. 2023;15(4):1146. doi:10.3390/PHARMACEUTICS15041146
98. Ozsoy Y, Gungor S, Cevher E. Nasal Delivery of High Molecular Weight Drugs. *Molecules*. 2009;14(9):3754–3779. doi:10.3390/molecules14093754
99. Wong AD, Ye M, Levy AF, Rothstein JD, Bergles DE, Searson PC. The Blood-Brain Barrier: an Engineering Perspective. *Front Neuroeng*. 2013;6. doi:10.3389/fneng.2013.00007
100. Henriques P, Bicker J, Silva S, Doktorovová S, Fortuna A. Nasal-PAMPA: a Novel Non-Cell-Based High Throughput Screening Assay for Prediction of Nasal Drug Permeability. *Int J Pharm*. 2023;643:123252. doi:10.1016/j.ijpharm.2023.123252
101. Taymouri S, Varshosaz J. Effect of Different Types of Surfactants on the Physical Properties and Stability of Carvedilol Nano-Niosomes. *Adv Biomed Res*. 2016;5(1):48. doi:10.4103/2277-9175.178781
102. Imran M, Titilayo B, Adil M, et al. Ascorbyl Palmitate: a Comprehensive Review on Its Characteristics, Synthesis, Encapsulation and Applications. *Process Biochem*. 2024;142:68–80. doi:10.1016/J.PROCBIO.2024.04.015

103. Mekasha YT, Chali BU, Feissa AB, Godena GH, Hassen HK, Wega SS. Quality Evaluation of the Azithromycin Tablets Commonly Marketed in Adama, and Modjo Towns, Oromia Regional State, Ethiopia. *PLoS One*. 2023;18(3):e0282156. doi:10.1371/JOURNAL.PONE.0282156
104. Mazumder R, Mahanti B, Majumdar S, Pal R, Chowdhury AD. Response Surface Method for Optimization of Prepared Satranidazole Powder Layered Pellets. *Future J Pharm Sci*. 2021;7(1):1–11. doi:10.1186/S43094-021-00337-W
105. Öztürk AA, Yenilmez E, Yazan Y. Dexketoprofen Trometamol-Loaded Eudragit® RL 100 Nanoparticle Formulation, Characterization and Release Kinetics. *Acta Pharma Sci*. 2019;57:1. doi:10.23893/1307-2080.APS.05705
106. Ekenna IC, Abali SO. Comparison of the Use of Kinetic Model Plots and DD Solver Software to Evaluate the Drug Release from Griseofulvin Tablets. *J Drug Delivery Ther*. 2022;12(2–S):5–13. doi:10.22270/JDDT.V12I2-S.5402
107. Basiri L, Rajabzadeh G, Bostan A. Physicochemical Properties and Release Behavior of Span 60/Tween 60 Niosomes as Vehicle for α -Tocopherol Delivery. *LWT*. 2017;84:471–478. doi:10.1016/j.lwt.2017.06.009
108. Elfadl AA, Boughdady M, Meshali M. New Peceol™/Span™ 60 Niosomes Coated with Chitosan for Candesartan Cilexetil: perspective Increase in Absolute Bioavailability in Rats. *Int J Nanomed*. 2021;16:5581–5601. doi:10.2147/IJN.S324171
109. Shi Q, Li F, Yeh S, Wang Y, Xin J. Physical Stability of Amorphous Pharmaceutical Solids: nucleation, Crystal Growth, Phase Separation and Effects of the Polymers. *Int J Pharm*. 2020;590:378–5173. doi:10.1016/j.ijpharm.2020.119925
110. Chen Q, Ji Y. Thermodynamic Mechanism of Physical Stability of Amorphous Pharmaceutical Formulations. *Ind Eng Chem Res*. 2023;62(3):1596–1605. doi:10.1021/ACS.IECR.2C02953/ASSET/IMAGES/LARGE/IE2C02953_0012.JPEG
111. Jüptner A, Scherließ R. Investigation of Powder Properties and Application Aspects Impacting Nasal Deposition of Spray-Dried Powders in a Nasal Cast. *Eur J Pharm Biopharm*. 2025;2025:114666. doi:10.1016/j.ejpb.2025.114666
112. Doub WH, Suman JM, Copley M, Goodey AP, Hosseini S, Mitchell JP. Laboratory Performance Testing of Aqueous Nasal Inhalation Products for Droplet/Particle Size Distribution: an Assessment from the International Pharmaceutical Aerosol Consortium on Regulation and Science (IPAC-RS). *AAPS Pharm Sci Tech*. 2023;24(7):1–13. doi:10.1208/S12249-023-02665-X/TABLES/4
113. Pina Costa C, Nižić Nodilo L, Silva R, et al. In Situ Hydrogel Containing Diazepam-Loaded Nanostructured Lipid Carriers (DZP-NLC) for Nose-to-Brain Delivery: development, Characterization and Deposition Studies in a 3D-Printed Human Nasal Cavity Model. *Int J Pharm*. 2023;644:123345. doi:10.1016/J.IJPHARM.2023.123345
114. Dayal P, Shaik MS, Singh M. Evaluation of Different Parameters That Affect Droplet-size Distribution from Nasal Sprays Using the Malvern Spraytec®. *J Pharm Sci*. 2004;93(7):1725–1742. doi:10.1002/jps.20090
115. Casula E, Manconi M, Vázquez J, et al. Design of a Nasal Spray Based on Cardiospermum Halicacabum Extract Loaded in Phospholipid Vesicles Enriched with Gelatin or Chondroitin Sulfate. *Molecules*. 2021;26(21):6670. doi:10.3390/molecules26216670
116. Patterlini V, Guareschi F, D'Angelo D, et al. Clinically Relevant Characterization and Comparison of Ryaltris and Other Anti-Allergic Nasal Sprays. *Pharmaceutics*. 2024;16(8). doi:10.3390/PHARMACEUTICS16080989/S1
117. Abourehab MAS, Khamas A, Genedy S, et al. Sesame Oil-Based Nanostructured Lipid Carriers of Nicergoline, Intranasal Delivery System for Brain Targeting of Synergistic Cerebrovascular Protection. *Pharmaceutics*. 2021;13(4):581. doi:10.3390/pharmaceutics13040581
118. League-Pascual JC, Lester-McCully CM, Shandilya S, et al. Plasma and Cerebrospinal Fluid Pharmacokinetics of Select Chemotherapeutic Agents Following Intranasal Delivery in a Non-Human Primate Model. *J Neurooncol*. 2017;132(3):401–407. doi:10.1007/s11060-017-2388-x
119. Huang Q, Chen X, Yu S, Gong G, Shu H. Research Progress in Brain-Targeted Nasal Drug Delivery. *Front Aging Neurosci*. 2023;15:1341295. doi:10.3389/FNAGI.2023.1341295/BIBTEX
120. Formica ML, Real DA, Picchio ML, Catlin E, Donnelly RF, Paredes AJ. On a Highway to the Brain: a Review on Nose-to-Brain Drug Delivery Using Nanoparticles. *Appl Mater Today*. 2022;29:101631. doi:10.1016/J.APMT.2022.101631
121. Pokorski M, Marczak M, Dymecka A, Suchocki P. Ascorbyl Palmitate as a Carrier of Ascorbate into Neural Tissues. *J Biomed Sci*. 2003;10(2):193–198. doi:10.1007/BF02256054
122. Pokorski M, Marczak M. Stability of Ascorbyl Palmitate Molecule in the Rat. *J Physiol Pharmacol*. 2005;56:197.
123. Tuesuwan B, Mueannoorn W, Jamnongtanachot P, et al. Basis to Aid Crisis: favipiravir Oral Solution for Hospital Compounding During COVID-19 Drug Shortage. *J Pharm Sci*. 2023;112(2):610–617. doi:10.1016/j.xphs.2022.10.026
124. Ammar HO, Haider M, Ibrahim M, El Huffy NM. In vitro and in vivo Investigation for Optimization of Niosomal Ability for Sustainment and Bioavailability Enhancement of Diltiazem after Nasal Administration. *Drug Deliv*. 2017;24(1):414–421. doi:10.1080/10717544.2016.1259371
125. Mane SD, Thoh M, Sharma D, Sandur SK, Naidu KA. Ascorbyl Stearate Promotes Apoptosis Through Intrinsic Mitochondrial Pathway in HeLa Cancer Cells. *Anticancer Res*. 2016;36(12):6409–6417. doi:10.21873/ANTICANRES.11238
126. Zhang L, Li G, Lin B, He H, Zhou R, Jiang W. Ascorbyl Palmitate Ameliorates Inflammatory Diseases by Inhibition of NLRP3 Inflammasome. *Int Immunopharmacol*. 2024;131. doi:10.1016/J.INTIMP.2024.111915
127. Varshosaz J, Sadrai H, Alinagari R. Nasal Delivery of Insulin Using Chitosan Microspheres. *J Microencapsul*. 2004;21(7):761–774. doi:10.1080/02652040400015403

RESEARCH ARTICLE

 OPEN ACCESS



Development, *in vitro* and *ex vivo* characterization of lamotrigine-loaded bovine serum albumin nanoparticles using QbD approach

Maryana Salamah^{a,b} , Bence Sipos^a , Zsuzsanna Schelz^b , István Zupkó^b , Ágnes Kiricsi^c , Ágnes Szalencó-Tőkés^c , László Rovó^c , Gábor Katona^a , György Tibor Balogh^{d,e}  and Ildikó Csóka^a 

^aInstitute of Pharmaceutical Technology and Regulatory Affairs, Faculty of Pharmacy, University of Szeged, Szeged, Hungary; ^bInstitute of Pharmacodynamics and Biopharmacy, Faculty of Pharmacy, University of Szeged, Szeged, Hungary; ^cDepartment of Oto-Rhino-Laryngology and Head-Neck Surgery, University of Szeged, Szeged, Hungary; ^dDepartment of Pharmaceutical Chemistry, Semmelweis University, Budapest, Hungary; ^eCenter for Pharmacology and Drug Research & Development, Semmelweis University, Budapest, Hungary

ABSTRACT

The present study aimed to prepare and optimize lamotrigine-loaded bovine serum albumin nanoparticles (LAM-NP) using the Quality by Design (QbD) approach and to investigate both the *in vitro* and *ex vivo* effects of different cross-linking agents glutaraldehyde (GLUT), glucose (GLUC) and 1-(3-dimethylaminopropyl)-3-ethylcarbodiimide hydrochloride (EDC) on intranasal applicability. Cross-linked LAM-NP from EDC (NP-EDC-1) showed the lowest Z-average value (163.7 ± 1.9 nm) and drug encapsulation efficacy (EE%) of $97.31 \pm 0.17\%$. The drug release of GLUC cross-linked LAM-NP (NP-GLUC-9), glutaraldehyde cross-linked LAM-NP (NP-GLUT-2), and NP-EDC-1 at blood circulation conditions was higher than the initial LAM. The results of the blood-brain barrier parallel artificial membrane permeability assay (BBB-PAMPA) showed an increase in the permeability of LAM through the BBB with NP-GLUC-9 and an increase in flux with all selected formulations. The *ex vivo* study showed that LAM diffusion from the selected formulations through the human nasal mucosa was higher than in case of initial LAM. The cytotoxicity study indicated that BSA-NP reduced LAM toxicity, and GLUC 9 mM and EDC 1 mg could be alternative cross-linking agents to avoid GLUT 2% v/v toxicity. Furthermore, permeability through Caco-2 cells showed that nasal epithelial transport/absorption of LAM was improved by using BSA-NPs. The use of BSA-NP may be a promising approach to enhance the solubility, permeability through BBB and decrease the frequency of dosing and adverse effects of LAM.

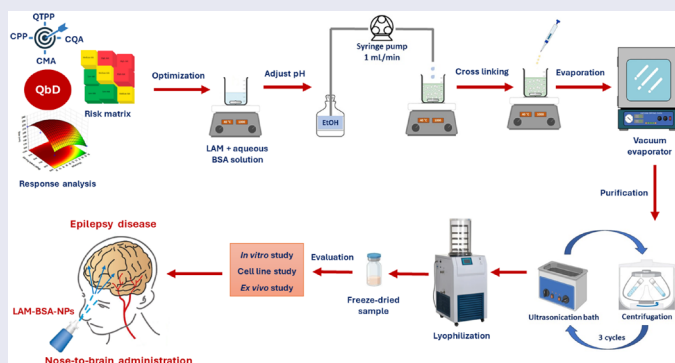
ARTICLE HISTORY

Received 4 September 2024
Revised 26 November 2024
Accepted 24 January 2025

KEYWORDS

Lamotrigine; bovine serum albumin; cross-linking; nanoparticles; quality by design; nasal delivery




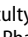
GRAPHICAL ABSTRACT




1. Introduction

Epilepsy is one of the most common neurological diseases, affecting around 50 million people worldwide according to the World Health Organization (WHO) (Do Canto et al., 2020; Manole et al., 2023; Yavuz et al., 2021). Additionally, the most

recent global burden of disease research ranks it as the second most serious neurological disease (Cano et al., 2021). Treatment of epilepsy remains challenging due to drug resistance to antiepileptic drugs, which is caused by several types of physiological barriers, including the blood-brain barrier (BBB) and the ATP-binding cassette (ABC) group of

CONTACT Gábor Katona  katona.gabor@szte.hu  Institute of Pharmaceutical Technology and Regulatory Affairs, Faculty of Pharmacy, University of Szeged, Eötvös street 6., H-6720 Szeged, Hungary; György Tibor Balogh  balogh.gyorgy.tibor@semmelweis.hu  Department of Pharmaceutical Chemistry, Semmelweis University, Högyes Endre Street 9, H-1092 Budapest, Hungary

 Supplemental data for this article can be accessed online at <https://doi.org/10.1080/10717544.2025.2460693>.

© 2025 The Author(s). Published by Informa UK Limited, trading as Taylor & Francis Group.

This is an Open Access article distributed under the terms of the Creative Commons Attribution-NonCommercial License (<http://creativecommons.org/licenses/by-nc/4.0/>), which permits unrestricted non-commercial use, distribution, and reproduction in any medium, provided the original work is properly cited. The terms on which this article has been published allow the posting of the Accepted Manuscript in a repository by the author(s) or with their consent.

transporters with P-glycoproteins (ABCB¹) (P-gp) (Saju, *n.d.*; Liu et al., 2014). P-gp limits the delivery of antiepileptic drugs to the site of action, decreasing the concentration of the drug in the brain, which requires the development of novel and effective treatment alternatives (Bonilla et al., 2022).

In recent years, albumin-based nanoparticles have been utilized as a drug delivery system due to their advantages, specifically to bypass different physiological barriers, such as BBB, and additionally to improve the efficacy and pharmacokinetics of drugs by controlling the particle size, solubility, permeability, drug release, stability *in vivo* and during storage (Jahanshahi and Babaei, 2008; Rahimnejad et al., 2012; Bennet and Kim, 2014). Abraxane® (human serum albumin-bound paclitaxel) is an example of the marketed albumin nanoparticles, which is approved by the US Food and Drug Administration (FDA) (Desai, 2016; Solanki et al., 2021).

Bovine serum albumin (BSA) has been widely used by scientists and researchers as a nanodrug delivery carrier (anticancer drugs (Wang et al., 2021; Yang et al., 2020; Sadeghzadeh et al., 2023), anti-epileptic drugs (Wilson et al., 2014; 2020), antibiotic (Arriagada et al., 2019; Zewde et al., 2021)). It has shown many advantages, including nontoxicity, high adsorption capacity, biodegradability, and biocompatibility (Galisteo-González and Molina-Bolívar, 2014; Sailaja and Vineela, 2014; Bronze-Uhle et al., 2017). BSA degraded to nontoxic compound *in vivo*, and it could be eliminated through the lungs or excreted in urine. This degradation could be chemical or catalyzed by enzymes. The most important mechanism of degradation of biodegradable polymers is a hydrolytic degradation (Tuovinen et al., 2002). In addition, it is used as a model protein for nanoparticle formulations, especially to encapsulate hydrophobic drugs, due to its properties as a pure, structurally stable, water soluble, inexpensive and simple protein (Rohiwal et al., 2015; Yang et al., 2017; Yadav and Yadav, 2021).

Lamotrigine (LAM), as a second-generation broad-spectrum antiepileptic drug, is used to treat epilepsy in pregnant (Avachat et al., 2022; Li and Meador, 2022), children and adults (He et al., 2012; Ji et al., 2021), as well as to maintain the treatment of bipolar I disorder (Patino et al., 2015). It belongs to class II drugs of the Biopharmaceutics Classification System (BCS) (very slightly soluble in water ~ 0.17 mg/mL) (Saju, *n.d.*; Singh et al., 2015). LAM has a pK_a value of 5.7 (Lalani et al., 2015; Abdelmonem et al., 2020). It is rapidly absorbed after oral administration, with an oral dose of 25 mg/day for the first 2 weeks, followed by an increase to 50 mg/day every 1 to 2 weeks (Ware et al., 2016; Praveen et al., 2019). LAM undergoes first-pass metabolism by an enzyme UGT1A4 (UDP-glucuronosyltransferase 1-4) in the liver, and is eliminated mostly via renal excretion (Nigam et al., 2019; Shankar Raman et al., 2021). According to recent studies, LAM is a substrate of P-gp, which may explain its limited access to the brain during treatment. To reach the required therapeutic level in the brain, a higher dose of LAM is administered. Due to this, the adverse effects of LAM are associated with an increase in blood concentration (Serralheiro et al., 2015), such as hepatotoxicity, leukopenia, thrombocytopenia, skin eruption, toxic epidermal necrosis, nausea, vomiting and headache (Gangurde et al., 2019).

For these reasons, alternative administration methods are needed to deliver LAM to the brain more effectively. Recently,

there has been a great deal of interest in using nanotechnology for intranasal administration to deliver therapeutic drugs directly to the brain and avoid hepatic metabolism (Clementino et al., 2021; Formica et al., 2022; Jeong et al., 2023). Drugs administered via the intranasal route have the opportunity to rapidly and easily bypass the BBB, cerebrospinal fluid (CSF), and the blood barrier of CSF through pathways along the olfactory and trigeminal nerves that innervate nasal passages and link the nasal cavity with the central nervous system (CNS) (Mistry et al., 2009; Alexander et al., 2019). Furthermore, it could reduce the amount of therapeutic molecules in the main organs, including the liver, spleen, and kidney, which could decrease adverse systemic effects (Lee and Minko, 2021).

To our knowledge, some LAM formulations for intranasal administration have already been successfully developed, such as nanosized nasal powder (Gieszinger et al., 2020), nanoliposomes (Praveen et al., 2019), thermoresponsive nasal gel (Serralheiro et al., 2015), cubosomal dispersion loaded in a thermosensitive *in situ* gel (Mohsen et al., 2023), however LAM-loaded BSA nanoparticles (LAM-NPs) seem to be a novel approach.

The purpose of the present study was to develop LAM-NPs using different types of cross-linking agents applying the Quality by Design approach (QbD) and to investigate their effect on drug release, cytotoxicity, and BBB permeability.

2. Materials

LAM (6-(2,3-dichlorophenyl)-1,2,4-triazine-3,5-diaminotese), was purchased from Teva Ltd. (Budapest, Hungary). BSA cell culture grade, ethanol (96% v/v), methanol 99.99% v/v (HPLC grade), glutaraldehyde (25% w/v), dimethyl sulfoxide (DMSO), mannitol, glucose, sodium chloride for physiological salt solution, and anhydrous Disodium hydrogen phosphate were purchased from Molar Chemicals Ltd. (Budapest, Hungary). Dodecane and hexane were purchased from Merck KGaA (Darmstadt, Germany). Polar brain lipid extract, porcine stomach mucin (Type III), 1-(3-dimethylaminopropyl)-3-ethylcarbodiimide hydrochloride (EDC) were purchased from Sigma Aldrich Co. Ltd. (Budapest, Hungary). Dulbecco's phosphate buffered saline (DPBS) was acquired from Capricorn Scientific GmbH (Ebsdorfergrund, Germany). As nasal dissolution medium, Simulated Nasal Electrolyte Solution (SNES) was freshly prepared, which consisted of 8.77 g sodium chloride (NaCl), 2.98 g potassium chloride (KCl), 0.59 g and anhydrous calcium chloride (CaCl₂) dissolved in 1000 mL of deionized water at pH 5.6 (Sipos et al., 2021). These chemicals were acquired from Sigma-Aldrich Co., Ltd. (Budapest, Hungary). In all experiments, the purified water was filtered using Milli-Q® Gradient Water Purification System (Merck Ltd., Budapest, Hungary). All reagents for cell line studies were purchased from Sigma-Aldrich Co. Ltd. (Budapest, Hungary) if not indicated otherwise.

3. Methods

3.1. Initial risk assessment

According to the International Council for Harmonization (ICH) of the Q8 (R2) pharmaceutical development guideline, the first step of the initial risk assessment based on QbD is

to define the Quality Target Product Profile (QTPP). QTPP describes the quality, safety, and efficacy characteristics of the drug product that will be achieved to confirm the desired quality (Tietje and Brouder, 2010). Then, according to QTPPs, the physical, chemical and biological characteristics critical to the were determined as Critical Quality Attributes (CQAs) (Ghose et al., 2021). The next step is to identify control factors, including Critical Material Attributes (CMAs) of the input materials and Critical Process Parameters (CPPs) of the production process (Soni et al., 2020). These steps were carried out according to ICH guideline Q9 (ICH guideline Q9 on quality risk management, 2015).

The risk assessment was performed after the risk identification process, where the mentioned attributes of the QbD methodology were established. A two-level risk assessment was performed using LeanQbD® software (QbD Works LLC, Fremont, CA, USA). At first, the relations between each assigned factor were investigated based on the basis of interdependence with each other. This was performed in two steps; first, the relations were assigned between the QTPP and CQA elements, describing the effect of CQAs on the QTPPs. This was repeated amongst the CMA/CPP and CQA elements, where the effect of individual material and product characteristics were described on the CQAs. The relations were described on a 3-level scale, where each relation was assigned with a 'HIGH', 'MEDIUM' or 'LOW' interdependence. The second step of the risk assessment was to quantify these relationships and identify the factors with the highest severity based on probability and software calculations. The calculations are expressed as severity scores and are depicted and analyzed on Pareto charts (Bartos et al., 2018; Kis et al., 2019). Based on the results of Pareto charts, the high-risk-level CQAs and CMAs/CPPs parameters were selected for further analysis using Design of Experimentation.

3.2. Preparation of nanoparticles by the coacervation method

3.2.1. Non-cross-linked lamotrigine-loaded bovine serum albumin nanoparticles (LAM-NP)

LAM-NP were prepared using a modified coacervation method (Piazzini et al., 2019; Wang et al., 2021). A certain amount of BSA was dissolved in 3 mL of 5 mM NaCl solution under magnetic stirring for 15 minutes at 40°C. A certain amount of LAM was added to the BSA solution and the pH value was adjusted to 8.0 with NaOH 0.1 N and the solution was kept stirring for 30 minutes. Then, using a syringe pump, 15 mL of ethanol (EtOH) was injected dropwise at a constant flow rate of 1 mL/min until turbidity appeared in the solution. After EtOH was evaporated at 40°C for 30 minutes under pressure using vacuum drying chambers (Binder GmbH, Tuttlingen, Germany), the pellet was then redispersed in purified water to its initial volume using an ultrasonication bath for 10 minutes. The resulting NPs were purified to eliminate the non-desolvated BSA and excipients, such as EtOH, by three centrifugation cycles (14000 rpm for 15 minutes at 4 ± 1°C) using a Hermle Z323 laboratory centrifuge (Hermle AG, Gossheim, Germany). The pellets were redispersed in purified water to the original volume by using an ultrasonication bath.

3.2.2. Cross-linked lamotrigine-loaded bovine serum albumin nanoparticles

The effect of cross-linking agents on the optimal LAM-NP formulation was investigated. For the stabilization of nanoparticles, different crosslinkers were studied, including 5% (v/v) of glutaraldehyde solution (GLUT), glucose (GLUC), and 1-ethyl-3-(3-dimethylaminopropyl) carbodiimide hydrochloride (EDC), as shown in Table 1. The cross-linking reaction was conducted for 2 h incubation time at 40°C temperature using a magnetic stirrer. Then, EtOH was evaporated using a vacuum evaporator at 40°C for 30 minutes, and the pellets were redispersed in purified water to its initial volume using an ultrasonication bath for 10 minutes. After that, the formulations were purified as previously described.

3.2.3. Freeze-drying

Freeze-drying was conducted with a Scanvac, CoolSafe 100-9 Pro type apparatus (LaboGeneApS, Lyngby, Denmark). 1.5 mL of all formulations was lyophilized in the presence of 5% w/v mannitol as a cryoprotectant. Freeze-drying was carried out at – 40°C for 16 h under a pressure of 0.012 mbar with an additional 4 h of secondary drying at 25°C. The process was controlled by the Scanlaf CTS16a02 software. The samples were then stored in the refrigerator until further investigation.

3.3. Design of experiments (DoE)

A Design of Experiments (DoE) is a potent statistical approach that may be used to analyze the impact of numerous factors that affect the therapeutic product, as well as a potent instrument for collecting enough data. The application of DoE improves the understanding of the process, resulting in process improvement and cost savings (Pandey et al., 2017). DoE was conducted using a 3³ factorial design to study the relationship between independent variables (amount of BSA, amount of LAM and stirring speed) and their responses on average hydrodynamic diameter (Z-average) and encapsulation efficiency (EE%), as the most critical parameters of the quality of the final product based on the risk assessment

Table 1. Cross-linking agents that used to stabilize the optimal LAM-NP formulation.

Cross-linking agents		Formulation code
GLUT (% v/v)	2 %	NP-GLUT-2
	4 %	NP-GLUT-4
	8 %	NP-GLUT-8
GLUC (mM)	3 mM	NP-GLUC-3
	6 mM	NP-GLUC-6
	9 mM	NP-GLUC-9
EDC (mg)	0.5 mg	NP-EDC-0.5
	1 mg	NP-EDC-1
	1.5 mg	NP-EDC-1.5

Table 2. Independent variables of the 3³ factorial design selected after the risk assessment.

Independent variables	Levels		
	Low (-1)	Medium (0)	High (+1)
X1: Amount of BSA (mg)	10	20	30
X2: Amount of LAM (mg)	10	20	30
X3: Stirring speed (rpm)	500	750	1000

(Table 2). The TIBCO Statistica® 13.4 software (Statsoft Hungary, Budapest, Hungary) was used for DoE, quadratic response surface analysis of 2D and 3D plots, and to construct a second-order polynomial model.

The relationship of the variables on the response can be analyzed by the following second-order Eq. (1):

$$Y = \beta_0 + \beta_1 X_1 + \beta_2 X_2 + \beta_3 X_3 + \beta_{11} X_1^2 + \beta_{22} X_2^2 + \beta_{33} X_3^2 + \beta_{12} X_1 X_2 + \beta_{13} X_1 X_3 + \beta_{23} X_2 X_3 \quad (1)$$

where Y is the response variable (Y_1 for Z-average and Y_2 for EE%); β_0 is a constant; β_1 , β_2 , and β_3 are linear coefficients; β_{12} , β_{13} , and β_{23} are interaction coefficients between the three factors; and β_{11} , β_{22} , and β_{33} are quadratic coefficients.

3.4. Determination of average hydrodynamic diameter, polydispersity index, and zeta potential

Dynamic light scattering using a Zetasizer (Malvern Instrument) has been applied as a noninvasive process analytical technology (PAT) tool to analyze the average hydrodynamic diameter (Z-average), polydispersity index (PDI), and zeta potential (ZP). Samples were redispersed in purified water and appropriately diluted (1:10), and then filled with folded capillary cells. Measurement was performed at 25°C with a refractive index of 1.33. All measurements were performed in triplicate, the results were presented as means \pm SD.

3.5. Quantitative analysis by RP-HPLC-DAD

Chromatographic analysis was performed using an Agilent 1260 HPLC (Agilent Technologies, San Diego, CA, USA) and Kinetex® C18 column (5 μ m, 150 mm \times 4.6 mm, 100 Å). The mobile phase consisting of Methanol: Phosphate buffer (pH 3.5, 10 mM) in the ratio (30:70, v/v). The injection volume was 10 μ L. The isocratic elution was carried out for 8 minutes at a flow rate of 1.0 mL/min at 30°C. Chromatograms were detected at 275.4 nm using the UV-VIS diode array detector at a retention time of 6.126 minutes. The regression coefficient of the calibration was 0.9997, while the limit of quantification (LOQ) and the limit of detection (LOD) of LAM were 0.016 and 0.049 ppm, respectively.

3.6. Encapsulation efficiency

The encapsulation efficiency (EE%) is defined by the percentage of LAM that is successfully entrapped into the nanoparticles. EE% was determined using the modified centrifugation method (Shah et al., 2021). First, 1 mL of each sample was centrifuged at 14000 rpm for 15 minutes at $4 \pm 1^\circ\text{C}$. Then, the clear supernatant solutions were diluted with methanol, filtered, and analyzed using RP-HPLC-DAD. All measurements were carried out in triplicate, the results were presented as means \pm SD. EE% was calculated using the following Eq. (2):

$$EE\% = \frac{C_{Total} - C_{Supernatant}}{C_{Total}} \times 100 \quad (2)$$

where C_{total} the initial concentration of LAM in the formulation, and $C_{supernatant}$ is the concentration of LAM in the supernatant after centrifugation.

3.7. In vitro drug release at nasal conditions

The selected formulations and the reference suspension of LAM, which were redispersed in SNES (pH 5.6, with a theoretical concentration of 2 mg/mL LAM), were tested using the modified paddle method (Hanson SR8 Plus (Teledyne Hanson Research, Chatsworth, CA, USA)) (Nigam et al., 2019). Pretreated dialysis membranes (Spectra/Por®, Spectrum Laboratories Inc., Rancho Dominguez, CA, USA) with a molecular weight cutoff value (MWCO) of 12-14 kDa were loaded with 1 mL of the reference suspension and the selected formulations. The bags were sealed at both ends. 100 mL of SNES was used as a dissolution medium. The measurement was carried out at 32°C at a paddle rotation speed of 50 rpm, while sampling was carried out for 30 minutes. After filtration, RP-HPLC-DAD was used to quantify the aliquots. Three parallel measurements were performed; Data were presented as means \pm SD.

3.8. Rapid equilibrium dialysis measurement (RED)

Time-dependent drug release patterns for the reference suspension of LAM and the selected formulations under blood circulation conditions were determined using the RED device (Thermo Scientific™, Waltham, MA, USA). The reference was prepared by suspending 2 mg of LAM in 1 mL of DPBS (pH 7.4) and then homogenizing it in an Eppendorf MixMate vortex mixer (Thermo Scientific™, Waltham, MA, USA) for 30 seconds. RED inserts (8K MWCO) were fitted into the reusable Teflon base plate. The donor chambers were then filled with 150-150 μ L of the reference LAM solution, as well as selected formulations redispersed in DPBS. 300 μ L of DPBS was used as acceptor phase and the base plate was covered with a sealing tape and incubated at 37°C on an orbital shaker (at 350 rpm) for 4 h. Aliquots were withdrawn at different times from acceptor chambers and immediately replaced with fresh DPBS (Katona et al., 2020). LAM concentrations were determined by using RP-HPLC-DAD. Five parallel measurements were performed; the data were presented as means \pm SD.

3.9. Determination of in vitro drug release kinetics

The model dependent approaches (including zero order, first order, Higuchi model, and Korsmeyer-Peppas model) were used to evaluate the release kinetics of LAM samples. DDSolver® add-in software (a menu-driven add-in program for Microsoft Excel) was used for the mathematical evaluation of the release kinetics, and the fitting of each model by comparing the rate constant (K), correlation coefficient (R^2), Akaike Information Criterion (AIC), and Model Selection Criterion (MSC) (Zhang et al., 2010; Pascoal et al., 2015; Abdul Rasool et al., 2021; Ameer, 2023).

3.10. In vitro permeability measurements

To evaluate the permeability (P_e , cm/s) of the initial suspension and the selected formulations, the parallel artificial membrane permeability assay specific to the blood-brain barrier (BBB-PAMPA) was employed (Katona et al., 2020). A 10 mM LAM solution was prepared in dimethylsulfoxide (DMSO), which was further diluted with SNES to obtain the 100 μ M reference donor solution. The filter donor plate (MultiscreenTM-IP, MAIPN4510, pore size 0.45 μ m; Millipore, Merck Ltd., Budapest, Hungary) was coated with 5 μ L of lipid solution (12 mg of porcine brain polar lipid extract dissolved in 420 μ L hexane and 180 μ L dodecane). The donor plate was inserted to the acceptor plate (Multiscreen Acceptor Plate, MSSACCEPTOR; Millipore, Merck Ltd., Budapest, Hungary), which contained 300 μ L of DPBS solution (pH 7.4). 150–150 μ L of reference LAM solution, as well as of the selected formulations redispersed with SNES (with a nominal concentration of 2 mg/mL of LAM) were transferred to the donor plate lipid membrane. The sandwich system was incubated at 37°C for 4 h (Heidolph Titramax 1000, Heidolph Instruments, Schwabach, Germany). Then, the PAMPA sandwich plates were separated and the LAM concentrations in the donor and acceptor chambers were determined using RP-HPLC-DAD. The effective permeability and membrane retention of the drugs were calculated using the following Eq. (3):

$$P_e = -\frac{2.303 \cdot V_A}{A(t - \tau_{ss})} \cdot \log \left(1 - \frac{C_A(t)}{S} \right) \quad (3)$$

where P_e is the effective permeability coefficient (cm/s), A is the filter area (0.24 cm²), V_A is the volume of the acceptor phase (0.3 cm³), t is the incubation time (s), τ_{ss} is the time to reach steady state (s), $C_A(t)$ is the concentration of the compound in the acceptor phase at time point t (mol/cm³), and S is LAM solubility in the donor phase. The solubility of LAM in donor phase was determined after centrifugation (at 14,000 rpm, 15 minutes, Eppendorf Centrifuge 5804R, Thermo ScientificTM, Waltham, MA, USA) in Microcon Centrifugal Filter Devices (30,000 molecular weight (MWCO)) and 5 \times dilution of formulations in MeOH, using the same RP-HPLC-DAD system. The flux of the samples was calculated using the following Eq. (4):

$$Flux = P_e \cdot S \quad (4)$$

For each assay, six parallel measurements were made and data were presented as means \pm SD.

3.11. In vitro assessment of mucoadhesive property

First, mucin 1% (w/v) was prepared in SNES (pH 5.6) and the mixture stirred continuously overnight at 37°C. Subsequently, the size of the mucin particles was reduced to 200–300 nm using a probe sonicator for 1 minute. The suspension was then centrifuged at 4000 rpm for 20 minutes to remove the aggregates and the supernatant was used for the test (Saengkrit et al., 2018). For testing, the selected formulations (after redispersion in 1.5 mL of purified water) were incubated

with 1% (w/v) mucin suspension in the ratio 1:1 (v/v) at 25°C for 1, 2 and 3 h. After each time point, the zeta potential was measured using a Zetasizer (Malvern Instrument) as described previously. All measurements were carried out in triplicate, the results were presented as means \pm SD.

3.12. Cell-based studies

3.12.1. Cytotoxicity assay

Cytotoxicity was determined by the MTT assay on human colon adenocarcinoma (Caco-2) cell line. Caco-2 cells were kindly donated by Solvo Biotechnology (Szeged, Hungary). The cells were cultivated in Dulbecco's modified essential medium. The medium was supplemented with 10% fetal bovine serum, 1% non-essential amino acids, and 1% antibiotic-antimycotic complex (penicillin, streptomycin, amphotericin B). Cells were incubated at 37°C in a humidified atmosphere containing 5% CO₂. Cells were seeded in 96-well plates (50,000 cells/well) and after overnight incubation, test compounds were added at six different concentrations (5, 10, 25, 50, 100, and 250 μ M for lamotrigine) and incubated for two hours under cell culture conditions. Finally, 20 μ L of 5 mg/mL MTT solution was pipetted to each well and incubated for an additional 4 h. Then, the medium was removed and the precipitated formazan crystals were dissolved in DMSO by shaking at 37°C for 30 minutes. Absorbances were measured at 545 nm using a microplate reader (SPECTROstar Nano, BMG Labtech) (Mosmann, 1983). Cell viability was assessed using the statistical software GraphPad Prism 10.12 and was calculated using the following Eq. (5):

$$Cell\ viability\ \% = \frac{Mean\ OD\ of\ sample}{Mean\ OD\ of\ control\ group} \times 100 \quad (5)$$

where OD represents the optical density, which is a measure of the absorbance of the samples (Rekha and Anila, 2019; Raj et al., 2023).

3.12.2. Permeability study on Caco-2 permeability model

The permeability coefficients across Human colon adenocarcinoma cells monolayer (Caco-2) were determined to predict the absorption of the tested formulations of lamotrigine. Caco-2 cells were harvested and seeded on filter supports (polycarbonate membrane, 0.4 μ m pore size, 1.12 cm² in 12 well plates, Corning Costar Co., Lowell, MA, USA) at a density of 300,000 cell/insert density. Cells were cultivated in 12-well plates with 1.5 mL medium in the acceptor and 0.5 mL of medium in the donor phase. The inserts were incubated at 37°C, 5% CO₂ concentration in humidified atmosphere for 21–29 days. The medium was changed every second day in the donor and acceptor phases.

The tightness of the Caco-2 cell layer was verified by measuring transepithelial electric resistance (TEER), which represents the closure of the cell layer of the epithelial barrier. TEER was measured with a Millipore Millicell ERS-2 voltohmmeter (Merck, USA) combined with STX-2 electrodes, and was calculated to the surface area of the monolayers as $\Omega \times$ cm². The cells were treated with the formulations when the cell layer reached steady-state TEER values.

During permeability experiments, the inserts were placed on 12-well plates containing 1.5 mL of physiological saline solution in the acceptor compartments (lower/base). In the donor compartments (upper/apical), the culture medium was changed and 0.5 mL of the tested formulations were added in saline. After incubation, samples were collected from the donor and acceptor compartments, and the lamotrigine concentrations were measured by RP-HPLC-DAD (Hubatsch et al., 2007). The apparent permeability coefficients (P_{app}) were determined according to the following Eq. (6) (Katona et al., 2021):

$$P_{app} = \frac{\Delta[C]_A \times V_A}{A \times [C]_D \times \Delta t} \quad (6)$$

where P_{app} is the apparent permeability (cm/s), $\Delta[C]_A$ is the difference in the concentration in the acceptor compartment after 120 minutes, $[C]_D$ is the initial concentration in the donor compartment, V_A is the volume of the acceptor compartment (1.5 mL) and A is the surface area available for permeability (1.1 cm²).

3.13. Ex vivo nasal permeability study on human nasal mucosa

Ex vivo transmucosal permeability of the selected formulations and reference suspension of LAM (with a theoretical concentration of 2 mg/mL) was performed in a modified Side-Bi-Side® type horizontal diffusion apparatus under the nasal conditions (Katona et al., 2022). Pieces of human nasal mucosa were collected during routine clinical daily nasal and sinus surgeries (septoplasty, FESS) under general or local anesthesia during which the surgical field was infiltrated with 1% Lidocain-Tonogen local injection and the mucosa was lifted from its base with a raspatorium or Cottle elevator. Transport from the operating room was performed in physiological saline. All investigations were carried out freshly after tissue removal. The experiments have been carried out with the approval of the institutional ethics committee of the University of Szeged (ETT-TUKÉB: IV/3880-1/2021/EKU). Six individuals (both female and male, aged from 30 to 60 years) participated in this study, coming for nose/sinus surgery at the University Oto-Rhino-Laryngology and Head-Neck Surgery. The inclusion criterion was that only intact nasal mucosa was considered for examination! The exclusion criterion was that patients with injured nasal mucosa were not considered for examination. The participants were briefed on the study procedures, and written informed consent was obtained from all subjects prior to conducting the procedure. Nasal mucosa was excised with a surgical scalpel into uniform segments with a diameter of 6 mm and membrane inserts were placed between donor and acceptor phases to provide an appropriate surface for permeability study (Sipos et al., 2023). The donor phase consisted of 8 mL of SNES, while the acceptor phase contained 9 mL of pH 7.4 DPBS. The temperature of both chambers was maintained at 32 ± 0.5 °C during the experiment using a heating circulator (ThermoHaake C 10-P5, Sigma-Aldrich Co., Ltd., Budapest, Hungary). For measurement, both the LAM reference suspension and the selected formulations were redispersed in 1 mL

of SNES, and added to the donor phase of the diffusion apparatus. Both the donor and acceptor compartments were continuously stirred at 300 rpm using magnetic stirrers. Aliquots from the acceptor phase (100 µL) were withdrawn at predetermined time points (5, 10, 15, 30, and 60 minutes) and replaced with fresh DPBS. LAM concentration was determined using the same RP-HPLC-DAD. Further biopharmaceutical evaluation was performed to determine different permeation parameters, such as the steady-state flux (J_{ss}) and permeability coefficient (K_p), using the following equations:

$$J_{ss} = \frac{m_t}{A \times t} \quad (7)$$

$$K_p = \frac{J_{ss}}{C_d} \quad (8)$$

where, J_{ss} is the steady-state flux (µg/cm²/h), m_t is the permeated drug quantity through the nasal mucosa, A the surface of the membrane insert (0.785 cm²), t the duration of the investigation, K_p the permeability coefficient (cm/h) and C_d the drug concentration in the donor phase (µg/cm³).

Moreover, the theoretical human steady-state plasma concentration (C_{ss}) of the drug, which estimates the concentration of the drug that could be reached in the blood after nasal administration, was obtained using the following Eq. (9) (Espinoza et al., 2019):

$$C_{ss} = J_{ss} \frac{A}{Cl_p} \quad (9)$$

where J_{ss} is the steady-state flux, A is the surface area of the nasal mucosa used for the permeation study (cm²), and Cl_p is the plasmatic clearance (human Cl_p value for LAM is 1.63 L/h (Tuba Incecayir, 2009)).

The enhancement ratio (ER) was calculated according to the following Eq. (10) (Abdullah et al., 2011):

$$ER = \frac{J_{ss} \text{ formulation}}{J_{ss} \text{ Reference}} \quad (10)$$

4. Statistical analysis

All results are expressed as mean ± SD. GraphPad Prism version 10.12 software (GraphPad Software, San Diego, CA) was used for the statistical analysis. A one-way analysis of variance (ANOVA) and Tukey's post-hoc test were performed to compare the groups. A significant level was set at a p value < .05. Where, (ns) means non-significant, *p-value < .05, **p-value < .01, and ***p-value < .001, ****p-value < .0001.

5. Results and discussion

5.1. Initial risk assessment

Quality by Design provides an efficient tool for quality-focused drug research and development processes in the early phase of preclinical academic research as well (Beg et al., 2019).

Based on the extended R&D QbD model, risk assessment must be implemented in the design and structure of the research flow to minimize risk factors that affect the quality, safety and efficacy (Pallagi et al., 2018; Rigamonti et al., 2023). There is a clinical need for the treatment of epilepsy in current medicine where patient adherence must be built into the dosage form, thus nasal administration is of paramount importance. Utilizing the advantageous combined properties of this alternative drug delivery route with albumin-based nanoparticles, the QTPP is as follows: a low-dose lamotrigine-loaded BSA nanoparticle containing nasal liquid formulation, providing sustained release due to its moderately high mucoadhesive properties and due to its favorable nanoparticle characteristics, prospering enhanced uptake at nasal and BBB region conditions. Critical Quality Attributes (CQAs), which have a significant influence on QTPP and hence the quality and efficacy of nanoparticles, were selected based on previous studies (Fatouh et al., 2017; Danaei et al., 2018; Alshweiat, 2019; Vitorino et al., 2020; Ghose et al., 2021; Hussain et al., 2021), including: nanocarrier properties, release profile, permeability profile, mucoadhesivity, and safety (the QTPPs, their target and justification of selecting CQAs were presented in Table 3).

The next step after the setup of the QTPPs was the interdependence rating-based risk assessment process. CMAs/CPPs were determined according to previous studies, including the amount of BSA, the amount of drug, the pH value, EtOH: water ratio, EtOH flow rate, stirring speed (rpm), incubation time (BSA with the drug), temperature and ionic strength (Galisteo-González and Molina-Bolívar, 2014; Gieszinger et al., 2017; Tarhini et al., 2018; Chaw and Olaitan, 2019; Wang et al., 2021; Yellanki et al., 2021).

In this study, the relations between each QTPP – CQA and CMA/CPP – CQA elements were evaluated using a risk estimation matrix (REM) to define the risk level (Figure 1).

The results indicate that high relations occur regarding the basic nanoparticle characteristics, such as the Z-average value and EE%. It is also considerable that two types of permeability rate can be found whilst conducting this research design, indicating different influencing factors at various ratios. The nanoparticle characteristics mentioned were implemented through the factorial design process later on. To quantify these results, using the software, Pareto charts were generated (Figures 2 and 3).

The probability rating also indicates that the main characteristics of the nanoparticles have the highest influence on the quality of the formulation and nasal applicability with the target of reaching the CNS. During the factorial design process, thus the following were considered: as main investigated independent factors, the stirring speed and the amount of the two main components: LAM and BSA were selected, while the pH was fixed at 8. Their effect on the Z-average and the encapsulation efficiency was investigated.

5.2. Preparation of nanoparticles

The coacervation method is one of the most commonly used processes to prepare protein nanoparticles. The use of a desolvating agent reduces the solubility of BSA, leading to phase separation and conformation changes in the protein structure that result in coacervation or precipitation of the protein in the form of nanoparticles (Lohcharoenkal et al., 2014).

The pH of the BSA solution and its ionic strength influence the particle size. The particle size decreases when using

Table 3. QTPP elements and CQAs for the development of LAM-NP.

QTPPs	Target	Justification
Dosage form	Nasal powder	To improve the solubility, bioavailability and stability of LAM (Masserini, 2013).
Therapeutic indication	Epilepsy	Lamotrigine, a synthetic phenyltriazine with antiepileptic properties (Singh et al., 2015).
Route of administration	Intranasal	A quick, easy and safe method of drug administration. bypasses the BBB, avoids hepatic first-pass metabolism, offers a highly vascularized absorption surface area with high permeation ability (Gangurde et al., 2019; de Barros et al., 2022).
Site of action	Central nervous system (CNS)	LAM acts by inhibiting sodium currents by selective binding to the inactive sodium channel, suppressing the release of the excitatory amino acid, glutamate (Shankar Raman et al., 2021).
Nanocarrier properties	Low particle size (Z-average < 250 nm)	Small particle size determines the biological fate, <i>in vivo</i> distribution, targeting abilities, and toxicity of a drug delivery system. It also affects the stability of the nanoparticles, drug loading, and drug release (Şahin et al., 2020).
	Narrow polydispersity index (PDI < 0.3)	PDI value of nanoparticles is an important physical characteristic. It is used to describe the degree of nonuniformity of a size distribution of particles. Values below 0.3 are considered acceptable and indicate a homogenous of vesicles (Danaei et al., 2018; De Oliveira et al., 2018).
	Relatively high zeta potential (ZP > ± 30 mV)	ZP is a function of dispersion stability. If ZP is higher than ± 30 mV, the dispersion is physically stable and aggregation between particles is inhibited (Şahin et al., 2020).
	High Encapsulation Efficiency (EE% > 75%)	EE% is a crucial physicochemical property of nanoparticles. It is critical to minimize the frequency of administration, increase patient compliance, and limit the consumption of materials/excipients and related adverse effects (Li et al., 2022).
Release profile at CSF conditions	Release rate higher than initial LAM	To confirm expected solubility which is important for better absorption, and to improve the pharmacokinetics of LAM.
Permeability profile (nasal mucosa)	Permeability rate higher than initial LAM	To enhance the absorption through the nasal epithelium into the systemic circulation hence to the brain (Zhang et al., 2013; Huang et al., 2023).
Permeability profile (BBB)	Permeability rate higher than initial LAM	To improve the bioavailability and therapeutic effect of LAM, because BBB is a typically rate-limiting factor for the availability of therapeutic drugs that penetrate the brain (He et al., 2018; Patharapankal et al., 2023).
Mucoadhesivity	High mucoadhesive properties (decreasing in ZP value)	A useful indication of adhesion properties is a decrease in ZP value after incubation with mucin, which overcomes nasal mucociliary clearance and lengthens residence time in the nasal cavity (Radwan et al., 2022).
Safety	Nontoxic	To reduce the toxicity of LAM and its adverse effects.

A	QTPP	Dosage form	Therapeutic indication	Route of administration	Site of action	Nanocarrier properties	Release profile at CSF conditions	Permeability profile	Mucoadhesivity	Safety
	CQA									
	Average hydrodynamic diameter	HIGH	HIGH	HIGH	HIGH	HIGH	HIGH	HIGH	HIGH	MEDIUM
	Polydispersity index	MEDIUM	MEDIUM	MEDIUM	MEDIUM	HIGH	HIGH	HIGH	MEDIUM	MEDIUM
	Zeta potential	MEDIUM	LOW	MEDIUM	MEDIUM	HIGH	LOW	MEDIUM	HIGH	LOW
	Encapsulation efficiency	HIGH	LOW	HIGH	HIGH	HIGH	HIGH	HIGH	LOW	MEDIUM
	Drug release rate	MEDIUM	MEDIUM	MEDIUM	LOW	LOW	HIGH	MEDIUM	LOW	LOW
	Permeability rate (nasal mucosa)	MEDIUM	HIGH	MEDIUM	MEDIUM	LOW	LOW	HIGH	MEDIUM	MEDIUM
	Permeability rate (BBB)	MEDIUM	HIGH	MEDIUM	HIGH	LOW	LOW	HIGH	MEDIUM	MEDIUM
	Mucoadhesive properties	MEDIUM	MEDIUM	HIGH	LOW	LOW	MEDIUM	MEDIUM	HIGH	MEDIUM

B	CMA/CPP	Amount of BSA	Amount of LAM	BSA: LAM incubation time	pH	EtOH : water ratio	EtOH flow rate	Ionic strength	Stirring speed	Temperature
	CQA									
	Average hydrodynamic diameter	HIGH	HIGH	MEDIUM	HIGH	HIGH	MEDIUM	MEDIUM	HIGH	MEDIUM
	Polydispersity index	HIGH	HIGH	MEDIUM	HIGH	HIGH	MEDIUM	MEDIUM	HIGH	MEDIUM
	Zeta potential	MEDIUM	LOW	MEDIUM	MEDIUM	MEDIUM	MEDIUM	MEDIUM	LOW	LOW
	Encapsulation efficiency	HIGH	HIGH	MEDIUM	HIGH	MEDIUM	MEDIUM	MEDIUM	HIGH	MEDIUM
	Drug release rate	MEDIUM	MEDIUM	LOW	LOW	LOW	LOW	LOW	LOW	LOW
	Permeability rate (nasal mucosa)	MEDIUM	MEDIUM	LOW	LOW	LOW	LOW	LOW	LOW	LOW
	Permeability rate (BBB)	MEDIUM	MEDIUM	LOW	LOW	LOW	LOW	LOW	LOW	LOW
	Mucoadhesivity	MEDIUM	MEDIUM	LOW	LOW	LOW	LOW	LOW	LOW	LOW

Figure 1. Risk estimation matrix (REM) of QTPPs-CQAs (A) and CMAs/CPPs-CQAs (B). The relations between the elements were assigned with 'high', 'medium' or 'low' risk level.

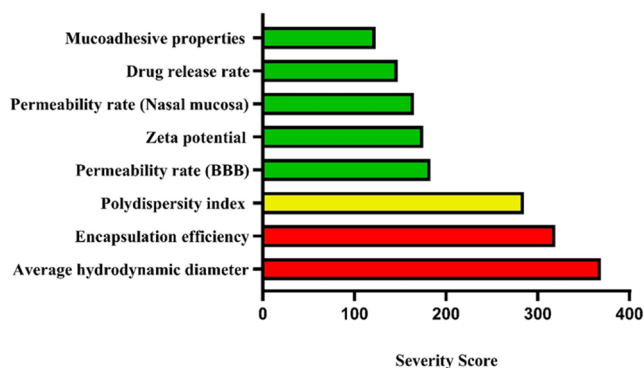


Figure 2. Pareto chart of the CQA parameters.

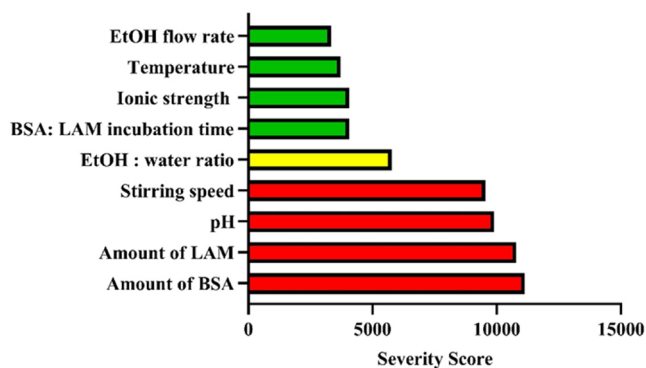


Figure 3. Pareto chart of the CMAs/CPPs parameters.

pH values of 7-9, higher than the isoelectric point of BSA (IEP ~4.7) (Chaw and Olaitan, 2019). In our preliminary study, we obtained small and uniform nanoparticles at pH 8. This was confirmed with previous studies (Satya Prakash, 2010; Yedomon et al., 2013). Sebak et al. found that at pH greater than 7, the particle diameter was reduced, and at pH 8 the particles had optimal size and narrow size distribution at approximately 175–200 nm. Nanoparticles prepared at a higher pH of 8–8.2, when investigated with SEM, revealed uniform and spherical particles (Satya Prakash, 2010).

NaCl was used to enhance the colloidal stability of BSA-NPs. It affects BSA molecules coagulation by shielding the surface charge of the protein molecule and altering their electrostatic properties (Rohiwal et al., 2015). In our preliminary study, the use of 5 mM NaCl at pH 8 led to the preparation of a more stable BSA solution and the formation of smaller particle sizes compared to the use of 10 mM NaCl. This was confirmed with previous studies (Galisteo-González and Molina-Bolívar, 2014; Rohiwal et al., 2015). Rohiwal et al. concluded that at low salt concentrations, the stability of NPs

increases. As long as the ionic strength is low, the electrical repulsion is greater than the van der Waals attraction; therefore, the NPs remain suspended (Rohiwal et al., 2015).

Different amounts of BSA (10, 20, 30 mg) were dissolved in 3 mL of 5 mM NaCl under magnetic stirring (500, 750, 1000 rpm) at 40°C for 15 minutes (Wang et al., 2021). Then, different amounts of LAM (10, 20, 30 mg) were added to the BSA solution and kept stirring at 40°C for 30 minutes. Maghsoudi et al. found that 30 minutes is enough for complete interaction between the drug and protein (Maghsoudi et al., 2008).

EtOH has been selected as a desolvating agent for BSA (Bansal et al., 2011). The addition of ethanol reduces the ratio of water available to keep BSA dissolved, resulting in the shrinkage of the hydrated BSA chains, and at a particular point the degree of hydration will be low and the protein chains will precipitate as nanoparticles (Syed et al., 2020). The use of EtOH also improves the solubility of LAM in water by increasing the temperature to 40°C (Zarghampour et al., 2021), and this will enhance the EE% of LAM (Rahimnejad et al., 2012). In this study, we used 15 mL of EtOH (5 times higher volume than the BSA solution). It was suitable for the BSA to become supersaturated, precipitate, and result in the formation of small and uniform particles with a narrow size distribution (Galisteo-González and Molina-Bolívar, 2014).

The EtOH flow rate was fixed at 1 mL/min. Tarhini et al. studied the effect of EtOH injection rate, and they found that the supersaturation rate and degree rise together in order with the ethanol injection rate, leading to the formation of smaller nanoparticles. Above a rate of ethanol addition of 0.5 mL/min, this impact is negligible (Tarhini et al., 2018).

The use of constant stirring of the aqueous and organic phases at high speed (500, 750, 1000 rpm) leads to the subsequent precipitation of the organic phase and binding to the BSA solution which produces nanoparticles (Yellanki et al., 2021). However, these nanoparticles should be treated with a cross-linker agent to avoid redissolution and reduce enzymatic degradation (Wang et al., 2008).

5.3. Design of Experimentation (DoE)

The high-risk parameters were studied using DoE to reduce their risk to a low level by controlling these parameters in the specific accepted range. In this study, we fixed the pH value at 8 and studied the effect of BSA amount (X_1), LAM amount (X_2) and the stirring speed (X_3) on the Z-average (Y_1) and EE% (Y_2) of the prepared nanoparticles at 3 levels (Table 4).

By comparing statistical variables such as the probability value (p-value), the multiple correlation coefficient (R^2), and adjusted multiple correlation coefficient (adjusted R^2), the best-fit empirical model was used to forecast the link between control factors and response factors (Supplementary Table S1 and S2).

As shown in Table 4, all LAM-NP formulations had an accepted particle size according to our CQA (ranged from 168.900 ± 4.036 to 223.233 ± 2.236 nm). Z-average, PDI and ZP are considered important parameters which could influence

Table 4. Dependent and independent factors of the 3³ factorial design. Results are presented as mean ± SD.

Formulation Code	Independent factors			Response	
	BSA (mg)	LAM (mg)	Stirring speed (rpm)	Z-average (nm)	EE (%)
LAM-NP-1	10	10	500	184.900 ± 0.818	62.760 ± 4.526
LAM-NP-2	10	20	1000	212.500 ± 1.734	83.007 ± 4.293
LAM-NP-3	10	30	750	218.833 ± 3.003	89.290 ± 2.881
LAM-NP-4	20	10	1000	205.766 ± 2.514	66.564 ± 3.942
LAM-NP-5	20	20	750	223.233 ± 2.236	83.273 ± 5.602
LAM-NP-6	20	30	500	182.733 ± 1.582	89.585 ± 3.445
LAM-NP-7	30	10	750	195.866 ± 0.850	64.843 ± 2.094
LAM-NP-8	30	20	500	168.900 ± 4.036	86.531 ± 3.112
LAM-NP-9	30	30	1000	173.800 ± 1.249	91.776 ± 2.455

the release, endocytosis-dependent cellular uptake, biodistribution and stability (Danaei et al., 2018; Hoseini et al., 2023). PDI values showed a narrow particle size distribution (PDI < 0.3), which means the potential for the formation of uniform nanoparticles with lower aggregation and hence improved the stability (Dutta et al., 2018) (as shown in Supplementary Table S3). However, PDI values < 0.5 reported to be acceptable, while PDI values > 0.5 means a broader size distribution. In addition, the narrow PDI values suggest that LAM-NPs had a larger surface area to volume ratio, which increases the contact surface with the dissolution medium, leading to increased rate of dissolution.

All formulations had negative ZP (from -33.733 ± 1.289 to -27.966 ± 0.288 mV), indicating higher physical stability due to the electrostatic repulsive forces that prevent albumin nanoparticles from aggregating (Neves et al., 2016). The potential for aggregation of nanoparticles in blood circulation is a critical concern in evaluating the embolism, which could impact the in vivo biodistribution. Nanoparticles can be uptake by the reticuloendothelial systems (such as liver, spleen), which leads to decrease the half-life in the bloodstream (Liu et al., 2013; Zelepukin et al., 2024). The smaller the particle, the higher the surface energy, thus smaller particles aggregate more readily than larger particles. Therefore, the enhancement in the electrostatic repulsive force will prevent the aggregation. Hence the particle size and zeta potential have an impact on the aggregation. Nanoparticles with Z-average values < 200 nm and ZP > |±30 mV| are able to bypass BBB and escape from the reticuloendothelial system (Masserini, 2013). In addition, ZP is a critical parameter to evaluate the ability of nanoparticles to bypass the BBB. Cationic nanoparticles expected to transport the drugs across BBB more efficiently than anionic nanoparticles due to the negative charge of BBB. However, this could prevent the permeability across BBB. Lockman et al. evaluated the effect of neutral, anionic and cationic charged nanoparticles on BBB integrity and brain permeability. Their study showed that anionic nanoparticles at lower concentrations had no effect on BBB integrity, and higher brain uptake rates (Lockman et al., 2004). Therefore, the prepared LAM-NP formulations are physically stable and have longer residence time inside the brain without being effluxed by time (Ammar et al., 2018). The negative value of ZP is due to the terminal groups of BSA of negative charges that are positioned on the surfaces of the NPs. Furthermore, the EE% was higher than 75%

(CQA) except in the LAM-NP-1, LAM-NP-4, and LAM-NP-7 formulations.

The potential for aggregation of nanoparticles in blood circulation is a critical concern in evaluating the embolism, which could impact the *in vivo* biodistribution. Nanoparticles can be uptake by the reticuloendothelial systems (such as liver, spleen), which leads to decrease the half-life in the bloodstream (Liu et al., 2013; Zelepukin et al., 2024). The smaller the particle, the higher the surface energy, thus smaller particles aggregate more readily than larger particles. Therefore, the enhancement in the electrostatic repulsive force will prevent the aggregation. Hence the particle size and zeta potential have an impact on the aggregation. Nanoparticles with Z-average values $< 200\text{nm}$ and $\text{ZP} > |\pm 30\text{mV}|$ are able to bypass BBB and escape from the reticuloendothelial system (Masserini, 2013).

5.3.1. The effect of independent factors on the average hydrodynamic diameter (Y_1)

A quadratic equation describing the individual main effects of X_1 , X_2 , and X_3 on Y_1 was generated by the reduced linear mathematical model, as presented in Eq. (11):

$$Y_1 = 196.281 - 12.944X_1 - 1.861X_2 + 9.255X_3 + 3.994X_1^2 + 3.947X_2^2 + 12.272X_3^2 - 3.455X_1X_2 \quad (11)$$

The regression coefficient (R^2) of the surface plot was 0.999, the adjusted R^2 was 0.997 and the MS Residual was 0.022, indicating a proper correlation. The R^2 values demonstrate how well the predicted model fits the experimental data, and its value should be closer to 1. The R^2 adjusted is another modified form of R^2 that demonstrates the number of terms present in the model (Naman et al., 2021).

Analysis of variance (ANOVA) was applied as statistics, with a 95% confidence interval level where the variable was considered significant if the p-value $< .05$. The results showed that the p-values of the model for Y_1 were less than .05, which justifies the fact that the quadratic model is significant. The model factors such as X_1 , X_3 , X_1^2 were significant (p-value $< .05$). The equation in terms of actual factors can be used to make predictions about the response for given levels of each factor. According to these results, the increase in the amount of BSA led to a decrease in the Z-average (significant effect). Similar results obtained by other authors (Wang et al., 2008; Rahimnejad et al., 2012; Rohiwal et al., 2015). Furthermore, the effect of LAM amount was insignificant and negligible on Z-average. The results showed that the Z-average increased with increasing stirring speed, but after a certain stirring speed, the Z-average was unaffected by the rate of stirring (Figure 4). Then, it started to decrease with increasing stirring speed. A similar result was obtained by Rahimnejad et al. (Rahimnejad et al., 2012).

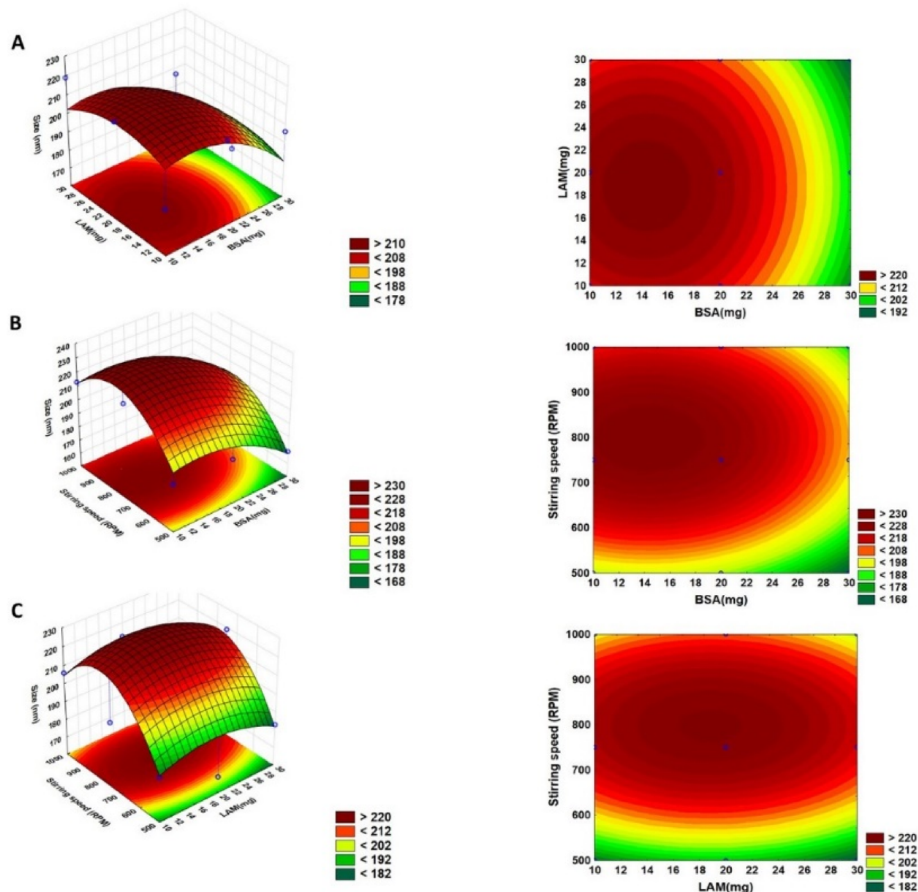


Figure 4. Contour plots (2D) and response surface plots (3D) of selected independent factors on Z-average; (a): BSA amount (X_1) and LAM amount (X_2), (B): BSA amount (X_1) and stirring speed (X_3), (C): LAM amount (X_2) and stirring speed (X_3).

5.3.2. The effect of independent factors on EE%

A quadratic equation describing the individual main effects of X_1 , X_2 , and X_3 on Y_2 was generated by the reduced linear mathematical model, as presented in Eq. (12):

$$Y_2 = 79.737 + 1.348X_1 + 12.747X_2 + 3.4X_2^2 \quad (12)$$

The regression coefficient (R^2) of the surface plot was 0.992 the adjusted R^2 was 0.988 and the MS Residual was 1.545, which indicates a proper correlation. The results showed that the p-values of the model for Y_2 are less than .05, which justifies the fact that the quadratic model is significant. The model factors such as X_1 , X_2 , X_2^2 were significant (p-value < .05, p-value < .001, p-value < .001, respectively), and had positive effects. The results showed that the EE% increased with increasing amount of BSA (Figure 5). Similar results obtained by other authors (Sailaja and Vineela, 2014; Yadav and Yadav, 2021). This can be related to the availability of higher amounts of polymer for entrapment. Moreover, the EE% increased with increase of the LAM amount. Maghsoudi et al. found that EE% increases with drug concentration. This is due to the increase in the amount of adsorbed drug on BSA molecules and at the same time to the increase in the concentration of entrapped drug (Maghsoudi et al., 2008).

Based on these data, the optimal LAM-NP was prepared using the following: BSA (30mg), LAM (30mg), and stirring

speed (1000rpm). The particle size was 173.800 ± 1.248 nm with a narrow particle size distribution ($PDI = 0.212 \pm 0.005$), a negative ZP value (-29.800 ± 0.070 mV) and high EE% ($91.776 \pm 2.455\%$).

This particle size and negative ZP are optimal for achieving a long-circulating system and increasing permeability through the BBB and into the brain (Masserini, 2013; Zaman et al., 2018). This formulation will be used for further investigations.

5.4. Cross-linked lamotrigine-loaded bovine serum albumin nanoparticles

Crosslinking is essential for nanoparticle preparation, affecting the stability, bio-decomposability and drug release from the nanocarrier system due to the impact on Z-average, PDI, ZP, and EE% (Niknejad and Mahmoudzadeh, 2015; Tanjung et al., 2024). The optimal LAM-NP was treated with different types and concentrations of cross-linkers to evaluate both the *in vitro* and *ex vivo* effects. The used cross-linkers act as stabilizers for the BSA nanoparticles (which bind two molecules of BSA with each other) and as functionalized group (which bond BSA and free LAM with each other).

To understand the chemical interaction between BSA and LAM, Patil et al. used molecular docking studies (Patil et al.,

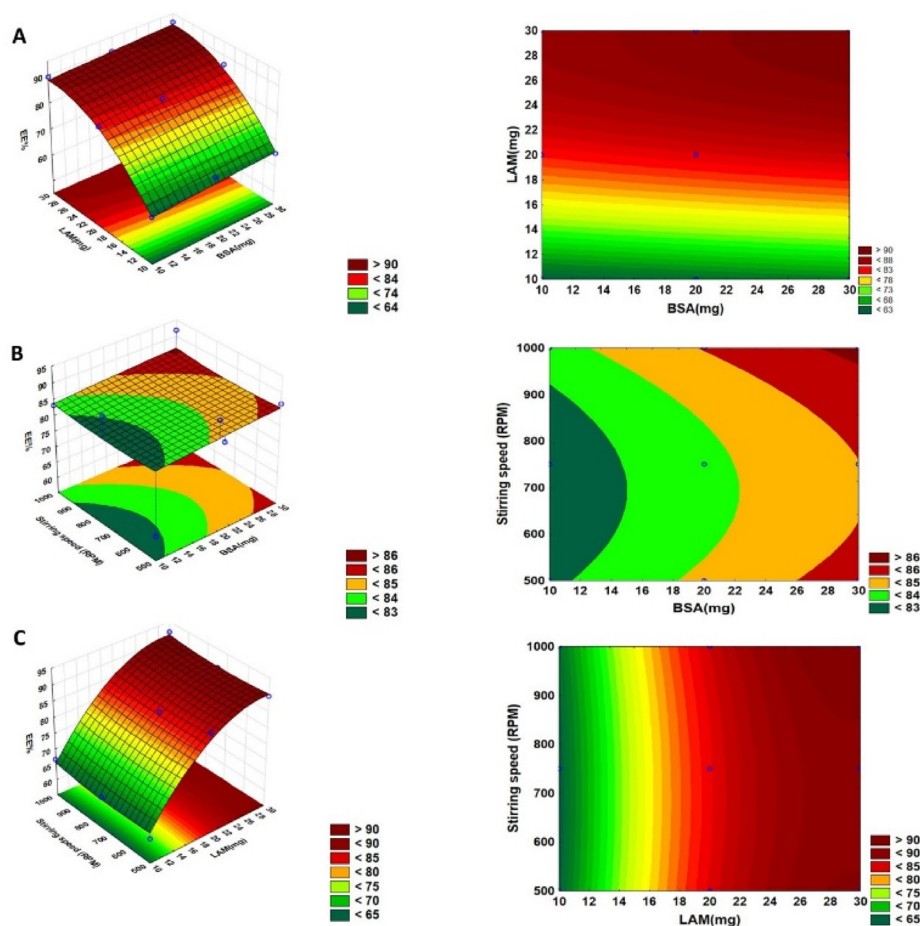


Figure 5. Contour plots (2D) and response surface plots (3D) of selected independent factors on EE%; (a): BSA amount (X_1) and LAM amount (X_2), (B): BSA amount (X_1) and stirring speed (X_3), (C): LAM amount (X_2) and stirring speed (X_3).

2024). The docking results showed that LAM has a high affinity for binding BSA, and it binds to subdomain IIA of domain II which is a drug binding site I (Sudlow Site I) in BSA. The possible interactions between LAM and residues of BSA were presented in [Supplementary Scheme 1](#), which included: alkyl, pi-alkyl, van der Waals, conventional hydrogen bonds, and carbon-hydrogen bonds.

GLUT is a chemical cross-linker, which is usually used to prepare albumin nanoparticles using the coacervation method (Prajapati et al., 2021). The amount of GLUT has a great influence on the physical properties such as the Z-average and ZP of the nanoparticles.

However, due to the toxicity effects of GLUT, other chemical cross-linkers such as GLUC and EDC were used in this study as alternatives to avoid the toxic aldehyde residues in the nanoparticles. Aldehyde groups of GLUT react with amino residues (such as the lysine amino acid of BSA) via a nucleophilic reaction to form Schiff bases which could react with other amino residues of the same or other BSA molecules (in the neutral to alkaline environment), thus preventing re-solution of BSA molecules and forming a network of cross-linked BSA molecules (Zuo et al., 2015; Jahanban-Esfahlan et al., 2016; Chaw and Olaitan, 2019) ([Supplementary Scheme 2](#)). In addition, this reaction could happen with the primary amine of free LAM which decreases the free amount of LAM, thus increasing EE%.

GLUC has a carbonyl group; therefore, it is also suitable as an eco-friendly cross-linker. The mechanism of crosslinking can be described by protein glycation, a nonenzymatic reaction, in which the carbonyl group of GLUC interacts with the nucleophilic amino group of the amino acid (N terminal residues of lysine and arginine) to produce a Schiff base (Ledesma-Osuna et al., 2008; Rahman and Khalil, 2022). Then, it undergoes an Amadori rearrangement to form a more stable ketoamine, which undergoes a series of rearrangement and cyclization reactions to produce heterogeneous compounds known as Advanced Glycation End products (AGEs), some AGEs act as cross-linkers (as shown in [Supplementary Scheme 2](#)) (Yang et al., 2022). The primary amines of free LAM could be sites of this nucleophilic reaction. The use of GLUC offers many advantages, such as low toxicity, long-term stability, and biocompatibility (Barbinta-Patrasco et al., 2023). EDC is a zero-space cross-linker. It forms peptide bands between carboxyl and amide groups of amino acids in stabilized nanoparticles to form active O-urea, creating an amide link with amino groups and releasing water-soluble, easily removable isourea (Jahanban-Esfahlan et al., 2016; Kalidasan et al., 2016; Katona et al., 2022). The primary amines of free LAM could be sites of this nucleophilic reaction ([Supplementary Scheme 3](#)).

As demonstrated in [Figure 6](#), increasing the concentration of GLUC and GLUT resulted in a significant increase in the Z-average. NP-GLUC-3, NP-GLUT-2 and NP-EDC-1 had the smallest Z-average (200.933 ± 2.993 , 168.900 ± 2.151 , and 163.766 ± 1.955 nm, respectively). All GLUC formulations were within the target particle size range (<250 nm). Furthermore, increasing the amount of EDC from 0.5 to 1 mg resulted in a decrease in Z-average due to the increase in the degree of crosslinking, however, NP-EDC-1.5 showed an increase in Z-average, which could be attributed to particle aggregation.

The effect of cross-linking on EE% is demonstrated in [Figure 7](#). It was revealed, NP-GLUC-9, NP-GLUT-2 and NP-EDC-1.5 had the highest percentage of EE ($98.104 \pm 0.154\%$, $97.401 \pm 0.104\%$, $97.388 \pm 0.175\%$, respectively). The concentration of GLUC or the amount of EDC had no significant impact on EE%. However, increasing the concentration of GLUT resulted in a significant decrease in EE% (p -value $< .0001$). This might be explained by increasing the degree of crosslinking, hence the potential for LAM to be incorporated within the BSA structure decreases (due to reduce the availability of BSA amino residues for the interaction with LAM), resulting in a low encapsulation efficiency. The comparison of EE% results of cross-linked formulations with non-cross-linked LAM-NP can be seen in [Supplementary Figure 1](#).

Based on these results, the selected formulations were NP-GLUC-9, NP-GLUT-2, and NP-EDC-1 (according to the highest EE% and the accepted Z-average value) which were used for further investigations.

Freeze-drying is a frequently applied gentle drying technique in the pharmaceutical industry because it has many advantages, such as simple water removal, increased material stability, and enhanced physicochemical properties and pharmacokinetics of drugs (Bhosale et al., 2021). [Table 5](#) showed Z-average, PDI, ZP and EE% for the selected formulations after freeze-drying.

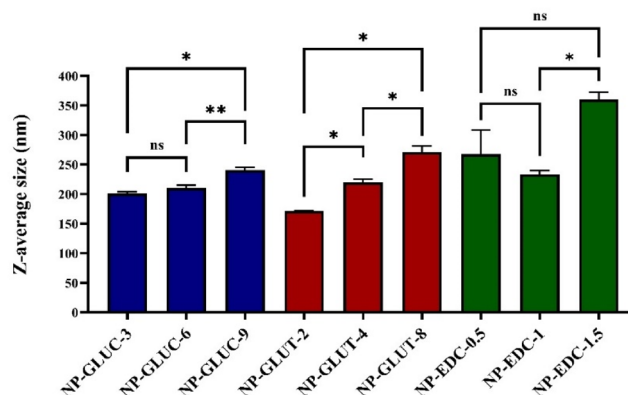


Figure 6. Effect of the type and concentration of the cross-linking agents on the Z-average.

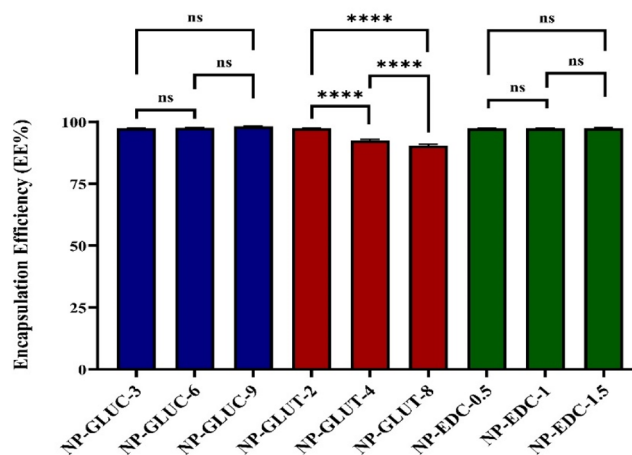
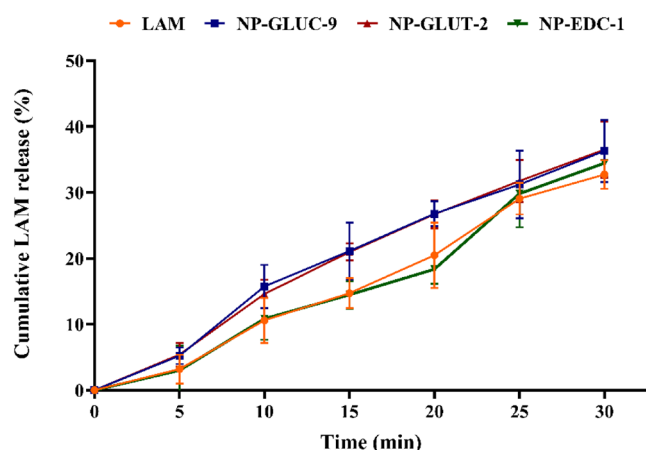


Figure 7. Effect of the type and concentration of cross-linking agents on EE%.

Table 5. Z-average, PDI, ZP, and EE% for the selected formulations after freeze-drying. Results are presented as mean \pm SD.

Optimal formulations	Z-average size (nm)	PDI	ZP (mV)	EE (%)
NPs-GLUC-9	211.100 \pm 1.942	0.123 \pm 0.013	- 38.401 \pm 3.937	98.104 \pm 0.154
NPs-GLUT-2	171.900 \pm 0.301	0.118 \pm 0.007	- 41.800 \pm 0.711	97.401 \pm 0.104
NPs-EDC-1	163.766 \pm 1.955	0.157 \pm 0.010	- 33.966 \pm 0.585	97.307 \pm 0.168

**Figure 8.** Cumulative *in vitro* release profile of the selected formulations in comparison with the initial LAM. Results are expressed as means \pm SD ($n=3$).

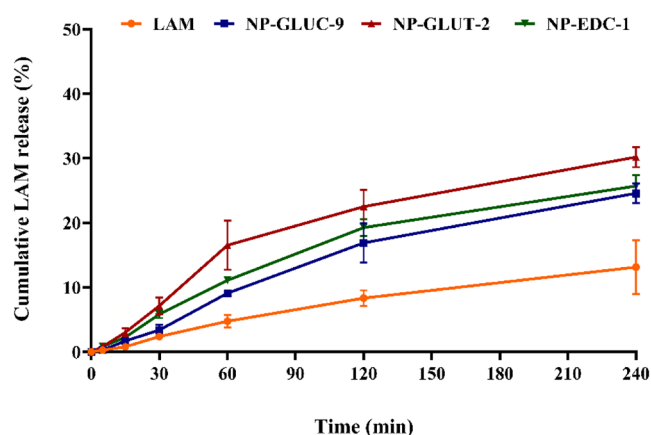
5.5. *In vitro* drug release at nasal conditions

A critical step in the development of intranasal formulations is the *in vitro* drug release test under nasal conditions, which evaluates the behavior of the drug carrier in the nasal cavity. LAM is a BCS Class II drug, and its dissolution is the rate-limiting step for its absorption. Furthermore, bioavailability is significantly impacted by the dissolution profile, which may be directly related to the drug's safety and effectiveness. The result of cumulative *in vitro* release of the selected formulations in SNES is presented in Figure 8. After 10 minutes, NP-GLUC-9 and NP-GLUT-2 showed higher drug release compared to other cross-linker agents and the initial LAM. There was no significant effect of the type of crosslinker on the release profile for all formulations up to 30 minutes. Since LAM is a weak base, it may not have dissociated efficiently above its pK_a value (5.7), which limits drug solubilization at pH 5.6, which could be responsible for the lower degree of drug release from nanoparticles.

5.6. Rapid equilibrium dialysis measurement (RED)

Rapid equilibrium dialysis (RED) is an accurate and reliable method for determining the degree to which a compound binds to plasma proteins. Drug binding to plasma proteins, such as albumin or alpha-1 acid glycoprotein, can limit the drug concentration available to act at the target receptor or enzyme (free drug hypothesis) (Waters et al., 2008). Therefore, it is important to measure the unbound drug to study its pharmacokinetics.

The *in vitro* drug release of LAM from the selected formulations and from the initial suspension was investigated at blood circulation conditions (pH 7.4). *In vitro* release studies using PBS (pH 7.4) medium were used to predict the *in vivo* behavior of drug delivery system using *in vitro-in vivo*

**Figure 9.** Rapid equilibrium dialysis (RED) of the selected formulations in comparison with the initial LAM. Results are expressed as means \pm SD ($n=5$).

correlation (IVIVC). D'Souza et al. evaluated IVIVC for olanzapine PLGA microsphere, and the results showed an excellent correlation between *in vitro* drug release (using PBS, pH 7.4) and the amount of drug absorbed *in vivo* (D'Souza et al., 2014).

As shown in Figure 9, the release of LAM from the selected formulations increased compared to the initial LAM (~1.8 to 2.3-fold). This improvement in release rate could be due to the pH-dependent solubility of LAM (Abdelmonem et al., 2020), and due to the high encapsulation efficiency, the smaller particle size, and the BSA-NP, which provides a greater surface area that enhances the drug release from the formulations. The LAM release profile for the selected formulations showed a biphasic pattern with an initial burst release of the drug in the first hour and a sustained release after 4 h.

5.7. *In vitro* drug release kinetics

The release of LAM from the biodegradable albumin nanoparticles followed two mechanisms: albumin degradation and diffusion through the pores (Mohanraj et al., 2013). The release kinetics of the selected formulations were compared with initial LAM (at pH 5.6 and 7.4) using DDSolver® (Supplementary Table S4 and S5). The model with the highest R^2 , the smallest AIC, and the highest MSC values is the best kinetics model (Pascoal et al., 2015; Abdul Rasool et al., 2021). The release kinetics resulted at pH 5.6 showed that NP-GLUC-9 and NP-GLUT-2 profiles fitted first-order kinetic model, which means that LAM release rate is concentration-dependent. NP-EDC-1.5 release profile fitted the Korsmeyer-Peppas kinetic model. The release exponent 'n' value was 1.245 ($n > 0.89$), which reflects the super case II transport mechanism (Ahmed et al., 2019), hence the release is ruled by the macromolecular relaxation of the polymeric chains. The release kinetics resulted at pH 7.4 showed that all selected formulations were fitted Korsmeyer-Peppas kinetic

model. The release exponent 'n' values for all formulations refers to anomalous transport (non-Fickian) ($0.45 < n < 0.89$), which means that the drug release is due the both Fickian diffusion, and swelling and relaxation of the drug delivery system matrix.

5.8. In vitro permeability measurements

The BBB-PAMPA assay, using porcine brain lipids, has been widely used to improve the prediction of BBB penetration. According to the pattern established in the literature for the prediction of BBB permeation, drugs can be classified into three groups (Di et al., 2003):

1. 'CNS +': (high BBB permeation predicted); $Pe (10^{-6} \text{ cm/s}) > 4.0$.
2. 'CNS': (low BBB permeation predicted); $Pe (10^{-6} \text{ cm/s}) < 2.0$.
3. 'CNS +/-': (BBB permeation uncertain); $Pe (10^{-6} \text{ cm/s})$ from 4.0 to 2.0.

The results of the BBB-PAMPA permeability of the selected formulations compared to the reference are presented in Table 6. NP-GLUC-9 showed higher permeability through brain lipid compared to other formulations and the initial LAM.

PAMPA was used to investigate the passive transcellular diffusion of poorly water-soluble drugs, but has difficulty predicting paracellular and active transport, as well as probable membrane retention of lipophilic drugs (Sun et al., 2017; Berben et al., 2018). As shown in Figure 10, the selected formulations showed a higher LAM flux compared to the initial LAM. This result could be explained by the improvement in the solubility of LAM as a result of the use of BSA-NPs as a drug carrier.

However, PAMPA is incapable of providing an accurate description of the permeability process at the BBB, the PAMPA permeability results should be supported by a cell-dependent model (Caco-2). A similar result was obtained by Nožinić et al. (Nožinić et al., 2010).

5.9. In vitro assessment of mucoadhesive property

Nasal mucociliary clearance is a major issue for nasal delivery, as it can reduce the residence time of a liquid or powder formulation to 15–30 minutes (Salade et al., 2019; Marcello and Chiono, 2023). In this study, we used electronic theory to assess the mucoadhesive properties of the selected formulations by measuring ZP through the interaction of negatively charged nanoparticles after incubation with mucin 1% (1:1 v/v) for 0, 1, 2 and 3 h (Figure 11). Mucin 1% showed a

Table 6. The BBB-PAMPA Permeability results of the selected formulations in comparison with the initial LAM. Results are expressed as means \pm SD ($n=6$).

Formulation	BBB-PAMPA permeability $Pe (10^{-6} \text{ cm/s})$	BBB-PAMPA assay classification
LAM	10.094 ± 0.775	CNS +
NP-GLUC-9	10.621 ± 1.166	CNS +
NP-GLUT-2	5.334 ± 0.471	CNS +
NP-EDC-1	4.859 ± 0.811	CNS +

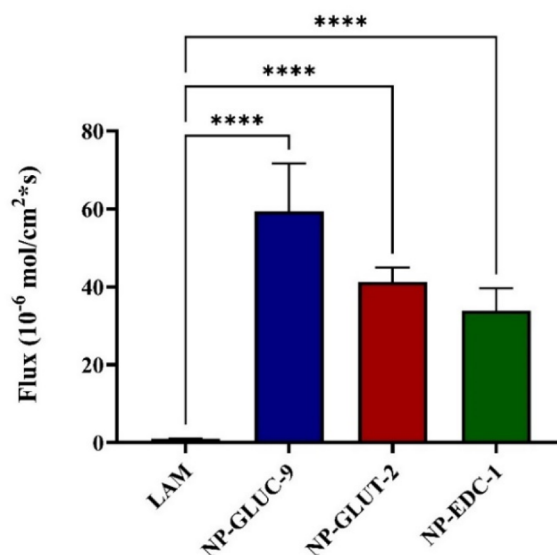


Figure 10. Fluxes of the PAMPA permeability study of the selected formulations in comparison with the initial LAM. Results are expressed as means \pm SD ($n=6$).

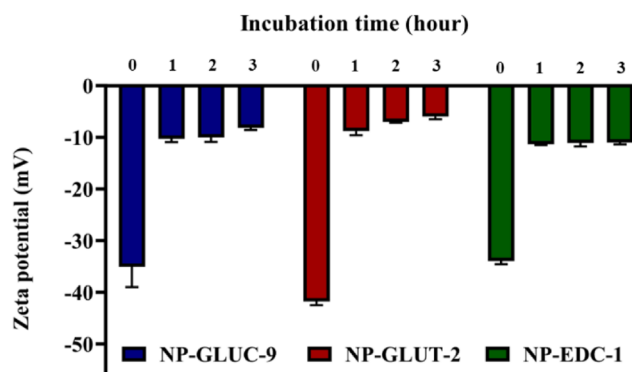


Figure 11. ZP of the selected formulations before and after incubation with mucin as an indicator of mucoadhesion. Results are expressed as means \pm SD ($n=3$).

negative ZP of $-4.753 \pm 0.364 \text{ mV}$ (with a particle size of $232.600 \pm 3.900 \text{ nm}$). NP-GLUC-9, NP-GLUT-2, and NP-EDC-1 showed a high decrease in ZP (from -38.401 ± 3.937 to $-8.170 \pm 0.390 \text{ mV}$, -41.800 ± 0.711 to $-6 \pm 0.501 \text{ mV}$, -33.966 ± 0.585 to $-11 \pm 0.360 \text{ mV}$, respectively) after 3 h of incubation with mucin 1%, almost equal to mucin. A possible explanation is the formation of a mucin layer covering NPs to a great extent (Radwan et al., 2021). This result confirmed the higher degree of interaction of nanoparticles with mucin, which means a better adhesion property. The close contact of the nanoparticles with the mucosa and the particular interactions with mucin all contribute to an increase in nasal residence time (Trenkel and Scherließ, 2021). Therefore, the use of albumin nanoparticles increases the residence time of the drug at the application site, improves drug absorption into the systemic circulation, and enhances its bioavailability.

5.10. Cytotoxicity assay

The percentage of cell viability was measured after 2 h of incubation (Figure 12). Cells tested with initial LAM at a concentration of 5–250 μM showed a significant decrease in cell

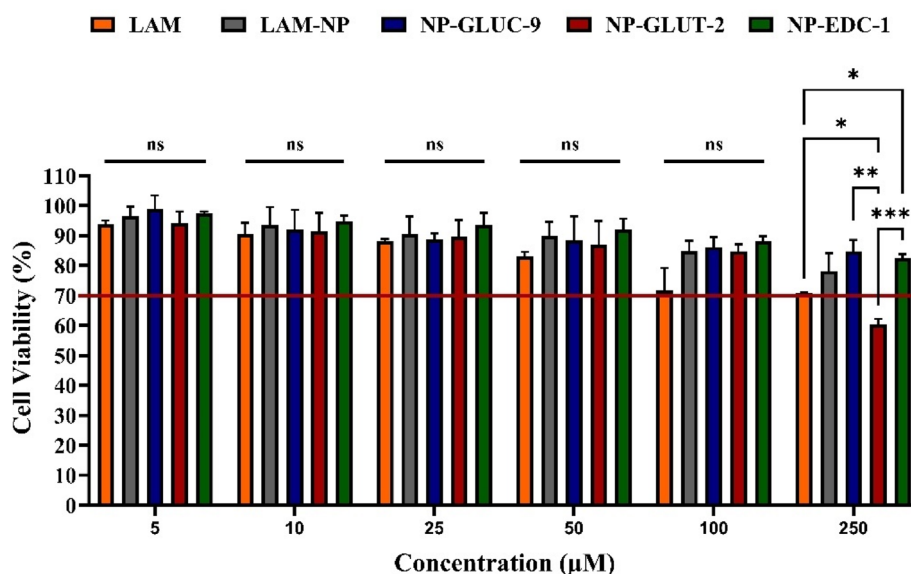


Figure 12. Cell viability % of the selected formulations in comparison to the initial LAM and LAM-NP. Results are expressed as means \pm SD ($n=3$).

viability from $93.802 \pm 1.289\%$ to $70.713 \pm 2.050\%$. Cells treated with LAM-NP showed a decrease in cell viability from $96.598 \pm 3.099\%$ to $78.183 \pm 5.919\%$, which could be explained by low stability, as a result of not using a cross-linker agent, and the potential for enzymatic degradation to release LAM from LAM-NP faster than from cross-linked NPs. Furthermore, cells treated with the selected formulations showed a higher viability value compared to the initial LAM at a concentration of 5–250 μM , except NP-GLUT-2 which showed toxicity at a concentration of 250 μM due to the toxicity of aldehyde residuals. This result indicated that BSA-NPs could be a suitable and compatible drug delivery system for LAM to decrease its toxicity. A similar result was obtained by Shankar Raman et al. (Shankar Raman et al., 2021). They studied the cytotoxicity of LAM polymeric nanoparticles using Vero cells in the concentration ranging between 10 and 50 $\mu\text{g/mL}$. Their study showed that the viability of cells was higher than the initial LAM, which confirmed the suitability of the nanoparticles as a drug delivery system for safe therapy at lower dose. Other study using neuroblastoma cell line was done to evaluate the cytotoxicity of lamotrigine-loaded PLGA nanoparticles in the concentration ranging between 0.625 and 50 $\mu\text{g/mL}$ showed similar results (Nigam et al., 2019). Nigam et al. found that the cytotoxicity of LAM was dose-dependent.

Our results also showed that GLUC 9 mM and EDC 1 mg could be an alternative to avoid the toxicity of GLUT 2% v/v. All formulations were nontoxic up to 100 μM concentration (cell viability $> 70\%$ (Cannella et al., 2019)), therefore the cell permeability study was conducted at that concentration.

5.11. Permeability study on the Caco-2 cell monolayer

The main problem associated with the nose-to-brain drug delivery is poor penetration across the nasal cavity, hence lower concentrations of drug bypassing the BBB (Nigam et al., 2019). The Caco-2 cell line derived from human colon

adenocarcinoma is considered the most common *in vitro* model used for the investigation and prediction of transcellular-based absorption, including passive diffusion, active transport, efflux, and paracellular transport. Caco-2 cells form a tight paracellular barrier, therefore, these cells are employed as models for the prediction of nasal absorption, and as a result, the brain penetration (Nožini et al., 2010; Awortwe et al., 2014; Wang et al., 2019; Furubayashi et al., 2020). As reported by Furubayashi et al., the function of Caco-2 was relatively similar to that of the rat nasal epithelial tissue, which indicated the ability of these cell lines to predict the drug absorption from the nasal cavity of the rat (Furubayashi et al., 2020). In addition, Caco-2 cells show a good correlation when compared with BBB models, in case of passive-diffusion drugs, despite cytoarchitectural differences and other dissimilarities from BBB models (Veszeka et al., 2018). However, Caco-2 cells don't take into consideration the impact of mucin, nasal mucus, clearance, and other physiological factors that restrict drug permeation (Boyuklieva et al., 2023). Therefore, the *in vitro* permeability results should be supported with *ex vivo* and *in vivo* study.

The permeability of LAM from the selected formulations compared to the initial LAM at a concentration of 100 μM is presented in Figure 13. The results showed a higher P_{app} value compared to pure LAM (non-significant effect). This indicates that BSA-NPs may improve LAM nasal absorption by promoting transport into cells and overcoming nasal mucosa permeability and the limited absorption time available due to fast mucociliary clearance. Furthermore, Caco-2 cells also express numerous metabolic enzymes such as cytochrome P450 isoenzymes (CYP450) and some phase II enzymes (e.g. glutathione-S-transferases, sulfotransferase and glucuronidase (Van Breemen and Li, 2005)) which may degrade BSA-NP and release LAM.

NP-EDC-1 showed a higher P_{app} value compared to other formulations and initial LAM, which could be attributed to the nanosized particle ($< 200\text{nm}$) and the high EE% ($97.307 \pm 0.168\%$).

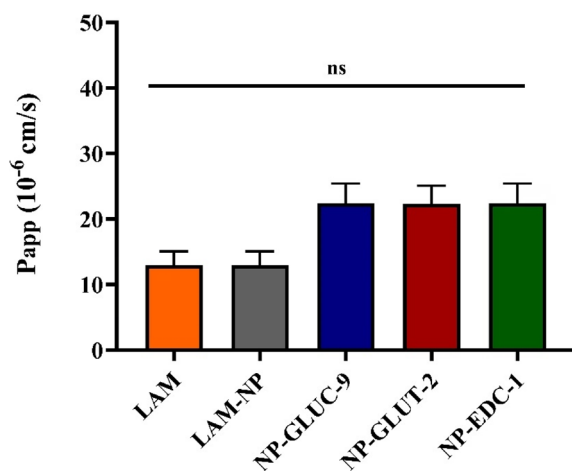


Figure 13. P_{app} value of the selected formulations compared to the initial LAM and LAM-NP at a concentration of 100 μ M. Results are expressed as means \pm SD ($n=3$).

5.12. Ex vivo nasal permeability study on human nasal mucosa

The ex vivo model is simple, time- and cost-effective, which provide accurate predictions for the absorption through the nasal cavity and hence the penetration cross BBB. However, this model has drawbacks, including the restricted tissue viability window, and interindividual variables (such as age, diet, and pathology) which could potentially affect the tissue morphology that can contribute to variability.

The nasal epithelium has relatively high permeability because there are only two cell layers that separate the nasal lumen from a thick network of blood vessels in the lamina propria (Mara Mainardes et al., 2006). Drugs can penetrate the blood circulation through the respiratory epithelium or the trigeminal nerve ends, and hence the brain; or they can penetrate the CSF or the brain directly through the olfactory neurons or the olfactory epithelial cells through the olfactory epithelium. Furthermore, the use of bioadhesive polymers, such as BSA, increased the residence time of the formulations in the nasal cavity, which could improve absorption while preventing damage to the nasal mucosa.

In this study, we used nasal tissue from the olfactory mucosa (could be identified by its yellowish color, whereas the respiratory mucosa is pink (Salade et al., 2019)), which covers only 10% of the human nasal cavity (Fortuna et al., 2022). Therefore, this could influence the delivery of the drug to the target site (olfactory mucosa used for CNS delivery, while respiratory mucosa used for systemic delivery (Fortuna et al., 2022)), hence this study evaluated the brain delivery only through the olfactory mucosa.

As shown in Figure 14, the selected formulations had a higher amount of LAM that diffused through the human nasal mucosa to the acceptor chamber in 60 minutes in comparison with initial LAM (260.608 ± 0.657 , 628.050 ± 1.692 , 637.494 ± 2.043 , and $841.711 \pm 2.088 \mu\text{g}/\text{cm}^2$ for LAM, NP-GLUC-9, NP-GLUT-2, and NP-EDC-1 respectively). Exposure time of 60 minutes is considered sufficient for nasal excipients/drugs due to rapid nasal mucociliary clearance (Rassu et al., 2020). Reduced mucociliary clearance might explain the enhanced permeability of BSA-NPs by increasing the

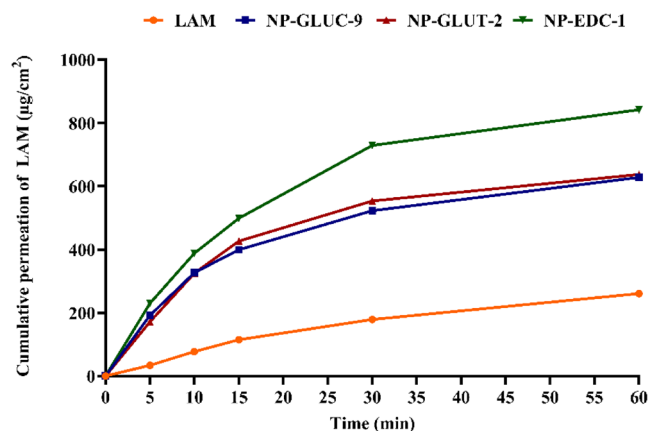


Figure 14. Ex vivo permeability study of the optimal formulations in comparison with initial LAM on human nasal mucosa. Results are expressed as means \pm SD ($n=3$).

Table 7. Permeation and prediction parameters for the selected formulations in comparison with the initial LAM. Results are expressed as means \pm SD ($n=3$).

Sample	Flux ($\mu\text{g}/\text{cm}^2/\text{h}$)	Kp (cm/h)	ER	Css ($\mu\text{g}/\text{mL}$)
LAM	4.343 ± 0.010	0.006	–	2.091 ± 0.005
NP-GLUC-9	10.467 ± 0.028	0.018	2.409 ± 0.006	5.041 ± 0.013
NP-GLUT-2	10.624 ± 0.067	0.008	2.446 ± 0.019	5.116 ± 0.032
NP-EDC-1	14.072 ± 0.113	0.013	3.239 ± 0.028	6.777 ± 0.053

contact period of LAM with the mucus layer, which could transiently open the tight junctions, thereby facilitating the transport of the associated LAM at the mucosal surface. However, when nanoparticles reach cells, the drug release mechanism may benefit from cell enzymes, which may cause nanoparticle structural biodegradation and influence release kinetics (Clementino et al., 2021).

NP-EDC-1 had the most diffuse LAM (with the smallest particle size of $163.766 \pm 1.955 \text{ nm}$). This result might be explained by considering that the typical size of intrinsic mucus intrinsic pores is 20–200 nm (Marcello and Chiono, 2023). Particles with diameters ranging from 100 to 700 nm can be transferred intracellularly through the nasal epithelium and perhaps to the brain via the olfactory neural pathway (Samaridou and Alonso, 2018; Clementino et al., 2021). Therefore, the smaller particle size with narrow size distribution may facilitate the pass through the pores and pathways leading to increase the absorption of LAM through the nasal epithelium, hence bypassing BBB.

The biopharmaceutical analyses, including the permeation and prediction parameters, of the selected formulations compared to the initial LAM were presented in Table 7. All optimal formulations had higher flux values, values of the permeability coefficient, enhanced ratio, and steady-state plasma concentration compared to the initial LAM.

6. Conclusions

The nasal cavity provides an alternative drug delivery for targeting the brain. The diffusion through the nasal mucosa could be affected by the pK_a , particle size, surface charge, mucoadhesion properties, and drug encapsulation, which are considered the most important parameters for improving

drug bioavailability by enhancing drug transport via nasal barriers through the interaction between the nanoparticles and the location of absorption.

In this study, LAM-loaded BSA nanoparticles were prepared using the coacervation method, and the QbD approach was used to optimize the method parameters. The optimal LAM formulation consisted of 30 mg BSA, 30 mg LAM, and a stirring speed of 1000 rpm for the preparation. The particle size obtained was 173.8 ± 1.248 nm, PDI of 0.212 ± 0.005 , ZP showed negative value (-29.8 ± 0.07 mV) and the EE% was sufficiently high ($91.776 \pm 2.455\%$). The optimal formulation was then prepared with different types and concentrations of cross-linking agents (GLUT, GLUC, and EDC) to investigate the appropriate alternatives for toxic GLUT. The concentration of each cross-linking agent was selected according to the highest EE% and accepted particle size; therefore, GLUT 2% v/v, GLUC 9 mM and EDC 1 mg was applied and their effect on drug release and permeability was investigated.

The selected formulations (NP-GLUC-9, NP-GLUT-2 and NP-EDC-1) showed a higher drug release at CSF conditions compared to nasal conditions, which could be due to the pH-dependent solubility of LAM. The PAMPA result showed an increase in the flux value of LAM through the BBB.

The *ex vivo* study showed a higher diffusion of LAM from the selected formulations through the human nasal mucosa compared to the initial LAM. The cytotoxicity study indicated that BSA-NP reduced LAM toxicity, and GLUC 9 mM and EDC 1 mg could be alternative cross-linking agents to avoid GLUT 2% v/v toxicity. Furthermore, permeability through Caco-2 cells showed that nasal absorption of LAM was improved by using BSA-NPs.

In summary, these findings demonstrate that LAM-loaded BSA nanoparticles could be promising in improving the bioavailability of LAM through nose-to-brain delivery system. However, *in vivo* investigation could be useful to evaluate the correlation between the *in vitro* method (release, permeation) and *in vivo* pharmacokinetics.

Ethical approval

This study was performed in line with the principles of the Declaration of Helsinki. Approval was granted by the institutional ethics committee of the University of Szeged (ETT-TUKEB: IV/3880-1/2021/EKU). The participants were briefed on the study procedures, and written informed consent was obtained from all subjects prior to conducting the procedure.

Author contributions

All authors contributed to the study conception and design. Conceptualization was performed by György Tibor Balogh and Gábor Katona; Methodology by Maryana Salamah, Bence Sipos, Zsuzsanna Schelz, István Zupkó György Tibor Balogh, Gábor Katona, Ágnes Kiricsi and Ágnes Szalencó-Tóké; Formal analysis and investigation by Maryana Salamah, Zsuzsanna Schelz, György Tibor Balogh and Gábor Katona; Writing - original draft preparation by Maryana Salamah; Writing - review and editing by György Tibor Balogh, Gábor Katona, István Zupkó, László Rovó and Ildikó Csóka; Funding acquisition by László Rovó and Ildikó Csóka; Resources by László Rovó, Ildikó Csóka, István Zupkó and György Tibor Balogh; Supervision by György Tibor Balogh, Gábor Katona, László Rovó and Ildikó Csóka. All authors read and approved the final manuscript.

Disclosure statement

No potential conflict of interest was reported by the author(s).

Funding

The publication was funded by The University of Szeged Open Access Fund (FundRef, Grant No. 7145). This work was supported by Project no. TKP2021-EGA-32 implemented with support provided by the Ministry of Culture and Innovation of Hungary from the National Research, Development and Innovation Fund, financed under the TKP2021-EGA funding scheme and by János Bolyai Research Scholarship of the Hungarian Academy of Sciences (G. Katona, BO/00251/21).

ORCID

Maryana Salamah  <http://orcid.org/0000-0003-3833-3233>
 Bence Sipos  <http://orcid.org/0000-0002-0131-4728>
 Zsuzsanna Schelz  <http://orcid.org/0000-0002-8519-4830>
 István Zupkó  <http://orcid.org/0000-0003-3243-5300>
 Ágnes Kiricsi  <http://orcid.org/0000-0002-4206-7145>
 Ágnes Szalencó-Tóké  <http://orcid.org/0000-0002-0024-8802>
 László Rovó  <http://orcid.org/0000-0003-1782-1756>
 Gábor Katona  <http://orcid.org/0000-0003-1564-4813>
 György Tibor Balogh  <http://orcid.org/0000-0001-8273-1760>
 Ildikó Csóka  <http://orcid.org/0000-0003-0807-2781>

Data availability statement

The datasets generated during and/or analyzed during the current study are available from the corresponding author on reasonable request.

References

- Abdelmonem R, Azer MS, Makky A, et al. (2020). Development, characterization, and in-vivo pharmacokinetic study of lamotrigine solid self-nanoemulsifying drug delivery system. *Drug Des Devel Ther* 14:4343–62. doi: [10.2147/DDDT.S263898](https://doi.org/10.2147/DDDT.S263898).
- Abdul Rasool BK, Mohammed AA, Salem YY. (2021). The optimization of a dimenhydrinate transdermal patch formulation based on the quantitative analysis of in vitro release data by DDSolver through skin penetration studies. *Sci Pharm* 89:33. doi: [10.3390/scipharm89030033](https://doi.org/10.3390/scipharm89030033).
- Abdullah GZ, Abdulkarim MF, Salman IM, et al. (2011). In vitro permeation and in vivo anti-inflammatory and analgesic properties of nanoscaled emulsions containing ibuprofen for topical delivery. *Int J Nanomedicine* 6:387–96. doi: [10.2147/IJN.S14667](https://doi.org/10.2147/IJN.S14667).
- Ahmed L, Atif R, Eldeen TS, et al. (2019). Study the using of nanoparticles as drug delivery system based on mathematical models for controlled release.
- Alexander A, Agrawal M, Uddin A, et al. (2019). Recent expansions of novel strategies towards the drug targeting into the brain. *Int J Nanomedicine* 14:5895–909. doi: [10.2147/IJN.S210876](https://doi.org/10.2147/IJN.S210876).
- Alshweiat A. (2019). QbD based control strategy of loratadine nanosuspensions and dry nanoparticles stabilized by Soluplus®. *FARMACIA* 67:729–35. doi: [10.31925/farmacia.2019.4.23](https://doi.org/10.31925/farmacia.2019.4.23).
- Ameer OZ. (2023). In vitro pharmaco-equivalence analysis of diclofenac potassium oral film-coated tablet relative to marketed generics. *J Pharm Pharmacogn Res* 11:585–94. doi: [10.56499/jppres23.1641_11.4.585](https://doi.org/10.56499/jppres23.1641_11.4.585).
- Ammar HO, Ghorab MM, Mahmoud AA, Higazy IM. (2018). Lamotrigine loaded poly-ε-(d,l-lactide-co-caprolactone) nanoparticles as brain delivery system. *Eur J Pharm Sci* 115:77–87. doi: [10.1016/j.ejps.2018.01.028](https://doi.org/10.1016/j.ejps.2018.01.028).
- Arriagada F, Günther G, Zabala I, et al. (2019). Development and characterization of florfenicol-loaded BSA nanoparticles as controlled release carrier. *AAPS PharmSciTech* 20:202. doi: [10.1208/s12249-019-1419-7](https://doi.org/10.1208/s12249-019-1419-7).

- Avachat C, Barry JM, Lyu X, et al. (2022). Management of anti-seizure medications during pregnancy: advancements in the past decade.
- Awortwe C, Fasinu PS, Rosenkranz B. (2014). Application of Caco-2 cell line in herb-drug interaction studies: current approaches and challenges. *J Pharm Pharm Sci* 17:1–19. doi: [10.18433/j30k63](https://doi.org/10.18433/j30k63).
- Bansal A, Kapoor D, Kapil R, et al. (2011). Design and development of paclitaxel-loaded bovine serum albumin nanoparticles for brain targeting. *Acta Pharm* 61:141–56. doi: [10.2478/v10007-011-0012-8](https://doi.org/10.2478/v10007-011-0012-8).
- Barbinta-Patrascu M-E, Iftimie S, Cazacu N, et al. (2023). Bio-entities based on albumin nanoparticles and biomimetic cell membranes: design, characterization and biophysical evaluation. *Coatings* 13:671. doi: [10.3390/coatings13040671](https://doi.org/10.3390/coatings13040671).
- Bartos C, Pallagi E, Szabó-Révész P, et al. (2018). Formulation of levodopa containing dry powder for nasal delivery applying the quality-by-design approach. *Eur J Pharm Sci* 123:475–83. doi: [10.1016/j.ejps.2018.07.061](https://doi.org/10.1016/j.ejps.2018.07.061).
- Beg S, Rahman M, Kohli K. (2019). Quality-by-design approach as a systematic tool for the development of nanopharmaceutical products. *Drug Discov Today* 24:717–25. doi: [10.1016/j.drudis.2018.12.002](https://doi.org/10.1016/j.drudis.2018.12.002).
- Bennet D, Kim S. (2014). Polymer nanoparticles for smart drug delivery. In: Sezer AD, ed. *Application of nanotechnology in drug delivery* [internet]. London, UK: InTech; [cited 2023 Jun 8]. Available at: <http://www.intechopen.com/books/application-of-nanotechnology-in-drug-delivery/polymer-nanoparticles-for-smart-drug-delivery>.
- Berben P, Bauer-Brandl A, Brandl M, et al. (2018). Drug permeability profiling using cell-free permeation tools: overview and applications. *Eur J Pharm Sci* 119:219–33. doi: [10.1016/j.ejps.2018.04.016](https://doi.org/10.1016/j.ejps.2018.04.016).
- Bhosale S, Kumbhar P, Patil O, et al. (2021). Lyophilization: principle, methods, and applications. *Drug Pharm Sci Archives* 1:10–14.
- Bonilla L, Esteruelas G, Ettcheto M, et al. (2022). Biodegradable nanoparticles for the treatment of epilepsy: from current advances to future challenges. *Epilepsia Open* 7:S121–S132. [cited 2023 Jun 8]; Available from: <https://onlinelibrary.wiley.com/doi/10.1002/epi4.12567> doi: [10.1002/epi4.12567](https://doi.org/10.1002/epi4.12567).
- Boyuklieva R, Zagorchev P, Pilicheva B. (2023). Computational, in vitro, and in vivo models for nose-to-brain drug delivery studies. *Biomedicine* 11:2198. doi: [10.3390/biomedicine11082198](https://doi.org/10.3390/biomedicine11082198).
- Bronze-Uhle E, Costa BC, Ximenes VF, Lisboa-Filho PN. (2017). Synthetic nanoparticles of bovine serum albumin with entrapped salicylic acid. *Nanotechnol Sci Appl* 10:11–21. doi: [10.2147/NSA.S117018](https://doi.org/10.2147/NSA.S117018).
- Cannella V, Altomare R, Chiramonte G, et al. (2019). Cytotoxicity evaluation of endodontic pins on L929 cell line. *Biomed Res Int* 2019: 3469525–doi: [10.1155/2019/3469525](https://doi.org/10.1155/2019/3469525).
- Cano A, Fonseca E, Ettcheto M, et al. (2021). Epilepsy in neurodegenerative diseases: related drugs and molecular pathways. *Pharmaceutics* 14:1057. doi: [10.3390/ph14101057](https://doi.org/10.3390/ph14101057).
- Chaw C, Olaitan V. (2019). Desolvation conditions for production of sulfasalazine based albumin nanoparticles: physical properties. *Pharm Front* [Internet]. [cited 2023 Jun 8]; Available at: https://pf.hapres.com/htmls/PF_1069_Detail.html
- Clementino AR, Pellegrini G, Banella S, et al. (2021). Structure and fate of nanoparticles designed for the nasal delivery of poorly soluble drugs. *Mol Pharm* 18:3132–46. doi: [10.1021/acs.molpharmaceut.1c00366](https://doi.org/10.1021/acs.molpharmaceut.1c00366).
- D'Souza S, Faraj JA, Giovagnoli S, Deluca PP. (2014). IVIC from long acting olanzapine microspheres. *Int J Biomater* 2014:407065–11. doi: [10.1155/2014/407065](https://doi.org/10.1155/2014/407065).
- Danaei M, Dehghankhold M, Ataei S, et al. (2018). Impact of particle size and polydispersity index on the clinical applications of lipidic nanocarrier systems. *Pharmaceutics* 10:57. doi: [10.3390/pharmaceutics10020057](https://doi.org/10.3390/pharmaceutics10020057).
- de Barros C, Portugal I, Batain F, et al. (2022). Formulation, design and strategies for efficient nanotechnology-based nasal delivery systems. *RPS Pharm Pharmacol Rep* 1:rqa003. doi: [10.1093/rpsppr/rqa003](https://doi.org/10.1093/rpsppr/rqa003).
- De Oliveira JK, Ronik DVF, Ascari J, et al. (2018). Nanoencapsulation of apocynin in bovine serum albumin nanoparticles: physicochemical characterization. *NANOASIA* 8:90–99. [cited 2023 Jun 8]. Available at: <http://www.eurekaselect.com/144977/article> doi: [10.2174/221068120666160822112408](https://doi.org/10.2174/221068120666160822112408).
- Desai N. (2016). Nanoparticle albumin-bound paclitaxel (Abraxane®). In: Otagiri M, Chuang VTG, eds. *Albumin in medicine* [internet]. Singapore: Springer Singapore, 101–19. [cited 2024 May 13]. Available at: [10.1007/978-981-10-2116-9_6](https://doi.org/10.1007/978-981-10-2116-9_6).
- Di L, Kerns EH, Fan K, et al. (2003). High throughput artificial membrane permeability assay for blood–brain barrier. *Eur J Med Chem* 38:223–32. doi: [10.1016/s0223-5234\(03\)00012-6](https://doi.org/10.1016/s0223-5234(03)00012-6).
- Do Canto AM, Donatti A, Gerald JC, et al. (2020). Neuroproteomics in epilepsy: what do we know so far? *Front Mol Neurosci* 13:604158. doi: [10.3389/fnmol.2020.604158](https://doi.org/10.3389/fnmol.2020.604158).
- Dutta L, Mukherjee B, Chakraborty T, et al. (2018). Lipid-based nanocarrier efficiently delivers highly water soluble drug across the blood–brain barrier into brain. *Drug Deliv* 25:504–16. doi: [10.1080/10717544.2018.1435749](https://doi.org/10.1080/10717544.2018.1435749).
- Espinoza LC, Silva-Abreu M, Clares B, et al. (2019). Formulation strategies to improve nose-to-brain delivery of donepezil. *Pharmaceutics* 11:64. doi: [10.3390/pharmaceutics11020064](https://doi.org/10.3390/pharmaceutics11020064).
- Fatouh A, Elshafeey A, Abdelbary A. (2017). Intranasal agomelatine solid lipid nanoparticles to enhance brain delivery: formulation, optimization and in vivo pharmacokinetics. *Drug Des Devel Ther* 11:1815–25. doi: [10.2147/DDDT.S102500](https://doi.org/10.2147/DDDT.S102500).
- Formica ML, Real DA, Picchio ML, et al. (2022). On a highway to the brain: a review on nose-to-brain drug delivery using nanoparticles. *Appl Mater Today* 29:101631. doi: [10.1016/j.apmt.2022.101631](https://doi.org/10.1016/j.apmt.2022.101631).
- Fortuna A, Schindowski K, Sonvico F. (2022). Editorial: intranasal drug delivery: challenges and opportunities. *Front Pharmacol* 13:868986. doi: [10.3389/fphar.2022.868986](https://doi.org/10.3389/fphar.2022.868986).
- Furubayashi T, Inoue D, Nishiyama N, et al. (2020). Comparison of various cell lines and three-dimensional mucociliary tissue model systems to estimate drug permeability using an in vitro transport study to predict nasal drug absorption in rats. *Pharmaceutics* 12:79. doi: [10.3390/pharmaceutics12010079](https://doi.org/10.3390/pharmaceutics12010079).
- Galisteo-González F, Molina-Bolívar JA. (2014). Systematic study on the preparation of BSA nanoparticles. *Colloids Surf B Biointerfaces* 123:286–92. doi: [10.1016/j.colsurfb.2014.09.028](https://doi.org/10.1016/j.colsurfb.2014.09.028).
- Gangurde PK, Ajitkumar B N, Kumar L. (2019). Lamotrigine lipid nanoparticles for effective treatment of epilepsy: a focus on brain targeting via nasal route. *J Pharm Innov* 14:91–111. doi: [10.1007/s12247-018-9343-z](https://doi.org/10.1007/s12247-018-9343-z).
- Ghose D, Patra CN, Ravi Kumar BVV, et al. (2021). QbD-based formulation optimization and characterization of polymeric nanoparticles of cinnacalcet hydrochloride with improved biopharmaceutical attributes. *Turk J Pharm Sci* 18:452–64. doi: [10.4274/tjps.galenos.2020.08522](https://doi.org/10.4274/tjps.galenos.2020.08522).
- Gieszinger P, Csóka I, Pallagi E, et al. (2017). Preliminary study of non-ionized lamotrigine containing products for nasal powder formulation. *Drug Des Devel Ther* 11:2453–66. doi: [10.2147/DDDT.S138559](https://doi.org/10.2147/DDDT.S138559).
- Gieszinger P, Katona G, Szabó-Révész P, Ambrus R. (2020). Stability study of nasal powder formulation containing nanosized lamotrigine. *APH* 90:27–31. doi: [10.33892/aph.2020.90.27-31](https://doi.org/10.33892/aph.2020.90.27-31).
- He D-k, Wang L, Qin J, et al. (2012). Population pharmacokinetics of lamotrigine in Chinese children with epilepsy. *Acta Pharmacol Sin* 33:1417–23. doi: [10.1038/aps.2012.118](https://doi.org/10.1038/aps.2012.118).
- He Q, Liu J, Liang J, et al. (2018). Towards improvements for penetrating the blood–brain barrier—recent progress from a material and pharmaceutical perspective. *Cells* 7:24. doi: [10.3390/cells7040024](https://doi.org/10.3390/cells7040024).
- Hoseini B, Jaafari MR, Golabpour A, et al. (2023). Application of ensemble machine learning approach to assess the factors affecting size and polydispersity index of liposomal nanoparticles. *Sci Rep* 13:18012. doi: [10.1038/s41598-023-43689-4](https://doi.org/10.1038/s41598-023-43689-4).
- Huang Q, Chen X, Yu S, et al. (2023). Research progress in brain-targeted nasal drug delivery. *Front Aging Neurosci* 15:1341295. doi: [10.3389/fnagi.2023.1341295](https://doi.org/10.3389/fnagi.2023.1341295).
- Hubatsch I, Ragnarsson EGE, Artursson P. (2007). Determination of drug permeability and prediction of drug absorption in Caco-2 monolayers. *Nat Protoc* 2:2111–9. doi: [10.1038/nprot.2007.303](https://doi.org/10.1038/nprot.2007.303).
- Hussain T, Paranthaman S, Rizvi SMD, et al. (2021). Fabrication and characterization of paclitaxel and resveratrol loaded soluplus polymeric

- nanoparticles for improved BBB penetration for glioma management. *Polymers* (Basel) 13:3210. doi: [10.3390/polym13193210](https://doi.org/10.3390/polym13193210).
- ICH guideline Q9 on quality risk management. (2015).
- Jahanban-Esfahlan A, Dastmalchi S, Davaran S. (2016). A simple improved desolvation method for the rapid preparation of albumin nanoparticles. *Int J Biol Macromol* 91:703–9. doi: [10.1016/j.ijbiomac.2016.05.032](https://doi.org/10.1016/j.ijbiomac.2016.05.032).
- Jahanshahi M, Babaei Z. (2008). Protein nanoparticle: a unique system as drug delivery vehicles. *AJOL* 7:4926–34.
- Jeong S-H, Jang J-H, Lee Y-B. (2023). Drug delivery to the brain via the nasal route of administration: exploration of key targets and major consideration factors. *J Pharm Investig* 53:119–52. doi: [10.1007/s40005-022-00589-5](https://doi.org/10.1007/s40005-022-00589-5).
- Ji L, Chen Y, Mao Z, et al. (2021). Efficacy and tolerability of lamotrigine in the treatment of focal epilepsy among children and adolescents: a meta-analysis. *Transl Pediatr* 10:807–18. doi: [10.21037/tp-20-379](https://doi.org/10.21037/tp-20-379).
- Kalidasan V, Liu XL, Herng TS, et al. (2016). Bovine serum albumin-conjugated ferrimagnetic iron oxide nanoparticles to enhance the biocompatibility and magnetic hyperthermia performance. *Nanomicro Lett* 8:80–93. doi: [10.1007/s40820-015-0065-1](https://doi.org/10.1007/s40820-015-0065-1).
- Katona G, Balogh GT, Dargó G, et al. (2020). Development of meloxicam-human serum albumin nanoparticles for nose-to-brain delivery via application of a quality by design approach. *Pharmaceutics* 12:97. doi: [10.3390/pharmaceutics12020097](https://doi.org/10.3390/pharmaceutics12020097).
- Katona G, Sabir F, Sipos B, et al. (2022). Development of lomustine and n-propyl gallate co-encapsulated liposomes for targeting glioblastoma multiforme via intranasal administration. *Pharmaceutics* 14:631. doi: [10.3390/pharmaceutics14030631](https://doi.org/10.3390/pharmaceutics14030631).
- Katona G, Sipos B, Budai-Szűcs M, et al. (2021). Development of in situ gelling meloxicam-human serum albumin nanoparticle formulation for nose-to-brain application. *Pharmaceutics* 13:646. doi: [10.3390/pharmaceutics13050646](https://doi.org/10.3390/pharmaceutics13050646).
- Katona G, Sipos B, Csóka I. (2022). Risk-assessment-based optimization favours the development of albumin nanoparticles with proper characteristics prior to drug loading. *Pharmaceutics* 14:2036. doi: [10.3390/pharmaceutics14102036](https://doi.org/10.3390/pharmaceutics14102036).
- Kis N, Kovács A, Budai-Szűcs M, et al. (2019). Investigation of silicone-containing semisolid in situ film-forming systems using QbD tools. *Pharmaceutics* 11:660. doi: [10.3390/pharmaceutics11120660](https://doi.org/10.3390/pharmaceutics11120660).
- Lalani J, Patil S, Kolate A, et al. (2015). Protein-functionalized PLGA nanoparticles of lamotrigine for neuropathic pain management. *AAPS PharmSciTech* 16:413–27. doi: [10.1208/s12249-014-0235-3](https://doi.org/10.1208/s12249-014-0235-3).
- Ledesma-Osuna AI, Ramos-Clamont G, Vázquez-Moreno L. (2008). Characterization of bovine serum albumin glycosylated with glucose, galactose and lactose. *Acta Biochim Pol* 55:491–7. doi: [10.18388/abp.2008_3054](https://doi.org/10.18388/abp.2008_3054).
- Lee D, Minko T. (2021). Nanotherapeutics for nose-to-brain drug delivery: an approach to bypass the blood brain barrier. *Pharmaceutics* 13:2049. doi: [10.3390/pharmaceutics13122049](https://doi.org/10.3390/pharmaceutics13122049).
- Li W, Chen J, Zhao S, et al. (2022). High drug-loaded microspheres enabled by controlled in-droplet precipitation promote functional recovery after spinal cord injury. *Nat Commun* 13:1262. doi: [10.1038/s41467-022-28787-7](https://doi.org/10.1038/s41467-022-28787-7).
- Li Y, Meador KJ. (2022). Epilepsy and pregnancy. *Continuum* (Minneapolis) 28:34–54. doi: [10.1212/CON.0000000000001056](https://doi.org/10.1212/CON.0000000000001056).
- Liu J-S, Wang J-H, Zhou J, et al. (2014). Enhanced brain delivery of lamotrigine with Pluronic® P123-based nanocarrier. *Int J Nanomed* 9:3923–35. doi: [10.2147/IJN.S62263](https://doi.org/10.2147/IJN.S62263).
- Liu X, Chen Y, Li H, et al. (2013). Enhanced retention and cellular uptake of nanoparticles in tumors by controlling their aggregation behavior. *ACS Nano* 7:6244–57. doi: [10.1021/nn402201w](https://doi.org/10.1021/nn402201w).
- Lockman PR, Koziara JM, Mumper RJ, Allen DD. (2004). Nanoparticle surface charges alter blood–brain barrier integrity and permeability. *J Drug Target* 12:635–41. doi: [10.1080/10611860400015936](https://doi.org/10.1080/10611860400015936).
- Lohcharoenkal W, Wang L, Chen YC, Rojanasakul Y. (2014). Protein nanoparticles as drug delivery carriers for cancer therapy. *Biomed Res Int* 2014:180549–12. doi: [10.1155/2014/180549](https://doi.org/10.1155/2014/180549).
- Maghsoudi A, Shojaosadati SA, Vasheghani Farahani E. (2008). 5-fluorouracil-loaded BSA nanoparticles: formulation optimization and in vitro release study. *AAPS PharmSciTech* 9:1092–6. doi: [10.1208/s12249-008-9146-5](https://doi.org/10.1208/s12249-008-9146-5).
- Manole A, Sirbu C, Mititelu M, et al. (2023). State of the art and challenges in epilepsy—a narrative review. *JPM* 13:623. doi: [10.3390/jpm13040623](https://doi.org/10.3390/jpm13040623).
- Mara Mainardes R, Cristina Cocenza Urban M, Oliveira Cinto P, et al. (2006). Liposomes and micro/nanoparticles as colloidal carriers for nasal drug delivery. *Curr Drug Deliv* 3:275–85. doi: [10.2174/15672010677731019](https://doi.org/10.2174/15672010677731019).
- Marcello E, Chiono V. (2023). Biomaterials-enhanced intranasal delivery of drugs as a direct route for brain targeting. *IJMS* 24:3390. doi: [10.3390/ijms24043390](https://doi.org/10.3390/ijms24043390).
- Masserini M. (2013). Nanoparticles for brain drug delivery. *ISRN Biochem* 2013:238428–18. doi: [10.1155/2013/238428](https://doi.org/10.1155/2013/238428).
- Mistry A, Stolnik S, Illum L. (2009). Nanoparticles for direct nose-to-brain delivery of drugs. *Int J Pharm* 379:146–57. doi: [10.1016/j.ijpharm.2009.06.019](https://doi.org/10.1016/j.ijpharm.2009.06.019).
- Mohanraj K, Sethuraman S, Krishnan UM. (2013). Development of poly(butylene succinate) microspheres for delivery of levodopa in the treatment of Parkinson's disease. *J Biomed Mater Res B Appl Biomater* 101:840–7. doi: [10.1002/jbm.b.32888](https://doi.org/10.1002/jbm.b.32888).
- Mohsen AM, Salama AAA, Asfour MH. (2023). Cubosome-based thermo-sensitive *in situ* gelling system for intranasal administration of lamotrigine with enhanced antiepileptic efficacy. *Pharm Dev Technol* 28:520–34. doi: [10.1080/10837450.2023.2216755](https://doi.org/10.1080/10837450.2023.2216755).
- Mosmann T. (1983). Rapid colorimetric assay for cellular growth and survival: application to proliferation and cytotoxicity assays. *J Immunol Methods* 65:55–63. doi: [10.1016/0022-1759\(83\)90303-4](https://doi.org/10.1016/0022-1759(83)90303-4).
- Naman S, Madhavi N, Singh B, et al. (2021). Implementing risk-based quality by design for development and optimization of flavored oral disintegrating mini tablets. *J Drug Delivery Sci Technol* 66:102799. doi: [10.1016/j.jddst.2021.102799](https://doi.org/10.1016/j.jddst.2021.102799).
- Neves AR, Queiroz JF, Reis S. (2016). Brain-targeted delivery of resveratrol using solid lipid nanoparticles functionalized with apolipoprotein E. *J Nanobiotechnology* 14:27. doi: [10.1186/s12951-016-0177-x](https://doi.org/10.1186/s12951-016-0177-x).
- Nigam K, Kaur A, Tyagi A, et al. (2019). Nose-to-brain delivery of lamotrigine-loaded PLGA nanoparticles. *Drug Deliv Transl Res* 9:879–90. doi: [10.1007/s13346-019-00622-5](https://doi.org/10.1007/s13346-019-00622-5).
- Niknejad H, Mahmoudzadeh R. (2015). Comparison of different crosslinking methods for preparation of docetaxel-loaded albumin nanoparticles. *Nožini D, Padovan J, Antolovi R. (2010). Assessment of macrolide transport using PAMPA, Caco-2 and MDCKII-hMDR1 assays. Croat Chem Acta 83:323–331.*
- Pallagi E, Ismail R, Paál TL, Csóka I. (2018). Initial risk assessment as part of the quality by design in peptide drug containing formulation development. *Eur J Pharm Sci* 122:160–9. doi: [10.1016/j.ejps.2018.07.003](https://doi.org/10.1016/j.ejps.2018.07.003).
- Pandey P, Bharadwaj R, Chen X. (2017). Modeling of drug product manufacturing processes in the pharmaceutical industry. *Predictive Modeling of Pharmaceutical Unit Operations*, 1–13. [Internet]. Elsevier; [cited 2023 Jun 8]. Available at: <https://linkinghub.elsevier.com/retrieve/pii/B9780081001547000016>
- Pascoal A, Da Silva PM, Coelho Pinheiro MN. (2015). Drug dissolution profiles from polymeric matrices: data versus numerical solution of the diffusion problem and kinetic models. *Int Commun Heat Mass Transfer* 61:118–27. doi: [10.1016/j.icheatmasstransfer.2014.12.011](https://doi.org/10.1016/j.icheatmasstransfer.2014.12.011).
- Patharapankal EJ, Ajiboye AL, Mattern C, Trivedi V. (2023). Nose-to-brain (N2B) delivery: an alternative route for the delivery of biologics in the management and treatment of central nervous system disorders. *Pharmaceutics* 16:66. doi: [10.3390/pharmaceutics16010066](https://doi.org/10.3390/pharmaceutics16010066).
- Patil V, Barale S, Patil P, et al. (2024). Spectroscopic investigations of conformational change in bovine serum albumin (BSA) with rising concentration of a mood stabilizing drug. *Lamotrigine*.
- Patino LR, Bruns KM, Witt NM, et al. (2015). Management of bipolar disorder in children and adolescents. *FOC* 13:25–36. doi: [10.1176/appi.focus.130121](https://doi.org/10.1176/appi.focus.130121).
- Piazzini V, Landucci E, D'Ambrosio M, et al. (2019). Chitosan coated human serum albumin nanoparticles: a promising strategy for nose-to-brain drug delivery. *Int J Biol Macromol* 129:267–80. doi: [10.1016/j.ijbiomac.2019.02.005](https://doi.org/10.1016/j.ijbiomac.2019.02.005).
- Prajapati R, Garcia-Garrido E, Somoza A. (2021). Albumin-based nanoparticles for the delivery of doxorubicin in breast cancer. *Cancers* (Basel) 13:3011. doi: [10.3390/cancers13123011](https://doi.org/10.3390/cancers13123011).
- Praveen A, Aqil M, Imam SS, et al. (2019). Lamotrigine encapsulated intra-nasal nanoliposome formulation for epilepsy treatment: formulation

- design, characterization and nasal toxicity study. *Colloids Surf B Biointerfaces* 174:553–62. doi: [10.1016/j.colsurfb.2018.11.025](https://doi.org/10.1016/j.colsurfb.2018.11.025).
- Radwan SE-S, El-Kamel AH, Zaki EI, et al. (2021). Hyaluronic-coated albumin nanoparticles for the non-invasive delivery of apatinib in diabetic retinopathy. *Int J Nanomed* 16:4481–94. doi: [10.2147/IJN.S316564](https://doi.org/10.2147/IJN.S316564).
- Radwan SE-S, El-Moslemany RM, Mehanna RA, et al. (2022). Chitosan-coated bovine serum albumin nanoparticles for topical tetradrine delivery in glaucoma: *in vitro* and *in vivo* assessment. *Drug Deliv* 29:1150–63. doi: [10.1080/10717544.2022.2058648](https://doi.org/10.1080/10717544.2022.2058648).
- Rahimnejad M, Najafpour G, Bakeri G. (2012). Investigation and modeling effective parameters influencing the size of BSA protein nanoparticles as colloidal carrier. *Colloids Surf A* 412:96–100. doi: [10.1016/j.colsurfa.2012.07.022](https://doi.org/10.1016/j.colsurfa.2012.07.022).
- Rahman N, Khalil N. (2022). Effect of glycation of bovine serum albumin on the interaction with xanthine oxidase inhibitor allopurinol: spectroscopic studies and molecular modeling. *J Mol Liq* 367:120396. doi: [10.1016/j.molliq.2022.120396](https://doi.org/10.1016/j.molliq.2022.120396).
- Raj A, Thomas RK, Vidya L, et al. (2023). Exploring the cytotoxicity on human lung cancer cells and DNA binding stratagem of camptothecin functionalised silver nanoparticles through multi-spectroscopic, and calorimetric approach. *Sci Rep* 13:9045. doi: [10.1038/s41598-023-34997-w](https://doi.org/10.1038/s41598-023-34997-w).
- Rassu G, Fancello S, Roldo M, et al. (2020). Investigation of cytotoxicity and cell uptake of cationic beta-cyclodextrins as valid tools in nasal delivery. *Pharmaceutics* 12:658. doi: [10.3390/pharmaceutics12070658](https://doi.org/10.3390/pharmaceutics12070658).
- Rekha S, Anila EI. (2019). *In vitro* cytotoxicity studies of surface modified CaS nanoparticles on L929 cell lines using MTT assay. *Mater Lett* 236:637–9. doi: [10.1016/j.matlet.2018.11.009](https://doi.org/10.1016/j.matlet.2018.11.009).
- Rigamonti N, Sebellin J, Pipitone F, et al. (2023). A method for risk assessment evaluating the safety, stability and efficacy in clinical practice of anticancer drug preparations in the centralized compounding unit of the veneto institute of oncology-IRCCS. *Pharmaceutics* 15:1429. doi: [10.3390/pharmaceutics15051429](https://doi.org/10.3390/pharmaceutics15051429).
- Rohiwal SS, Satvekar RK, Tiwari AP, et al. (2015). Investigating the influence of effective parameters on molecular characteristics of bovine serum albumin nanoparticles. *Appl Surf Sci* 334:157–64. doi: [10.1016/j.apsusc.2014.08.170](https://doi.org/10.1016/j.apsusc.2014.08.170).
- Rohiwal SS, Tiwari AP, Verma G, Pawar SH. (2015). Preparation and evaluation of bovine serum albumin nanoparticles for ex vivo colloidal stability in biological media. *Colloids Surf A* 480:28–37. doi: [10.1016/j.colsurfa.2015.04.017](https://doi.org/10.1016/j.colsurfa.2015.04.017).
- Sadeghzadeh F, Nasiraei Haghighi H, Ghiyamaty M, et al. (2023). *In vitro* and *in vivo* study on the anticancer effects of anethole-loaded bovine serum albumin nanoparticles surface decorated with chitosan and folic acid. *Cancer Nano* 14:24. doi: [10.1186/s12645-023-00181-y](https://doi.org/10.1186/s12645-023-00181-y).
- Saengkrit N, Saesoo S, Woramongkolchai N, et al. (2018). Dry formulations enhanced mucoadhesive properties and reduced cold chain handling of influenza vaccines. *AAPS PharmSciTech* 19:3763–9. doi: [10.1208/s12249-018-1181-2](https://doi.org/10.1208/s12249-018-1181-2).
- Şahin A, Tonbul H, Çapan Y, Seko I. (2020). Brain-targeted nanoparticles to overcome the blood-brain barrier. *jpt* 1:26–40. doi: [10.37662/jpt.2020.4](https://doi.org/10.37662/jpt.2020.4).
- Sailaja AK, Vineela C. (2014). Preparation and characterization of mefenamic acid loaded bovine serum albumin nanoparticles by desolvation technique using acetone as desolvating agent.
- Saju J. (n.d.). Formulation and evaluation of lamotrigine nanoparticles incorporated in-situ gel for epilepsy. 13.
- Salade L, Wauthoz N, Goole J, Amighi K. (2019). How to characterize a nasal product. The state of the art of *in vitro* and *ex vivo* specific methods. *Int J Pharm* 561:47–65. doi: [10.1016/j.ijpharm.2019.02.026](https://doi.org/10.1016/j.ijpharm.2019.02.026).
- Samaridou E, Alonso MJ. (2018). Nose-to-brain peptide delivery – the potential of nanotechnology. *Bioorg Med Chem* 26:2888–905. doi: [10.1016/j.bmc.2017.11.001](https://doi.org/10.1016/j.bmc.2017.11.001).
- Satya Prakash S. (2010). Human serum albumin nanoparticles as an efficient nospapine drug delivery system for potential use in breast cancer: preparation and *in vitro* analysis. *IJN* 5:525–532. doi: [10.2147/IJN.S10443](https://doi.org/10.2147/IJN.S10443).
- Serralheiro A, Alves G, Fortuna A, Falcão A. (2015). Direct nose-to-brain delivery of lamotrigine following intranasal administration to mice. *Int J Pharm* 490:39–46. doi: [10.1016/j.ijpharm.2015.05.021](https://doi.org/10.1016/j.ijpharm.2015.05.021).
- Shah P, Dubey P, Vyas B, et al. (2021). Lamotrigine loaded PLGA nanoparticles intended for direct nose to brain delivery in epilepsy: pharmacokinetic, pharmacodynamic and scintigraphy study. *Artif Cells Nanomed Biotechnol* 49:511–22. doi: [10.1080/21691401.2021.1939709](https://doi.org/10.1080/21691401.2021.1939709).
- Shankar Raman S, Narayanan VHB, Durai R. (2021). Lamotrigine nanoparticle laden polymer composite oral dissolving films for improving therapeutic potential of the hydrophobic antiepileptic molecule. *Assay Drug Dev Technol* 19:2–16. doi: [10.1089/adt.2020.992](https://doi.org/10.1089/adt.2020.992).
- Singh J, Garg R, Gupta GD. (2015). Enhancement of solubility of lamotrigine by solid dispersion and development of orally disintegrating tablets using 3² full factorial design. *J Pharm (Cairo)* 2015:828453–8. doi: [10.1155/2015/828453](https://doi.org/10.1155/2015/828453).
- Sipos B, Bella Z, Gróf I, et al. (2023). Soluplus® promotes efficient transport of meloxicam to the central nervous system via nasal administration. *Int J Pharm* 632:122594. doi: [10.1016/j.ijpharm.2023.122594](https://doi.org/10.1016/j.ijpharm.2023.122594).
- Sipos B, Csóka I, Budai-Szűcs M, et al. (2021). Development of dexamethasone-loaded mixed polymeric micelles for nasal delivery. *Eur J Pharm Sci* 166:105960. doi: [10.1016/j.ejps.2021.105960](https://doi.org/10.1016/j.ejps.2021.105960).
- Solanki R, Patel K, Patel S. (2021). Bovine serum albumin nanoparticles for the efficient delivery of berberine: preparation, characterization and *in vitro* biological studies. *Colloids Surf A* 608:125501. doi: [10.1016/j.colsurfa.2020.125501](https://doi.org/10.1016/j.colsurfa.2020.125501).
- Soni G, Kale K, Shetty S, et al. (2020). Quality by design (QbD) approach in processing polymeric nanoparticles loading anticancer drugs by high pressure homogenizer. *Heliyon* 6:e03846. doi: [10.1016/j.heliyon.2020.e03846](https://doi.org/10.1016/j.heliyon.2020.e03846).
- Sun H, Nguyen K, Kerns E, et al. (2017). Highly predictive and interpretable models for PAMPA permeability. *Bioorg Med Chem* 25:1266–76. doi: [10.1016/j.bmc.2016.12.049](https://doi.org/10.1016/j.bmc.2016.12.049).
- Syed A, Devi VK, Karwa P. (2020). Applying Taguchi design for the synthesis of albumin nanoparticles of methotrexate by desolvation technique. *J Pharm Sci* 10:39–44.
- Tanjung Y, Dewi M, Gatera V, et al. (2024). Factors affecting the synthesis of bovine serum albumin nanoparticles using the desolvation method. *Nanotechnol Sci Appl* 17:21–40. doi: [10.2147/NSA.S441324](https://doi.org/10.2147/NSA.S441324).
- Tarhini M, Benlyamani I, Hamdani S, et al. (2018). Protein-based nanoparticle preparation via nanoprecipitation method. *Materials* 11:394. doi: [10.3390/ma11030394](https://doi.org/10.3390/ma11030394).
- Tietje C, Brouder A, ed. (2010). International conference on harmonisation of technical requirements for registration of pharmaceuticals for human use. Handbook of transnational economic governance regimes [Internet]. Brill | Nijhoff, 1041–53. [cited 2022 Nov 2]. Available at: https://brill.com/view/book/edcoll/9789004181564/Bej.9789004163300.i-1081_085.xml.
- Trenkel M, Scherließ R. (2021). Nasal powder formulations: *in-vitro* characterisation of the impact of powders on nasal residence time and sensory effects. *Pharmaceutics* 13:385. doi: [10.3390/pharmaceutics13030385](https://doi.org/10.3390/pharmaceutics13030385).
- Tuba Incecayir IA. (2009). Pharmacokinetic modelling of lamotrigine from plasma concentrations in healthy volunteers. *JBABM* [Internet] [cited 2023 Jun 8]. Available at: <https://www.omicsonline.org/pharmacokinetic-modelling-of-lamotrigine-from-plasma-concentrations-in-healthy-volunteers-1948-593X.1000009.php?aid=365>
- Tuovinen LM, Peltonen SH, Suortti TM, et al. (2002). Enzymatic degradation of and bovine serum albumin release from starch–acetate films. *Biomacromolecules* 3:284–90. doi: [10.1021/bm015581e](https://doi.org/10.1021/bm015581e).
- Van Breenen RB, Li Y. (2005). Caco-2 cell permeability assays to measure drug absorption. *Expert Opin Drug Metab Toxicol* 1:175–85. doi: [10.1517/17425255.1.2.175](https://doi.org/10.1517/17425255.1.2.175).
- Veszela S, Tóth A, Walter FR, et al. (2018). Comparison of a rat primary cell-based blood-brain barrier model with epithelial and brain endothelial cell lines: gene expression and drug transport. *Front Mol Neurosci* 11:166. doi: [10.3389/fnmol.2018.00166](https://doi.org/10.3389/fnmol.2018.00166).
- Vitorino C, Silva S, Gouveia F, et al. (2020). QbD-driven development of intranasal lipid nanoparticles for depression treatment. *Eur J Pharm Biopharm* 153:106–20. doi: [10.1016/j.ejpb.2020.04.011](https://doi.org/10.1016/j.ejpb.2020.04.011).
- Wang G, Siggers K, Zhang S, et al. (2008). Preparation of BMP-2 containing bovine serum albumin (bsa) nanoparticles stabilized by polymer coating. *Pharm Res* 25:2896–909. doi: [10.1007/s11095-008-9692-2](https://doi.org/10.1007/s11095-008-9692-2).

- Wang L, Zhao X, Du J, et al. (2019). Improved brain delivery of pueraria flavones via intranasal administration of borneol-modified solid lipid nanoparticles. *Nanomedicine (Lond)* 14:2105–19. doi: [10.2217/nnm-2018-0417](https://doi.org/10.2217/nnm-2018-0417).
- Wang Y, Chen S, Yang X, et al. (2021). Preparation optimization of bovine serum albumin nanoparticles and its application for siRNA delivery. *Drug Des Devel Ther* 15:1531–47. doi: [10.2147/DDDT.S299479](https://doi.org/10.2147/DDDT.S299479).
- Ware K, Tillery E, Linder L. (2016). General pharmacokinetic/pharmacodynamic concepts of mood stabilizers in the treatment of bipolar disorder. *Ment Health Clin* 6:54–61. doi: [10.9740/mhc.2016.01.054](https://doi.org/10.9740/mhc.2016.01.054).
- Waters NJ, Jones R, Williams G, Sohal B. (2008). Validation of a rapid equilibrium dialysis approach for the measurement of plasma protein binding. *J Pharm Sci* 97:4586–95. doi: [10.1002/jps.21317](https://doi.org/10.1002/jps.21317).
- Wilson B, Lavanya Y, Priyadarshini SRB, et al. (2014). Albumin nanoparticles for the delivery of gabapentin: preparation, characterization and pharmacodynamic studies. *Int J Pharm* 473:73–9. doi: [10.1016/j.ijpharm.2014.05.056](https://doi.org/10.1016/j.ijpharm.2014.05.056).
- Wilson B, Selvam J, Mukundan GK, et al. (2020). Albumin nanoparticles coated with polysorbate 80 for the targeted delivery of antiepileptic drug levetiracetam into the brain. *Drug Deliv Transl Res* 10:1853–61. doi: [10.1007/s13346-020-00831-3](https://doi.org/10.1007/s13346-020-00831-3).
- Yadav P, Yadav AB. (2021). Preparation and characterization of BSA as a model protein loaded chitosan nanoparticles for the development of protein-/peptide-based drug delivery system. *Futur J Pharm Sci* 7:200. doi: [10.1186/s43094-021-00345-w](https://doi.org/10.1186/s43094-021-00345-w).
- Yang C, Di P, Fu J, et al. (2017). Improving the physicochemical properties of bicalutamide by complex formation with bovine serum albumin. *Eur J Pharm Sci* 106:381–92. doi: [10.1016/j.ejps.2017.05.059](https://doi.org/10.1016/j.ejps.2017.05.059).
- Yang F, Zhu D, Wang Z, et al. (2022). Role of advanced glycation end products in intervertebral disc degeneration: mechanism and therapeutic potential. *Oxid Med Cell Longev* 2022:1–12. doi: [10.1155/2022/7299005](https://doi.org/10.1155/2022/7299005).
- Yang Z, Zhang N, Ma T, et al. (2020). Engineered bovine serum albumin-based nanoparticles with pH-sensitivity for doxorubicin delivery and controlled release. *Drug Deliv* 27:1156–64. doi: [10.1080/10717544.2020.1797243](https://doi.org/10.1080/10717544.2020.1797243).
- Yavuz B, Yıldırım Ö, Yılmaz AG. (2021). A new approach in epilepsy treatment: nano-carrier systems. *A J Health Sci* 3:33–44.
- Yedomon B, Fessi H, Charcosset C. (2013). Preparation of bovine serum albumin (BSA) nanoparticles by desolvation using a membrane contactor: a new tool for large scale production. *Eur J Pharm Biopharm* 85:398–405. doi: [10.1016/j.ejpb.2013.06.014](https://doi.org/10.1016/j.ejpb.2013.06.014).
- Yellanki SK, Manoj A S, T M. (2021). Preparation and in vitro evaluation of metoprolol-loaded bovine serum albumin nanoparticles. *Asian J Pharm Clin Res* 14:213–217. doi: [10.22159/ajpcr.2021.v14i1.39738](https://doi.org/10.22159/ajpcr.2021.v14i1.39738).
- Zaman RU, Mulla NS, Braz Gomes K, et al. (2018). Nanoparticle formulations that allow for sustained delivery and brain targeting of the neuropeptide oxytocin. *Int J Pharm* 548:698–706. doi: [10.1016/j.ijpharm.2018.07.043](https://doi.org/10.1016/j.ijpharm.2018.07.043).
- Zarghampour A, Moradi M, Rahimpour E, et al. (2021). Solubility study of lamotrigine in the aqueous mixture of choline chloride based deep eutectic solvent at different temperatures. *J Mol Liq* 344:117935. doi: [10.1016/j.molliq.2021.117935](https://doi.org/10.1016/j.molliq.2021.117935).
- Zelepukin IV, Shevchenko KG, Deyev SM. (2024). Rediscovery of mononuclear phagocyte system blockade for nanoparticle drug delivery. *Nat Commun* 15:4366. doi: [10.1038/s41467-024-48838-5](https://doi.org/10.1038/s41467-024-48838-5).
- Zewde B, Atoyebi O, Gugssa A, et al. (2021). An investigation of the interaction between bovine serum albumin-conjugated silver nanoparticles and the hydrogel in hydrogel nanocomposites. *ACS Omega* 6:11614–27. doi: [10.1021/acsomega.1c00834](https://doi.org/10.1021/acsomega.1c00834).
- Zhang H, Lin C-W, Donovan MD. (2013). Correlation between nasal membrane permeability and nasal absorption rate. *AAPS PharmSciTech* 14:60–3. doi: [10.1208/s12249-012-9884-2](https://doi.org/10.1208/s12249-012-9884-2).
- Zhang Y, Huo M, Zhou J, et al. (2010). DDSolver: an add-in program for modeling and comparison of drug dissolution profiles. *Aaps J* 12:263–71. doi: [10.1208/s12248-010-9185-1](https://doi.org/10.1208/s12248-010-9185-1).
- Zuo H, Gu Z, Cooper H, Xu ZP. (2015). Crosslinking to enhance colloidal stability and redispersity of layered double hydroxide nanoparticles. *J Colloid Interface Sci* 459:10–6. doi: [10.1016/j.jcis.2015.07.063](https://doi.org/10.1016/j.jcis.2015.07.063).